Master's thesis

2020

Jan Groznik

NTNU
Norwegian University of
Science and Technology
Faculty of Engineering
Department of Energy and Process Engineering

Master's thesis

Jan Groznik

Boil-off gas handling from liquefied hydrogen storage

Håndtering av hydrogenavkok fra flytende hydrogen lager

June 2020

NTNU
Norwegian University of
Science and Technology

NTNU
Norwegian University of
Science and Technology

NTNU
Norwegian University of
Science and Technology

Boil-off gas handling from liquefied hydrogen storage

Håndtering av hydrogenavkok fra flytende hydrogen lager

Jan Groznik

Natural Gas Technology
Submission date: June 2020
Supervisor: Prof. Petter Nekså
Co-supervisor: Stian Trædal, SINTEF Energi AS
David Berstad, SINTEF Energi AS

Norwegian University of Science and Technology
Department of Energy and Process Engineering

Norwegian University of Science and Technology

Faculty of Engineering Science and Technology
Department of Energy and Process Engineering

EPT-M

MASTER WORK

for

Student Jan Groznik

Spring 2020

Boil-off gas handling from liquefied hydrogen storage

Håndtering av hydrogenavkok fra flytende hydrogen lager

Background and objective

There is an increasing concern related to climate change. This has led to the interest in using hydrogen as energy carrier and fuel for transportation, power production, industry and potentially other applications in order to avoid the end-use CO_2 emissions.

Norway has vast amounts of energy resources in form of natural gas and electricity from hydro- and wind power. A valorization of these resources to produce hydrogen may give great opportunities for Norway.

There are however several challenges related to the practical implementation of hydrogen as energy carrier. A suitable way of transporting larger amounts of hydrogen over long distances will be in liquid form at temperatures around -250 ºC, as liquid hydrogen (LH_2). Even with well insulated storage tanks, a certain heat inleak will create boil-off gas (BOG) that must be handled.

Reliquefaction of the boiloff gas is a likely possibility if it cannot be handled by pressure build-up in the storage tank or utilized in some other way. Reliquefaction is a frequently used method to handle boil-off from LNG. However, due to the low temperature of LH_2 a reliquefaction plant may become more complex.

The aim of this Master thesis work is to explore hydrogen boil-off gas handling by reliquefaction for various sizes of storage tanks.

The following tasks are to be considered:

1. Literature survey related to concepts and equipment for liquefaction and storage of hydrogen
2. Select a set of process concepts for reliquefaction of hydrogen BOG relevant for volume rates corresponding to different storage tank sizes, and if relevant, for on-shore and maritime applications
3. Modelling of the most relevant concepts and performing simulation/optimization for comparison in Hysys using the best available EoS with latest update of parameters for hydrogen and the refrigerants used

Address
N-7034 Trondheim
Norway

Location
K. Hejes vei 1b

Tel. +47 73 59 38 60
Fax +47 73 59 35 80
Org. no. NO 974 767 880

4. Validate the thermodynamic data of Hysys with data from the thermodynamic library ThermoPack
5. Comparing the concepts related to energy efficiency and other relevant parameters, such as complexity and component selection
6. Perform a simplified cost comparison of relevant concepts to investigate the feasibility of realizing reliquefaction plants for LH2 storage
7. Make a draft scientific paper based on the work performed
8. Propose a plan for further work

-- “ --

Department for Energy and Process Engineering, January 15, 2020

___Petter Nekså_____
Adjunct Prof. Petter Nekså
Supervisor

Co-Supervisor(s):
Stian Trædal SINTEF Energi AS
David Berstad SINTEF Energi AS

Summary

The main objective of the thesis was to develop concepts for hydrogen boil-off gas reliquefaction. Three different processes were simulated, analyzed, and compared: helium Brayton refrigeration cycle with two helium turbine expanders, hydrogen Claude refrigeration cycle with two hydrogen expanders, and Brayton refrigeration cycle with two expanders for the mixture of helium and neon called ”nelium”. Regarding assessed energy efficiency, the most efficient was the nelium Brayton refrigeration process, followed by the hydrogen Claude process, and the least efficient was the helium Brayton refrigeration cycle.

This research topic addresses an important aspect of using a relevant and promising energy source. This thesis provides a systematic approach to an energy efficiency evaluation of boil-off gas reliquefaction solutions as well as some general conclusions that can be made when comparing the options studied. Interestingly, one conclusion is that higher hydrogen feed pressure is not theoretically beneficial if compared to hydrogen liquefaction processes. Furthermore, findings suggest that the benefits of implementing the liquid hydrogen turbine expander instead of the Joule-Thomson valve do not justify implementation of a more complex, and more expensive, machinery. It was also concluded that the mixed refrigerant process with helium and neon would need to be significantly improved to be an attractive option for implementation. Adding hydrogen into the mix seems to be one of the most promising solutions.

This thesis provides general guidelines and insights regarding the handling of boil-off gas. Even though the focus of this master’s thesis was on reliquefaction processes of the entire boil-off gas, other alternatives for handling boil-off gas are discussed and compared.

Preface

This master's thesis was performed at the Norwegian University of Science and Technology (NTNU) Faculty of Engineering Science and Technology, and within the Department of Energy and Process Engineering in the Spring semester 2020. Supervisors of this project were Professor Petter Nekså from NTNU and SINTEF Energi AS, Stian Trædal from SINTEF ENERGI AS, and David Berstad from SINTEF ENERGI AS.

Due to novel circumstances imposed by COVID-19, several tasks were changed in comparison to the task description. First, regarding the simulation and Equations of State (EOS) for reasonable results within a reasonable time, due to mandated safety measures, including work from home, it was not possible to use all of the best available EOS with the latest parameters, as in the point 3 of the thesis description from January 15, 2020. Furthermore, it was not possible to validate thermodynamic data of Aspen HYSYS with the thermodynamic library from SINTEF, ThermoPack, as in the point 4., because it was not possible to get in contact with people responsible for ThermoPack. Point 6 was also not fulfilled because, based on the results, it was obvious that a more detailed design would be needed for a specific cost comparison; this should be done in future research steps.

In the end, I would like to sincerely thank my supervisors for all the help and support given throughout the project!

Table of Contents

List of Tables

List of Figures

Abbreviations

A ..... Heat exchanger area

An ..... Anergy

amb ..... Ambient

BOG ..... Boil-off gas

BOR ..... Boil-off rate

C_3 ..... Propane

c ..... Cold

CCS ..... Carbon capture storage

CNG ..... Compressed natural gas

CO ..... Carbon monoxide

CO_2 ..... Carbon dioxide

comp ..... Compressor

cons ..... Consumed

cum ..... Cumulative

dest ..... Destroyed

Displ ..... Piston displacement volume

E ..... Energy

e ..... Specific energy

Δex ..... Exergy difference

Ex ..... Exergy

$\dot{\mathrm{E}}$x ..... Exergy flow

ex ..... Specific exergy

exp ..... Expander

gas ..... Gas phase

GCU ..... Gas combustion unit

GHG ..... Green house gas

h ..... Specific enthalpy

H_2 ..... Hydrogen

h ..... Hot

He ..... Helium

HX ..... Heat exchanger

in ..... Inlet

KPI ..... Key performance indicators

LH_2 ..... Liquid hydrogen

liq ..... Liquid phase

LMTD ..... Logarithmic mean temperature difference

LNG ..... Liquefied natural gas

$\dot{m}$ ..... Mass flow

min ..... Minimum

no ..... Number

N_2 ..... Nitrogen

Ne ..... Neon

out ..... Outlet

P ..... Power

p ..... Pressure

PFHX ..... Plate-fin heat exchanger

Ref ..... Refrigerant

s ..... Specific entropy

SEC ..... Specific energy consumption

SNG ..... Synthetic natural gas

SWHX ..... Spiral-wound heat exchangers

T ..... Temperature

U ..... Heat transfer coefficient

W ..... Work

Q ..... Heat transfer duty

x ..... Mole concentration

η ..... Energy efficiency

ψ ..... Exergy efficiency

Chapter 1

Introduction

In recent years, heat records have been broken across the world, oceans have shown consistent temperature rise, extreme events have been occurring at higher rates, glaciers have been melting, seas have been rising. These, as well as a host of other indicators, illustrate that global changes are real and serve to thin out any remaining global climate change skeptics. Rapid climate change impells us to realize how quickly life on this planet could become unbearable, not only for us but also for other creatures. While climate changes are not historically new for humanity, this time the changes are more severe and rapid and, importantly, we are aware that humans are, at least partially, the cause. Society will sooner or later have to deal with these challenges in order to survive. According to the UN environmental report, sectors with the highest emission reduction potential are energy, electricity and heat production, industry, forestry, transport, and agriculture Programme (2019).

There have several alternatives proposed in different sectors on how to deal with this crisis, many of which include the use of hydrogen. It is expected that hydrogen technology will play an important, if not crucial, role in the future. However, there are still several challenges that must be overcome before fulfilling the promise of hydrogen. One of the challenges to be resolved is related to liquid hydrogen, specifically the question of how to most efficiently deal with boil-off gas. In our preliminary research, we proposed several options for the handling of boil-off gas in different circumstances. A consideration of these proposals within the context of this master's thesis can be found within the consideration for future research portion of the conclusion sections (Chapter 6) and proposals for further work (Chapter 7). However, the focus of this thesis is on reliquefaction options for hydrogen BOG, and the analysis is dedicated solely to these alternatives.

1.1 Background and motivation

Countries with vast resources of natural gas or other hydrocarbons could produce and export energy in the form of hydrogen rather than hydrocarbons. Alternatively, countries

with a significant amount of renewable energies such as solar, wind, and hydro could use the surplus produced electrical energy to then produce hydrogen via electrolysis and use it as an energy storage form. Norway is a prime example of interest in both alternatives' applications and should be leading the research on hydrogen, including its liquid form which has a significantly higher energy density in comparison to the gas. However, liquid gases are always accompanied by boil-off gas due to heat inleaks and subsequent evaporation. Therefore, dealing with boil-off gas is an important aspect of a promising energy form.

BOG in liquid hydrogen is inevitable and thus necessitates proper handling. While in literature there are a plethora of studies related to liquefied natural gas, research on the handling of hydrogen BOG is sparse. Reliquefaction is especially complex in the case of LH_2 because of lower temperature, the penetration of hydrogen molecules through materials, ortho-para conversion, and other similar specific issues.

The scope of this thesis includes exploring and developing general concepts to efficiently handle hydrogen BOG for different applications, as well as providing a systematic approach to analyzing and comparing the efficiency of different concepts. The focus of these general concepts is on reliquefaction processes.

1.2 Thesis structure

The thesis is structured in the following chapters:

- **Chapter 1: Introduction:** Arguments are given as to why the research scope of this thesis is important and relevant. While the topic is currently not researched yet thoroughly, this is expected to change.
- **Chapter 2: Theory and literature review:** An overview of relevant literature related to liquefaction processes for LNG and liquid hydrogen, BOG handling for LNG and liquid hydrogen, and process equipment in liquid hydrogen industry. Furthermore, basic theoretical concepts are presented, and the equations of state for the simulations of processes related to liquid hydrogen are discussed. Some relevant specific concepts are explained in relation to cryogenics, particularly LNG and liquid hydrogen fields.
- **Chapter 3: Concepts for liquid hydrogen boil-off gas reliquefaction:** In this chapter, several concepts related to hydrogen BOG reliquefaction are presented as the basis for explaining and understanding processes that are the subject of the research topic.
- **Chapter 4: Process simulation:** Simulation procedural steps and specific assumptions used for simulations are laid out.
- **Chapter 5: Final results and analysis:** The main simulation results are presented. Reliquefaction processes are compared directly based on the predefined key performance indicators.

- **Chapter 6: Conclusion:** The research results are discussed and conclusions are drawn based on the research experience; limitations of this thesis are considered.
- **Chapter 7: Proposal for future research**: Further research ideas are listed and recommendations proposed.

Chapter 2

Theory and literature review

This chapter provides a review of existing technologies related to liquefaction, reliquefaction, and handling of boil-off gas for hydrogen and liquefied natural gas. An overview of concepts used in practice, equipment, and existing levels of BOG rates from different types of storage tanks are presented. This chapter begins with a short introduction into liquefaction processes, continuing with LNG specifics and practice, before ending the chapter by presenting hydrogen specifics. These specifics include cryogenic components needed for hydrogen liquefaction, equations of states necessary to carry out simulations, and similar.

2.1 Thermodynamics of liquefaction processes

Before reviewing the existing liquefaction processes in LNG and LH_2 industries, it is important to present how liquefaction processes are analyzed. Given are the definition of energy and exergy efficiencies, key performance indicators of these processes, specific energy consumption, and other characteristics.

One of the important parameters regarding liquefaction is energy efficiency - in the broadest sense it is defined as a ratio between useful output energy and consumed input energy:

$$\eta = \frac{\sum E_{out}}{\sum E_{in}} \tag{2.1}$$

In the above general formula of efficiency, energy can be in any form, including thermal, electrical and mechanical energy. Specifically to liquefaction processes, the most common use of liquefaction efficiency is in the form presented below (Marmolejo-Correa and Gundersen, 2012):

$$\eta = \frac{E_{liq} + x \sum W_{exp}}{E_{gas} + \sum W_{comp}} \tag{2.2}$$

In Equation 2.2, the energy of produced liquid and produced work from expanders are considered for energy outputs, while energy inputs consist of the energy of a gas phase at

the beginning and work needed for compression, which includes pumps and compressors. However, it is not possible to utilize produced work from expanders completely, thus x is a fraction of utilization. Furthermore, in certain cases, including BOG handling, it is hard to utilize it at all, and this case x is equal to 0. Usually, specific energy is used to compare different processes, to indicate the energy needed for a given amount of product. The main goal of the process is to consume the least possible amount of energy for a given amount of product; the best processes have the lowest specific energy. Specific energy is defined as the ratio between consumed energy and mass flow of the product at the outlet, in the case of LNG and hydrogen, these are the liquid products at the end:

$$e = \frac{E_{cons}}{\dot{m}_{out}} \tag{2.3}$$

All energies forms are the sum of exergy Ex and anergy A, where exergy represents maximum useful work, while anergy represents the part of the energy which cannot be converted at all:

$$E = Ex + An \tag{2.4}$$

In general, there are three types of energy involved in a conversion. First, some energies can be converted to any other form of energy without any limitations, and these energies include mechanical work, electrical energy, etc. In these cases, the amount of anergy equals zero, and all energy consists of exergy. The second type of energy can be partially converted, and energy consists of both exergy and anergy, for example, heat. The third type is the energy that cannot be converted at all and consists just of anergy. A typical example is the internal energy of ambient.

According to the first law of thermodynamics, all processes have a constant sum of exergy and anergy. However, according to the second law of thermodynamics, in every ideal and reversible process exergy stays constant, while for every real and irreversible process at least part of exergy is converted into anergy (Rant, 2001).

For any refrigeration or cryogenic liquefaction cycle, exergy efficiency is defined as a ratio between minimum specific energy required for a reversible process and consumed specific energy (Marmolejo-Correa and Gundersen, 2012):

$$\psi = \frac{e_{min}}{e_{real}} \tag{2.5}$$

Minimum specific energy for refrigeration is derived from the second law of thermodynamics, and it is defined as the exergy change between the state 1, usually gas phase, and the state 2, liquid phase at certain pressure:

$$e_{min} = \Delta ex = h_2 - h_1 - T_{amb}(s_2 - s_1) = SEC \tag{2.6}$$

To analyze the process, it is also very important to determine the exergy efficiencies of the main process equipment, such as compressors, heat exchangers, valves, turbines, and similar. Therefore, it is important to define the exergy efficiencies of these components and consequently their irreversibilities. These equations are presented in the last part of this chapter.

2.2 Liquefied natural gas

Knowledge and experiences from liquefied natural gas is an important source to develop new concepts for liquid hydrogen transportation. Both LNG and LH_2 offer better economic solutions than pipeline gas when the gas market is located far away from the source (Yang and Ogden, 2007). Furthermore, both of these fuels offer flexibility to the sellers and buyers, which is in the case of pipelines limited to the existing network.

Natural gas liquefaction is done by cooling to the temperature around $-162\,°\mathrm{C}$, which is significantly higher than hydrogen liquefaction temperature at ambient pressure equal to $1013.25\,\mathrm{mbar}$ and has an expansion ratio, which is a ratio between the normal volume of the gas phase and liquid phase of the same mass, around 600 (Vaudolon, 2000). All process chain to make LNG is very complex, but relevant for our thesis is just a part related to liquefaction of natural gas and handling of boil-off gas during transportation and storage. LNG is colorless cryogenic liquid with a density range from $430\,\mathrm{kg\,m^{-3}}$ to $520\,\mathrm{kg\,m^{-3}}$ (Vaudolon, 2000), and it shares many cryogenic properties with liquid hydrogen. The main problem of all cryogenic liquids is the evaporation of LNG due to imperfect insulation, which leads to heat leaks into a reservoir and consequent pressure increase. To release the pressure, it is necessary to release boil-off gas from the reservoir. As a result of methane emissions concerning BOG venting, regarding safety for personnel and equipment and energy losses for LNG and LH_2, it is necessary to handle BOG. Knowledge from the LNG industry about BOG handling could help develop appropriate technology also in the case of LH_2.

2.2.1 Liquefaction processes for liquefied natural gas

There are several ways how to liquefy NG, but only the main processes will be described here. In 2018, the largest part of existing capacity represents Air products process, the most common liquefaction process with $41\,\%$ of the market share is Air product propane pre-cooled mixed refrigerant process (UNION, 2019). The other important alternatives are ConocoPhillips optimized cascade process, Air Products propane precooled single mixed refrigerant, AP-X also from Air Products, where refrigerants are either nitrogen or methane, and Linde mixed fluid cascade process. Natural gas is a mixture of different hydrocarbons and other gases, which means that it has a gliding cooling curve. Intuitively, this means that a good boiling refrigerant mixture has a heating curve with a changing gradient, which in theory leads to a closer gap between the hot and cold composite curves. On the other side, gas refrigerants have less changing gradient and the gap is in theory larger, which results in larger entropy generation and consequently decreasing efficiency. A cascade process is characterized by several multi-stage pure or mixed refrigerant cycles and heat is absorbed in distinct temperature levels. The idea is to follow closely the cooling curve by splitting it into several parts and using different refrigerants at each one. The goal is to try to find the best refrigerant at each level and closing the gap.

One of the best examples of the cascade process for LNG is the ConocoPhillips Optimized cascade process with aluminum heat exchangers. In this case, three pure refrigerants are

propane, ethylene, or IUPAC name ethene and methane. Their properties are easily determined, which ensures smooth operation. Optimization ensures a closed approach between NG stream and refrigerant streams, and refrigerants with good heat integration properties lead to high efficiency. Furthermore, it is worth noticing that this process possesses high flexibility and availability because each refrigerant stream can be controlled separately. The main problem with this process is that it has a high capital cost due to a large number of process equipment (Fahmy et al., 2016a), (ConocoPhillips, 2013).

Air Products propane precooling and mixed refrigerant is the most widely used process for LNG plants. It consists of propane precooling in several stages using kettle type evaporators. Liquefaction and subcooling are done with the mixed refrigerant liquefaction cycle, where a mixture of propane, ethane, methane, and nitrogen is used. In this case, coil-wound heat exchangers are used, and these heat exchangers have been constantly improving in terms of size. It possesses high efficiency due to a good fit of composite curves and technology is well established. It is also believed to be the most cost-effective and reliable process for base-load operation (Fahmy et al., 2016b), (Airproducts, 2013).

The AP-X process was developed to increase train capacity. In comparison to AP-C_3MR, subcooling is done with the third N_2 expander cycle. The main advantage is that the nitrogen cycle ensures smaller duty on propane and mixed refrigerant cycles, decreasing flow rates of both, reducing the size of the equipment. This means that this process has higher train capacity and it has high efficiency and low production cost. However, the main problem is that scaling up the economy is worse than for the AP-C_3MR process, due to continuing size improvements of coil-wound heat exchangers (Pearsall and Schmidt, 2012), (Airproducts, 2013).

Dual mixed refrigerants use two separate mixed refrigerant cycle for subcooling, where this is usually a mixture of ethane and propane and another mixed refrigerant for liquefaction and subcooling, and it is offered by both Air Products and Royal Dutch Shell PLC. Recently, the DMR process gained momentum, because, in comparison to propane pre-cooled mixed refrigerant process, its advantages are lower specific energy consumption, larger train capacity, and less flammable refrigerant. However, this technology has been only implemented into few plants and there are still some challenges related to the complexity of the process. In general, it has similar efficiency to AP-C_3MR in tropical climates, but it is more efficient in colder climates (Khan et al., 2016), (Vikse et al., 2018).

Linde and Equinor, at the time Statoil, developed the Mixed Fluid Cascade cycle, where three different mixed refrigerants are used for precooling, liquefaction and subcooling. The first cycle uses plate-fin heat exchangers, and liquefaction and subcooling use coil-wound heat exchangers. Precooling mixed refrigerant varies depending on ambient temperature, which can ensure the closest gap between the feed and the refrigerant at different ambient conditions. Higher efficiency than the cascade process is the main advantage. However, at the start, there were plenty of problems with startup and operation (Ding et al., 2017), (Linde, 2019a).

The single mixed refrigerant process has just one multi-component refrigerant for precooling, liquefaction and subcooling. This makes a simple and flexible process with lower capital costs. However, the power consumption is higher and the overall efficiency is lower in comparison to other processes, thus it is mostly used for small scale LNG and offshore applications (Moein et al., 2015).

Another option is to use a single-phase gas as the refrigerant. In the LNG industry, this is most often nitrogen (N_2), but it can also use methane or mixture of methane and nitrogen and are generally used for small-scale or offshore LNG plants, BOG reliquefaction on board of LNG ships, trucks and similar. The simplest form of this process is usually a reversed Brayton cycle with just one expander and low efficiency. The process can be improved by using a separate precooling process and few expander stages, usually two or three. An alternative is to use feed gas as a refrigerant, which prevents problems with storage and import of additional refrigerant. AP-C_1 process can deliver natural gas at low or high pressure for the pipeline or as LNG. It can be also used to reliquefy BOG.

2.2.2 LNG boil-off gas handling

In general, most of the reliquefaction processes for BOG are derived from the reversed Brayton process, potentially sometimes Claude process. These processes in the LNG industry need to be simple to be economically viable, and this is most likely the case also for liquid hydrogen. For LNG, usually, the boil-off rate (BOR), which represents the amount of boil-off gas per stored volume in a given time, is between $0.1\,\%\,\mathrm{d}^{-1}$ to $0.8\,\%\,\mathrm{d}^{-1}$, mostly depending on the tank insulation, shape and size, ambient conditions and some other factors (Jang et al., 2011), (Romero et al., 2012).

Receiving terminals

At the receiving terminals, the best option is usually just to compress BOG to the pressure of export gas, or use it to generate heat and power. However, if there is no potential use for BOG, the best way is to reliquefy it. In the past, it was common to use a flare for BOG instead, but regulations do not allow it anymore due to potential methane emissions, which has a strong impact on the environment.

The main options to reliquefy BOG for larger capacity terminals with more than $1\,\mathrm{tonne}$ are usually based on the nitrogen refrigeration cycle due to simplicity and low maintenance, easy design, low investment cost and similar. A condenser operates at around $-161\,^{\circ}\mathrm{C}$ and pressures from $3\,\mathrm{bar}$ to $10\,\mathrm{bar}$. Conventionally, this has been done in the packed column, where BOG is a continuous phase. However, a better alternative in terms of size, cost, and weight is the static mixer (Liquide, 2017).

For smaller capacities, the best options are reliquefaction using a turbo-Brayton cycle or technology, where liquid nitrogen is stored at the lower temperature than LNG in the additional reservoir on site and then used in a heat exchanger to cool down and reliquefy LNG BOG (Liquide, 2017).

LNG Ships

Small size LNG carriers and LNG bunker vessels are equipped with cylindrical tanks, and they usually use N_2 reverse Brayton reliquefaction process. These smaller LNG carriers usually cannot use LNG in the engine, so the part of the equipment is also the gas combustion unit (GCU). GCU unit works as a kind of flare and it is simply used to manage boil-off gas. For smaller carriers, it is also possible to use the Turbo-Brayton cycle to subcool LNG and mix it with BOG. Consequently, heat and mass transfer cause absorption of BOG into LNG, thus liquefying it (Lee, 2017).

For larger tankers equipped with membrane tanks, there are two main alternatives. Some of the ships cannot use LNG in the main engines, so the solutions for BOG handling are similar to smaller ones. This means that they are equipped with a reliquefaction process and GCU. On the other hand, some of the LNG tankers can use LNG as a fuel in the main engines. Most of the existing LNG tankers are equipped with the MAN 2-stroke gas engine, which uses LNG high duty pumps to give pressure around $300\,\mathrm{bar}$ (solutions MAN, 2020). Furthermore, Burckhardt compression AG developed high-pressure compressors for BOG (Burckhardt, 2019). However, new LNG tankers usually prefer to use the WinGD engine, which uses a 2-stroke low-pressure engine with gas inlet pressure at $16\,\mathrm{bar}$, and in this case, BOG compression is not so consuming (Parker, 2019). In Japan, some LNG carriers use a steam boiler with a steam turbine as the main propulsion, but this solution is not popular in other countries due to more complex operation, which requires competent operators and they are hard to find. Otherwise, these tankers are also equipped with N_2 reverse Brayton liquefaction process and GCU (Fernandez et al., 2017).

Other ships, which use LNG as a fuel for the main engine, such as cruise ships, container vessels and similar, are usually equipped with LNG storage tanks and LNG pumping system to the main engine. Most of these ships are not equipped with reliquefaction processes, but they have GCU. At the moment, intensive research and development are focused on trying to improve the handling of the boil-off gas on ships (Kim et al., 2019).

LNG Trucks

For LNG trucks, there were some proposals to use different methods to liquefy or use BOG, instead of venting it once the certain pressure was reached. This was a big problem when a truck has not been in operation for some time and a significant amount of BOG was generated in the tank, resulting in high pressure. In this case, the pressure safety valve would open and release BOG, due to safety. In this case, GHG emissions are significant, because global warming potential of methane is 34, which means that emissions of $1\,\mathrm{kg}$ of methane is equal to $34\,\mathrm{kg}$ of CO_2 (Myhre et al., 2013).

Most of the studies have been more focused on reducing BOG, rather than handling it. However, main ideas for handling BOG was related to fueling stations for LNG, where BOG inside truck reservoirs would be transported from trucks to the stations. There, BOG could be treated in several different ways depending on the initial design, such as injecting BOG into the gas grid if the station is connected to it, cogeneration of heat and power if

there is sufficient demand or compressing BOG, and using it as compressed natural gas if there is a part of the station, which offers also CNG for other vehicles (Leclercq and Desrumaux, 2018).

Furthermore, there have not been many studies that focused on the treatment of BOG during the voyage. Even fewer truck manufacturers decided to implement any solutions related to BOG. However, this might change shortly with the implementation of new rules in the European Union. These solutions include using gas burner for BOG to generate heat which can be used to heat an engine coolant or catalysts, use BOG to run an engine or solid oxide fuel cells to generate heat and electricity, or compressing BOG, cooling it to the ambient temperature and then expanding, thus liquefying it (Gunnarsson and Heland, 2015).

2.3 Liquid hydrogen

Hydrogen is the most abundant element in the universe and it represents around $90\,\%$ of atoms. Furthermore, hydrogen and helium were first elements to form in our universe, and stars at the beginning consists mainly of hydrogen plasma. Hydrogen is also the lightest element in the periodic system, and it is colorless, odorless, tasteless, non-toxic, and highly flammable gas at the atmospheric conditions. Hydrogen exists in nature in two stable isotopes, protium and deuterium, and one unstable isotope called radioactive tritium. However, most of the existing hydrogen is protium and also hydrogen isotopes with higher numbers of neutrons have been synthesized. At the standard conditions, atomic hydrogen is extremely rare and it usually exists in molecule form as H_2. However, because it can easily form covalent compounds with most non-metal elements, on Earth it is mostly found in water or organic compounds, thus it needs to be converted from these materials. Historically, most of the hydrogen has been produced with steam reforming of natural gas. However, in the last years' other means of production have become competitive; for example water electrolysis, auto-thermal reforming of natural gas, low-temperature oxidation of coal, and similar. In general, there are four different types of "hydrogen"; brown hydrogen, which is produced from fossil fuels such as coal; grey hydrogen, which is produced from natural gas; blue hydrogen, which is produced from natural gas with the implementation of CCS (carbon capture storage); and green hydrogen, which is produced from renewable electricity through water electrolysis (IRENA, 2019).

In the past, most of the hydrogen was used in refineries for hydrocracking of hydrocarbons, ammonia synthesis, or the Haber-Bosch process, where ammonia for fertilizers is produced from nitrogen and hydrogen, and also the production of methanol with synthesis gas (a mixture of H_2 and CO). Recently, hydrogen has gained importance as a transportation fuel mainly due to the option to be used in fuel cells, where hydrogen reacts with atmospheric oxygen to form water, simultaneously releasing electric and heat energy. Different researchers and companies started developing also hydrogen gas turbines and hydrogen internal combustion engines, which are modified petrol engines as alternative propulsion systems. Furthermore, hydrogen seems like one of the most promising

solutions to store a high amount of renewable energy to balance the production and consumption of electricity in the future grids connected to renewable energy sources. Wind and solar energy production cannot balance grid consumption, so humans must develop an efficient way to ensure the flexibility of future electricity grids. One of the most popular public solutions would be batteries, but their very low energy density makes them not suitable for large amounts of energy, and this renders hydrogen a better alternative. There are several alternatives to store hydrogen. The main alternatives are compressed, liquid and cryo-compressed hydrogen, chemical storage, such as hydrides, ammonia and so on, underground storage in depleted gas and oil fields, caverns, salt domes and similar; and the last, but not the least, the power to gas, where it can be injected into gas pipelines as hydrogen, SNG or biomethane (IRENA, 2019).

Liquid hydrogen has been used as rocket fuel for several years because from all known rocket propellants it possesses the highest specific impulse, which is a measure of how effectively an engine uses fuel. In the future, LH_2 will most likely be used as a fuel for heavy-duty vehicles (trucks, buses and similar), trains, ships (ferries, cruise ships, cargo ships and similar). Furthermore, when compared to compressed hydrogen, storing hydrogen as a cryogenic liquid is beneficial for several different reasons. First, it has higher energy density, because the density of liquid hydrogen at atmospheric pressure and temperature of $20\,\mathrm{K}$ ($-253.15\,°\mathrm{C}$) is around $70.8\,\mathrm{kg/m^3}$, while hydrogen as a gas has density around $0.09\,\mathrm{kg/m^3}$ at STP (p = $1013.25\,\mathrm{mbar}$, T = $0\,°\mathrm{C}$) and density of $40\,\mathrm{kg/m^3}$ at pressure $700\,\mathrm{bar}$ and temperature $15\,°\mathrm{C}$ (NCE, 2016). This means that LH_2 is cost-efficient for transportation of large volumes over long distances (Yang and Ogden, 2007). Another important advantage is hydrogen purity, required by ISO 14687-2 standard, which states that hydrogen purity must be more than $99.97\,\%$ (Bacquart et al., 2018), and in the case of LH_2 all impurities are frozen during liquefaction ensuring enough purity. It is also used in the high tech industry for the detection of fundamental particles and similar.

2.3.1 Liquefaction processes for liquid hydrogen

Sir James Dewar was the first who liquefied hydrogen. In 1898, he managed to liquefy hydrogen through the Joule-Thomson effect by precooling hydrogen compressed to $180\,\mathrm{bar}$ with liquid air hydrogen and then expanding it. The next year, he also managed to solidify hydrogen (Rowlinson, 2014). An important part of hydrogen liquefaction is that molecular hydrogen H_2 exists in two forms, depending on the spin direction of nuclei in both hydrogen atoms. If both spins of atoms are parallel (same direction), this results in higher rotational energy levels, and this form is called orthohydrogen. On the other hand, if both spins of atoms are anti-parallel (opposite direction) this means lower rotational energy levels, and this form is called parahydrogen. Equilibrium hydrogen is an equilibrium mixture of both spin isomers (Matthews et al., 2011). Normal hydrogen is represented by equilibrium composition at ambient conditions, with $75\,\%$ of orthohydrogen and $25\,\%$ of parahydrogen. At lower temperatures equilibrium composition consists mainly of parahydrogen, around $99.8\,\%$ at $20\,\mathrm{K}$, because it is a more stable form of hydrogen molecular form. The equilibrium composition is defined by Boltzmann distribution (Brun, 1997).

During the hydrogen liquefaction process, it is necessary to convert orthohydrogen to parahydrogen, because the equilibrium conversion reaction from ortho to para is highly exothermic, and it is larger than the heat of vaporization for liquid hydrogen in the tank. This results in large evaporation rates, in other words in high boil-off rates. However, the spontaneous conversion from ortho to para is very slow and it can take even several days (Ubaid et al., 2014).

Therefore, it is necessary to use catalysts to boost the conversion and these catalysts can be an iron oxide (Fe_2O_3), chromium oxides and nickel silicate (NiO_3Si) catalysts. The best option to do the conversion is during liquefaction. In the past, catalysts beds were placed between heat exchangers in a batch mode, but nowadays they are placed inside heat exchanger canals (Zhuzhgov et al., 2018). This is more efficient because the released heat is extracted continuously, while in the past it was extracted at the lower temperature, which means higher liquefaction work (McIntosh, 2015).

The minimum work for liquefaction of hydrogen from ambient (p= $3.27\,\mathrm{kW\,h\,kg^{-1}}$) is approximately $1.59\,\mathrm{kW\,h\,kg^{-1}}$ for cooling and $1.68\,\mathrm{kW\,h\,kg^{-1}}$ for liquefaction without ortho-para conversion and $3.92\,\mathrm{kW\,h\,kg^{-1}}$ ($2.24\,\mathrm{kW\,h\,kg^{-1}}$ for cooling) with the conversion. Nowadays, there are several different processes how to liquefy hydrogen. Most of them use hydrogen feed gas at pressure of $21\,\mathrm{bar}$, and this became standard for most of analyzed liquefaction cycles. However, there is a tendency to increase this pressure even further up to $80\,\mathrm{bar}$ (Ohlig and Decker, 2019).

At the industrial level, two processes are the most common. The first one is the helium reverse Brayton cycle presented in Figure 2.1, where helium is the refrigerant with LN_2 precooling. In this case, capital expenditures are lower because it is possible to use standardized equipment, especially the screw compressors with injected oil. However, the Brayton cycle has lower efficiency and high operational cost. The reported specific consumption is in the range from $12.3\,\mathrm{kWh/kg_{LH_2}}$ to $13.5\,\mathrm{kWh/kg_{LH_2}}$ (Ohlig and Decker, 2019). In this case, Mycom oil-filled compressors have efficiency in the range $50\,\%$ to $55\,\%$, while piston compressors for helium have efficiency in the range from $63\,\%$ to $67\,\%$ (Kuzmenko et al., 2004).

On the other side, the Claude cycle using hydrogen as a refrigerant with LN_2 precooling has higher efficiency (Bracha et al., 1994). This process is presented in Figure 2.2. The process has a lower operational cost, but capital expenditures are higher due to several reasons. The main reasons are related to H_2 refrigerant, where it is necessary to use non-standardized equipment, such as piston compressors for example, and also due to more strict safety measures, instrumentation and electrical equipment are more sophisticated and expensive as well. In this case, the reported specific energies are from $7.7\,\mathrm{kWh/kg_{LH_2}}$ to $12.7\,\mathrm{kWh/kg_{LH_2}}$ (Ohlig and Decker, 2019). The isothermal efficiency of hydrogen piston compressors at Linde Leuna plant is in the range $65\,\%$ to $70\,\%$, and the isentropic efficiency of a liquid expander is more than $85\,\%$. The resulting exergy efficiency reported in this article is $23.6\,\%$ (Berstad et al., 2010).

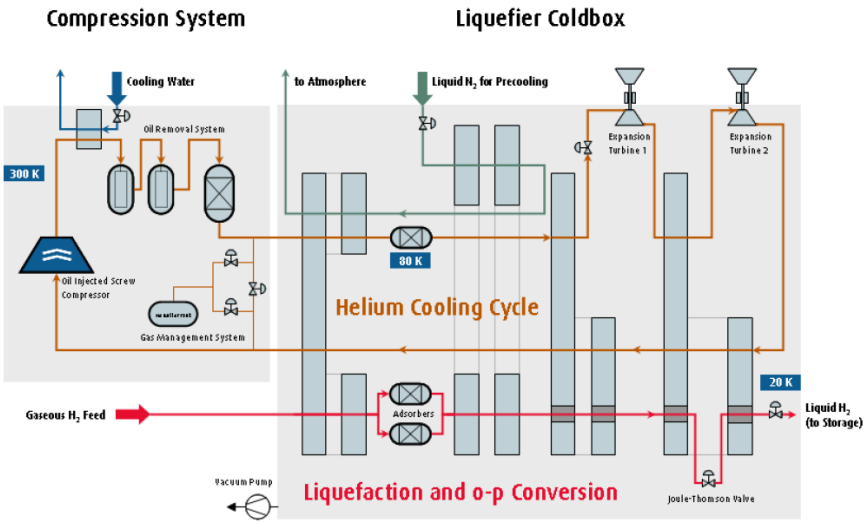

Figure 2.1: Process flow diagram of reverse Brayton cycle with helium refrigerant for liquefaction of hydrogen (Ohlig and Decker, 2019).

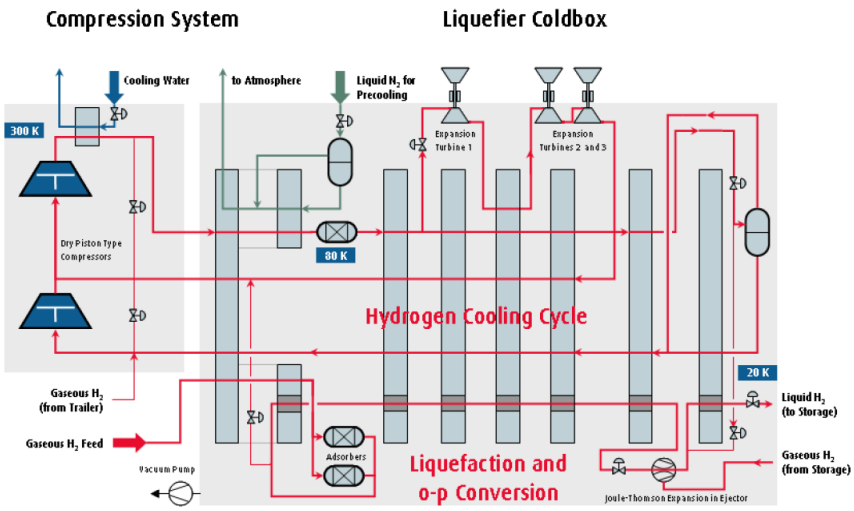

Figure 2.2: Process flow diagram of Claude cycle with hydrogen refrigerant for hydrogen liquefaction (Ohlig and Decker, 2019).

However, there are still challenges related to LH_2. The biggest challenge is how to reduce energy consumption. Therefore, several different processes have been developed with lower specific energy, and only the most interesting will be mentioned. This process presented in Figure 2.3 and developed for U.S. Department of Energy has four He refrigeration cycles, and in this case the specific energy consumption was between $7.4\,\mathrm{kWh/kg_{LH_2}}$

to $9.7\,\mathrm{kWh/kg_{LH_2}}$, or $30\,\%$ to $44\,\%$ exergy efficiency. In this case, the hydrogen compressor efficiency for the pilot was assumed $60\,\%$ and for helium, compressors $65\,\%$, while for the large scale hydrogen compressor efficiency and helium compressors efficiency were assumed $80\,\%$. The liquid expander for hydrogen was assumed $90\,\%$ and helium expanders were in $60\,\%$ to $75\,\%$ for the pilot and in range $83\,\%$ to $86\,\%$ for large scale liquefaction plant, $50\,\mathrm{t\,d^{-1}}$ (Shimko et al., 2008).

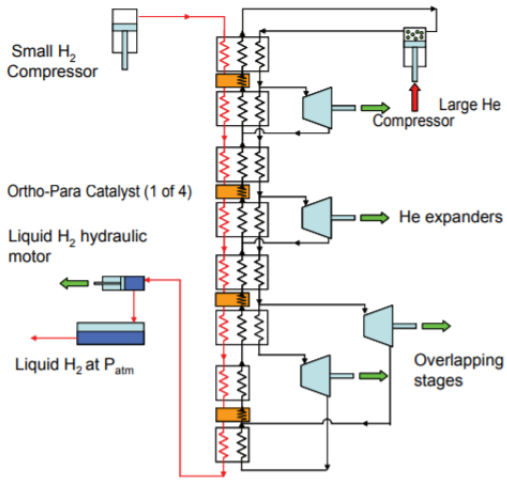

Figure 2.3: Process flow diagram for hydrogen liquefaction with four helium cycles (Shimko et al., 2008).

Another process uses four recuperative He Joule-Brayton cycles as presented in Figure 2.4, and in this case specific energy is predicted around $5.5\,\mathrm{kWh/kg_{LH_2}}$ and exergy efficiency of $45\,\%$. In this case, the liquefaction capacity was $10\,\mathrm{kg\,d^{-1}}$, polytropic efficiency of helium compressors was assumed to be $92\,\%$, polytropic efficiencies of helium turbines was in $88\,\%$ to $93\,\%$, while hydrogen turbine had $85\,\%$ efficiency (Valenti and Macchi, 2008).

Furthermore, in Figure 2.5 the process with mixture of different hydrocarbons, nitrogen and hydrogen as refrigerants and four helium refrigeration cycles resulted in SEC of $5.35\,\mathrm{kWh/kg_{LH_2}}$ and exergy efficiency of $54\,\%$. In this case, the capacity was $50\,\mathrm{t\,d^{-1}}$, while compressors and turbines isentropic efficiency were $80\,\%$ (Krasae-in et al., 2010).

Another interesting process employs two separate MR, the first one is a mixture of hydrocarbons, neon, and nitrogen, whereas the second is ”Nelium” refrigerant was introduced as a mixture of helium and neon. The process is presented in Figure 2.6. In this case SEC, is between $6.15\,\mathrm{kWh/kg_{LH_2}}$ to $6.48\,\mathrm{kWh/kg_{LH_2}}$ for mass flow of hydrogen feed at $1\,\mathrm{kg\,s^{-1}}$. The isentropic efficiency of hydrogen feed and He/Ne compressors is assumed $85\,\%$, while the efficiencies of He/Ne turbines is $90\,\%$ and the efficiencies of the liquid expanders for both hydrogen and He/Ne mixtures is $85\,\%$ (Berstad et al., 2010).

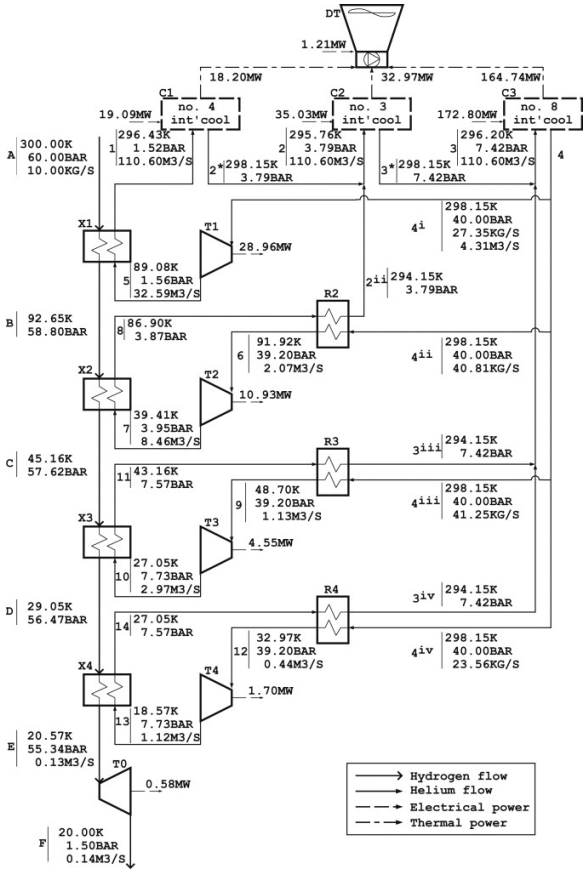

Figure 2.4: Process flow diagram for hydrogen liquefaction with four helium Joule-Brayton cycles (Valenti and Macchi, 2008).

An additional process with very low reported SEC used two separate MR cycles presented in Figure 2.7. The first MR cycle is composed of different hydrocarbons and the second one is the mixture of neon, helium, and hydrogen. The SEC is reported $4.36\,\mathrm{kWh/kg_{LH_2}}$ and exergy efficiency of $55.5\,\%$. In this case, the adiabatic efficiency of the compressors is $90\,\%$ and the expander adiabatic efficiency is $85\,\%$. Furthermore, compared to other studies, in this case, the pressure drops in all heat exchangers were neglected (Sadaghiani and Mehrpooya, 2017). In a different study that combined the previous process with an organic Rankine cycle and an absorption refrigeration system, the SEC of $4.02\,\mathrm{kWh/kg_{LH_2}}$ and exergy efficiency of $73.5\,\%$ was obtained. In this case, the adiabatic efficiencies of the compressors and the pumps are $90\,\%$ and the expander adiabatic efficiency is $85\,\%$ and there is no pressure drop (Ghorbani et al., 2019).

Recently, as part of the Hyper project, a new liquefaction cycle was developed. In this case, mixed refrigerant "PRICO" cycle is used to cool hydrogen to $114\,\mathrm{K}$ and then the hydrogen

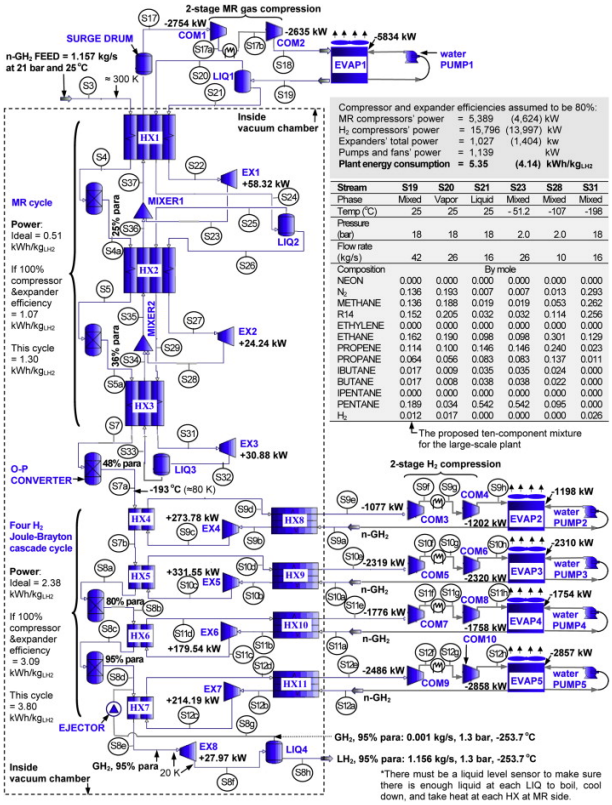

Stream	S19	S20	S21	S23	S28	S31
Phase	Mixed	Vapor	Liquid	Mixed	Mixed	Mixed
Temp (°C)	25	25	25	- 51.2	-107	-198
Pressure (bar)	18	18	18	2.0	2.0	18
Flow rate (kg/s)	42	26	16	26	10	16
Composition	By mole					
NEON	0.000	0.000	0.000	0.000	0.000	0.000
N_2	0.136	0.193	0.007	0.007	0.013	0.293
METHANE	0.136	0.188	0.019	0.019	0.053	0.262
R14	0.152	0.205	0.032	0.032	0.114	0.256
ETHYLENE	0.000	0.000	0.000	0.000	0.000	0.000
ETHANE	0.162	0.190	0.098	0.098	0.301	0.129
PROPENE	0.114	0.100	0.146	0.146	0.240	0.023
PROPANE	0.064	0.056	0.083	0.083	0.137	0.011
IBUTANE	0.017	0.009	0.035	0.035	0.024	0.000
BUTANE	0.017	0.008	0.038	0.038	0.022	0.000
IPENTANE	0.000	0.000	0.000	0.000	0.000	0.000
PENTANE	0.189	0.034	0.542	0.542	0.095	0.000
H_2	0.012	0.017	0.000	0.000	0.000	0.026

Figure 2.5: Process flow diagram for hydrogen liquefaction with mixture of hydrocarbons, nitrogen and hydrogen (Krasae-in et al., 2010).

Claude process is used to cool down hydrogen to 30 K. In this liquefaction also boil-off gas recompression is done in the ejector. The process flow diagram is presented in Figure 2.8. The specific energy consumption for this process was $7.05\,\mathrm{kW\,h\,kg^{-1}}$ and exergy efficiency of $39.1\,\%$ for liquefaction capacity rate of $125\,\mathrm{t\,d^{-1}}$ without turbine expander energy utilization. If boil-off gas reliquefaction rate is included in the calculation then specific energy consumption is $6.67\,\mathrm{kW\,h\,kg^{-1}}$ (Berstad et al., 2019).

Some other liquefaction alternatives have also been developed. For example, an active magnetic refrigerator has the potential to have very low specific energy consumption, be environmentally friendly, and cost-effective. However, this SEC was obtained by simulations or experimentally for a very low cooling capacity of $25.3\,\mathrm{W}$, which are not suitable for industrial hydrogen liquefaction (Numazawa et al., 2014). This might change in the future, but at the moment magnetic liquefaction is not a competitive technology. Also, there were few successful hydrogen liquefaction using different cryocoolers, but it has been done just for very small volumes as well, so it does not seem like a viable solution at the moment. For example, in one of the studies the science group developed

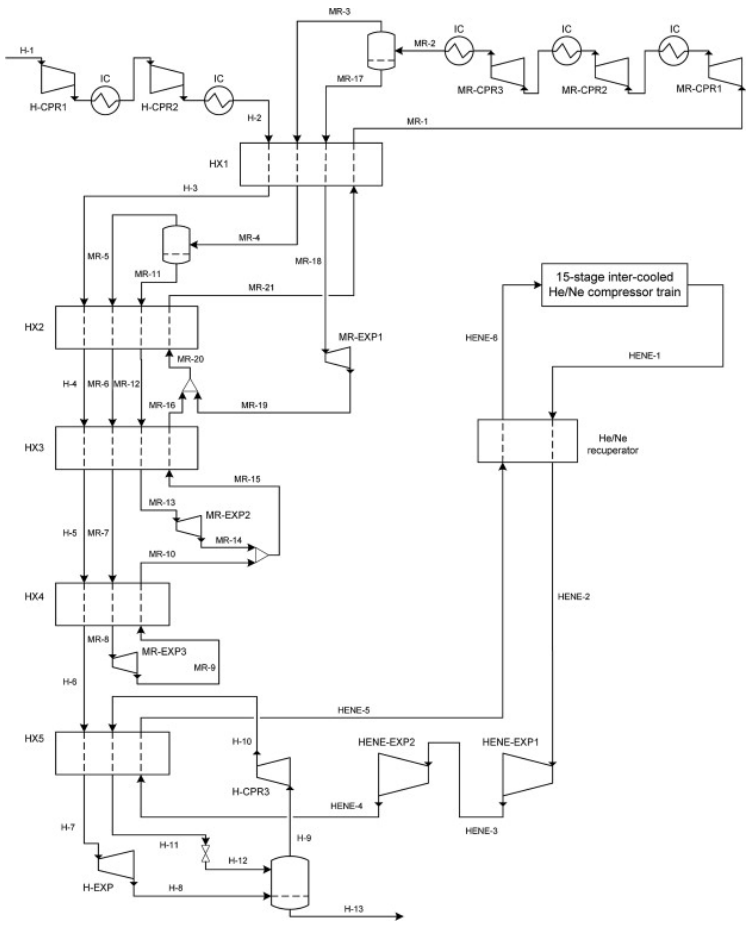

Figure 2.6: Process flow diagram for hydrogen liquefaction with two mixed refrigerants; mixture of hydrocarbons and nelium (Berstad et al., 2010).

Gifford-McMahon cryocooler for liquefaction of hydrogen, but with liquefaction rate of only $19.9\,\mathrm{L\,d^{-1}}$ (Nakano et al., 2010). Recently, Stirling type pulse tube cryocooler for hydrogen liquefaction was developed. However, it has cooling capacity of only $1.74\,\mathrm{W}$ at temperature $25\,\mathrm{K}$ (Huang et al., 2020). Furthermore, one of the studies combined LNG regasification and hydrogen liquefaction, and in this case, LNG first precools hydrogen feed to the temperature of $135\,\mathrm{K}$, then nitrogen cycle is used to reduce temperature to $80\,\mathrm{K}$ and hydrogen refrigeration loop is used to reach temperature of $22.7\,\mathrm{K}$. The reported specific energy consumptions were $3.15\,\mathrm{kWh/kg_{LH_2}}$ with significant amounts of LNG and $3.55\,\mathrm{kWh/kg_{LH_2}}$ with lower amounts of LNG. However, in this case, LNG production was not included in the results (Kuendig et al., 2008).

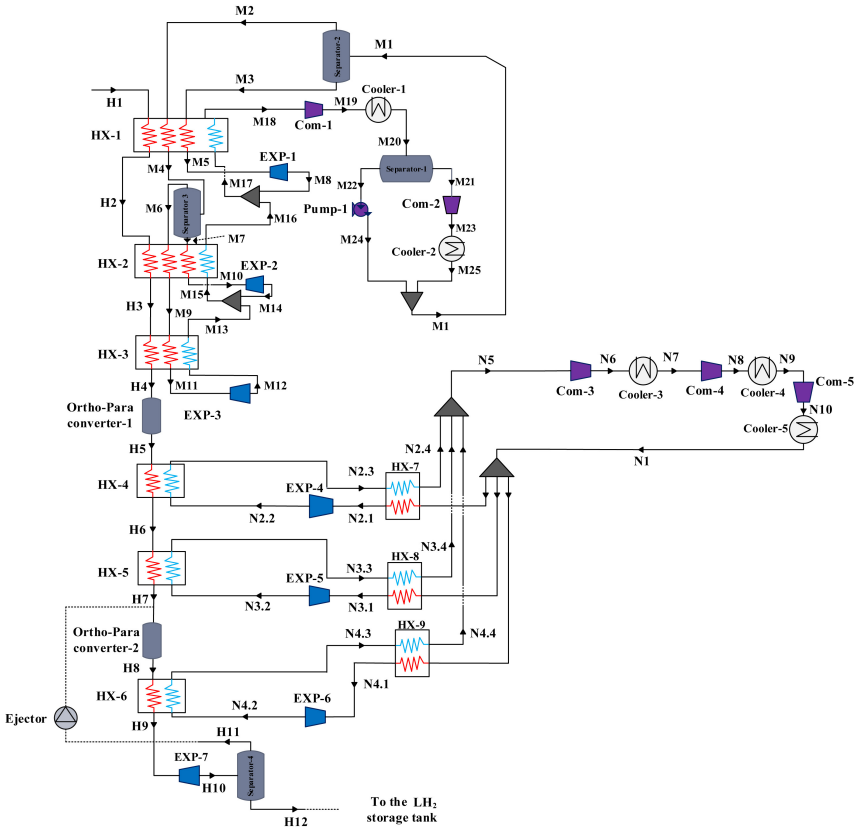

Figure 2.7: Process flow diagram for hydrogen liquefaction with two mixed refrigerants: mixture of hydrocarbons and mixture of neon, helium and hydrogen (Sadaghiani and Mehrpooya, 2017)

2.3.2 Liquid hydrogen boil-off gas handling

At the moment, there is not a lot of research dedicated to BOG in liquid hydrogen. Most of the relevant studies have been conducted by NASA as it is necessary to have zero boil-off storage to meet requirements for flights to outer space. One of the more interesting studies was related to zero boil-off gas methods, where Brayton cryocooler has been developed with a cooling capacity of 20 W at temperature 20 K. However, the main problem is that estimated heat leaks for infrastructure related to liquid hydrogen on Earth are significantly larger and it is necessary to develop much larger cryocoolers (Plachta et al., 2018).

On the other side, there were only a couple of other proposals. One of them included how to treat BOG for LH_2 carriers using LNG and H_2 as a fuel for propulsion and ancillary equipment. The process flow diagram of this process is presented in Figure 2.9 and in this case, only part of H_2 was reliquefied, while the other part was used as a fuel. The SEC was $3.3\,\mathrm{kWh/kg_{LH_2}}$ and exergy efficiency of $74.9\,\%$. In this case, the isentropic efficiencies of

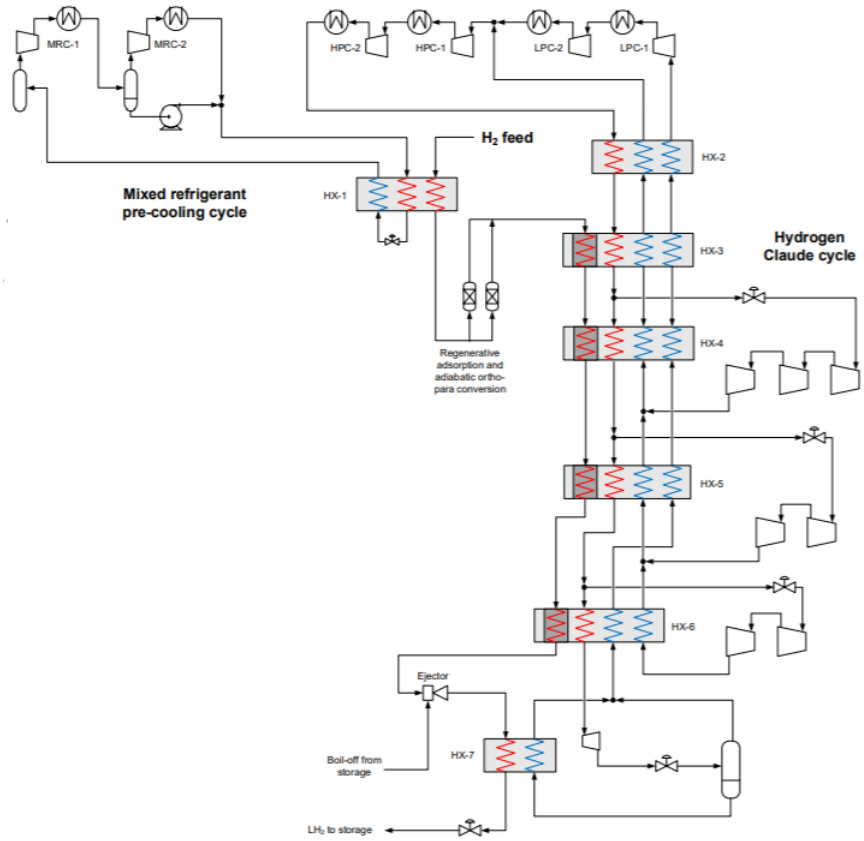

Figure 2.8: Process flow diagram for hydrogen liquefaction with mixed refrigeratn "PRICO" cycle and hydrogen Claude cycle (Berstad et al., 2019)

compressors and expanders were 85 % (Hyunyong et al., 2019).

A different alternative to treat boil-off gas called hydrogen reliquefier with Low-Pressure Extraction (LOPEX) was developed by the Linde group. In this case, cold boil-off gas with low pressure is heated up in the heat exchanger by cooling down part of the high-pressure boil-off gas. Then low-pressure BOG is separated into two streams, process and consumption. The process gas stream is first compressed and then cooled to ambient in an air cooler. Then it enters the same heat exchanger, where it exchanges heat with the cold gas from the tank reservoir. After that, there is an isenthalpic expansion in a Joule-Thomson valve to the reservoir pressure level. After the expansion, part of the gas is liquefied and is returned into the tank, while the gas-phase is returned into the process together with low-pressure hydrogen gas from the reservoir. The consumption hydrogen stream is used in fuel cells to give power to compressors. In other words: part of boil-off gas is used to reliquefy the rest of it. This process is very simple, produces higher

liquid fractions after the expansion due to a lower ratio between the refrigerant and cooling medium flow, does not require an additional energy source, if designed appropriately, and increases the overall efficiency (MWConsulting, 2007), (Linde, 2019b). One of the most important factors to consider is the price of hydrogen in comparison to electricity and natural gas. If the price of hydrogen is significantly higher than electricity and natural gas, it is probably better to reliquefy BOG and sell it as a fuel.

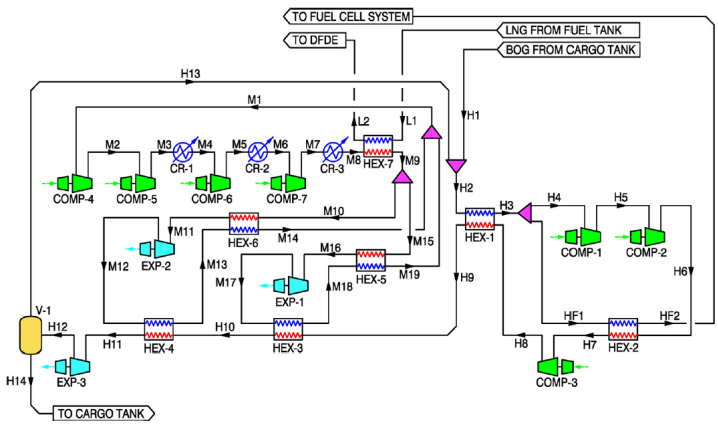

Figure 2.9: Process flow diagram for hydrogen liquefaction with mixture of hydrocarbons, nitrogen and hydrogen (Hyunyong et al., 2019)

2.3.3 Equipment for hydrogen liquefaction

Since one of the goals of this thesis is to design general concepts for reliquefying BOG for LH_2 and develop an approach on how to analyze and evaluate such concepts, it is important to analyze the state of the art of main equipment needed for these reliquefaction processes. These include compressors, heat exchangers, coolers, Joule-Thomson valves, and turbine expanders. Other equipment such as pumps, phase separators, pipelines, and more will not be analyzed within the scope of this thesis. Because of the LH_2 specifics described before in this chapter, also technologies involved need to be adequate.

Compressors

As seen from the review of hydrogen liquefaction processes, there is huge uncertainty regarding the efficiencies of compressors and turbines. In general, the most often used compressors in cryogenics are reciprocating or piston compressors, rotary screw compressors, and turbo compressors. At the moment in the case of hydrogen liquefaction, particularly electric driven piston compressors and rotary screw compressors are used (Ohlig and Decker, 2014), (McCoy and Douglass, 2014). Compressed fluid, compressor capacity, and compressor pressure ratio are the main parameters for selection. In general, screw and piston compressors are usually used for lower volume flows and higher total needed

compressor pressure ratios, while turbo compressors need to be used with higher volume flow rates (Grote and Feldhusen, 2014). The compressor energy consumption represents more than $90\,\%$ of total energy consumption for hydrogen liquefaction processes. The compressor efficiency has a significant impact on the exergy efficiency of the hydrogen liquefaction process. The most important factors defining the compressor efficiency are design, type of a compressor, and compressor capacity. Isentropic efficiencies for large compressors are about $65\,\%$ to $92\,\%$. The mechanical efficiency for a large compressor can be higher than $95\,\%$ (Cardella, 2018).

Oil-injected screw compressors are most common for helium compression in already built hydrogen liquefaction capacities below $3\,\mathrm{t\,d^{-1}}$(Ohlig and Decker, 2014). They possess rather low isentropic efficiency between $65\,\%$ to $75\,\%$ (Alekseev, 2015) and require a system to remove oil, but standardized compressors have quite low investment cost (CAPEX) and can achieve pressure ratios higher than 10 (Häring, 2007).

Reciprocating compressors use a piston to deliver gases at elevated pressure. They represent the state of the art technology for compression of feed and refrigerant gas hydrogen in cryogenics because they achieve high-pressure ratios even for very light gases such as hydrogen or helium. The main limitation of pressure ratio is the outlet temperature of the compressor, which should not exceed temperature around $420\,\mathrm{K}$ (Eifler et al., 2009). Large piston compressors can achieve isentropic efficiencies between $75\,\%$ to $92\,\%$ (Cardella et al., 2017b). For hydrogen compression, pressure ratio is usually between 2 to 3 (Grote and Feldhusen, 2014). Burckhardt Compression offers the largest outlet power at $40\,\mathrm{MW}$ (Cardella, 2018).

The main obstacle for the implementation of turbo compressors in hydrogen liquefaction processes is a very low-pressure ratio of compressor stages for substances with low molar mass, which is relevant for both hydrogen and helium. For example, it takes around 24 stages to compress hydrogen gas from $1\,\mathrm{bar}$ to $80\,\mathrm{bar}$. For this reason, the usage of mixture refrigerants with neon is considered to increase the molar mass of the refrigerant (Quack et al., 2015) (Skaugen et al., 2020). The efficiencies of these compressors are in the range $70\,\%$ to $88\,\%$ (Cardella et al., 2017a). Relatively high efficiencies, the lower operational cost in comparison to piston compressors, and small specific investment costs for common capacities make turbo compressors with integral gears a very promising solution for many cryogenics applications in the future (Grote and Feldhusen, 2014). However, at the moment they are not considered as a feasible option for hydrogen or helium compression, particularly for smaller capacities.

Heat exchangers

Counterflow plate-fin heat exchangers (PFHX) are most commonly used in the industry due to high surface area, achievable very low-temperature differences, low-pressure drops, and high compatibility between the streams (Häring, 2007). These heat exchangers are filled with catalysts due to necessary ortho-para hydrogen conversion (Skaugen et al., 2020). They are made of aluminum which has a thermal conductivity of $205\,\mathrm{W\,m^{-1}\,K}$ and

the pressure range is between $20\,\mathrm{bar}$ to $130\,\mathrm{bar}$. Exergy efficiency and design are strongly dependent on the size and the performance of heat exchangers in the liquefaction processes. Larger surface area and volume increase the efficiency of hydrogen liquefaction, but this also requires higher investments costs CAPEX. Therefore, manufacturing technology and transportation, available space, costs are important factors to consider when designing the heat exchangers (Cardella, 2018). In general, there are strong initiatives to try to reduce irreversibilities in the heat exchangers, because they result in higher exergy efficiency of the liquefaction process. Several studies have been conducted to reduce the exergy destruction in the heat exchangers (Wilhelmsen et al., 2018), (Skaugen et al., 2020).

An interesting alternative to PFXH is spiral-wound heat exchangers (SWHX), which are most often used in LNG liquefaction plants. However, plate-fin heat exchangers have preferred solutions because of the higher surface density, but there are some cases in which spiral-wound heat exchangers might be a better alternative (Skaugen et al., 2020).

Turbine expanders

Turbine expanders can be used to improve the process efficiency to use them instead of Joule-Thomson valves. In this case, the expansion in the turbine expander is polytropic and it is possible to remove more heat in comparison to the isenthalpic process in the Joule-Thomson valve (Niu et al., 2015). Turbine expanders are classified into two groups depending on the outlet phase of the product. The first alternative is dry expanders with the gas phase and the second one is a wet expander. The isentropic efficiencies of the expander are usually in the range of $70\,\%$ to $90\,\%$ (Bloch and Soares, 2001).

2.3.4 Irreversibilities and exergy efficiencies of process equipment

In this section, the equations for irreversibilities and exergy efficiencies of some process equipment will be presented. These are compressors, turbine expanders, heat exchangers, separators, and coolers. In all equations below, exergy flows of the stream are defined as followed (Thomas et al., 2011):

$$\dot{E}x_{flow} = (\dot{m}ex) = \dot{m}((h - h_{amb}) - T_{amb}(s - s_{amb})) \tag{2.7}$$

In the equation above, h_{amb} and s_{amb} represent specific enthalpy of the given material stream in ambient conditions. As seen from 2.10, the specific exergy ex increases when the temperature gets lower in the case of temperatures below ambient.

Compressors

Equations 2.8 and 2.9 are used to determine the exergy efficiency and exergy destruction of compressors (Hammad and Dincer, 2018), (Yuksel et al., 2017), (Sadaghiani and Mehrpooya, 2017).

$$\psi = \frac{\sum(\dot{m}ex)_{out} - \sum(\dot{m}ex)_{in}}{W_{comp}} \tag{2.8}$$

$$\dot{E}x_{dest} = \sum(\dot{m}ex)_{in} + W_{comp} - \sum(\dot{m}ex)_{out} \tag{2.9}$$

Turbine expanders

Equations 2.10 and 2.11 are used to determine the exergy efficiency and exergy destruction of turbine expanders (Yuksel et al., 2017), (Sadaghiani and Mehrpooya, 2017):

$$\psi = \frac{W_{turb}}{\sum(\dot{m}ex)_{in} - \sum(\dot{m}ex)_{out}} \tag{2.10}$$

$$\dot{E}x_{dest} = \sum(\dot{m}ex)_{in} - W_{exp} - \sum(\dot{m}ex)_{out} \tag{2.11}$$

Heat exchangers

Equations 2.12 and 2.13 are used to determine the exergy efficiency and exergy destruction of heat exchangers: (Yuksel et al., 2017), (Sadaghiani and Mehrpooya, 2017). In these equations, h represents the hot side, while c represents the cold side. In this case, fluids on the hot side increase their exergy and fluids on the cold side decrease their exergy as seen in Figure 2.10.

$$\psi = \frac{\sum(\dot{m}ex)_{out,h} - \sum(\dot{m}ex)_{in,h}}{\sum(\dot{m}ex)_{in,c} - \sum(\dot{m}ex)_{out,c}} \tag{2.12}$$

$$\dot{E}x_{dest} = \sum(\dot{m}ex)_{in} - \sum(\dot{m}ex)_{out} \tag{2.13}$$

Coolers and Joule-Thomson valves

For intercoolers, Joule-Thomson valves and aftercoolers the exergy efficiency and exergy destruction are defined in Equation 2.14 and Equation 2.15 (Yuksel et al., 2017), (Sadaghiani and Mehrpooya, 2017):

$$\psi = \frac{\sum(\dot{m}ex)_{out}}{\sum(\dot{m}ex)_{in}} \tag{2.14}$$

$$\dot{E}x_{dest} = \sum(\dot{m}ex)_{in} - \sum(\dot{m}ex)_{out} \tag{2.15}$$

2.3.5 Equation of states for simulation of hydrogen liquefaction processes

In general, the modified Benedict-Webb-Rubin equations of state are used for many simulations of processes with certain gases and helium and all hydrogen alternatives (normal hydrogen, parahydrogen, and orthohydrogen) are all part of this group. In this case, 32

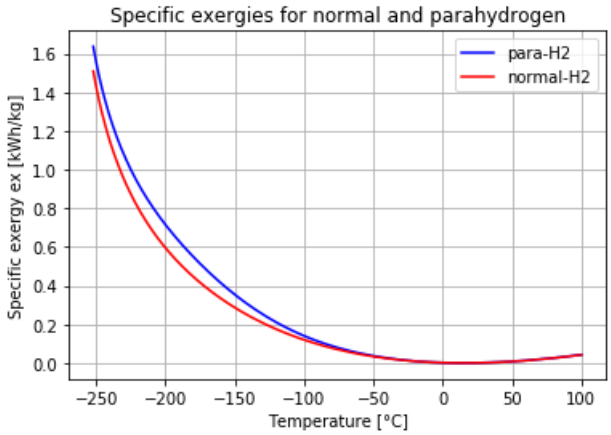

Figure 2.10: Specific exergy of normal and para hydrogen for different temperatures according to MBWR equations of state in Aspen HSYSY with ambient conditions at 15 °C and 1.013 bar

numerical parameters are modified to fit the empirical data (Kaviani et al., 2015), (Roder, 1975). The accuracy strongly depends on the availability of experimental data, and due to a large number of numerical parameters, these equations are rather complicated and time-consuming. In Aspen HYSYS help, they suggest using helium and hydrogen inside certain temperature and pressure ranges. In the last years, there have been few studies trying to improve these equations of state. The Helmholtz type of equations of state for ortho, para, and normal hydrogen were developed. They represent existing experimental data slightly better than MBWR, but they are even more time consuming (Leachman et al., 2009), (Leachman et al., 2017).

On the other side, in the last few years, there has been a strong focus on developing equations of states for different mixtures of hydrogen, helium, and neon. Soave-Redlich-Kwong and Peng–Robinson-Stryjek-Vera (PRSV) equations of state are most commonly used in the natural gas industry (Ashour et al., 2011), (Stryjek and Vera, 1986). Recently there was a study for equations of state regarding mixtures of natural gas, which also contain hydrogen and other gases, and it was concluded that PRSV and SRK-Twu equations of state fit the best experimental data in low-pressure regions (Zhang et al., 2020). In one of the more important studies, different equations of states were compared, and it was determined that Peng-Robinson equations give reasonable results and other equations of state were not much better for mixtures of helium and neon (Wilhelmsen et al., 2018). However, new sophisticated equations of state for mixtures of helium, neon, and hydrogen were developed, but they are too complex and time-consuming to use them for process simulation and optimization with normal personal computers (Aasen et al., 2020).

Chapter 3

Concepts for liquid hydrogen boil-off gas reliquefaction

In this chapter, the main concepts for reliquefaction of BOG are described. Based on the literature survey and research ideas, the focus of this research is on a limited number of concepts. The most promising concepts were chosen to be simulated in the Aspen HYSYS software. As explained in the previous chapters, heat inleak due to imperfect insulation causes evaporation of liquid. Evaporated gas needs to be handled to prevent a significant rise in pressure in reservoirs. It is expected that size of tank reservoirs for LH_2 will increase in the future, and then it will be especially important to handle the boil-off gas of storage tanks at receiving terminals, during voyages of LH_2 carriers, trucks, cruise ships, hydrogen filling stations and similar. The boil-off rate (BOR) is given as a percentage of the total stored volume of liquid per given time unit. Nowadays, BOR for LH_2 is between $0.1\,\%\,\mathrm{d}^{-1}$ to $0.3\,\%\,\mathrm{d}^{-1}$ (Ohlig and Decker, 2019), heavily depending on ambient conditions, insulation, size, shape, and design of storage tanks and some other factors.

There are several different reliquefaction processes, and what is the best option in each case depends on several different factors. These are quantity of BOG, prices of LH_2, available fuels, electricity, and industrial gases, requirements for export H_2 gas, requirements for electricity and heat energy, the complexity of these processes, operation of plants, vehicles and similar, capital and operation expenditures of these processes, and many more. In the scope of this thesis, the main target is to only develop and analyze BOG reliquefaction concepts, while comparing these reliquefaction processes with other alternatives. From several options, based on our previous work within the preliminary research, only the most promising solutions were included for analysis within this thesis.

All three selected boil-off gas reliquefaction processes use the same precooling process for hydrogen BOG precooling. In the scope of this thesis, precooling on the refrigerant

side will be neglected, because there are several options available and the best option depends on the availability of industrial gases, investment and operational costs, and many other factors as explained already before. To reduce the minimum theoretical liquefaction work of the studied processes, it is beneficial to compress BOG and precool it by using cold BOG from the tank in the first heat exchanger HX-1. Cold BOG from the reservoir is transferred to the heat exchanger where it is heated by the counterflow of the warm gas. Then it is compressed with intercooling in several stages. After the last compressor stage, it is cooled to the ambient temperature, in this case, water or air coolers can be used depending on the location, availability of water sources and other factors, and then fed back to the heat exchanger HX-1 where it is precooled with BOG from the tank. To reliquefy the full amount of hydrogen boil-off gas, it is necessary to have an additional refrigeration process. After that, there is an expansion in either a Joule-Thomson valve or a turbine expander.

In general, the Joule-Thomson valve is less efficient, but also less complex and cheaper, while the expander is more efficient but also more complex and more expensive. Furthermore, according to the Cryostar company, the market for pure hydrogen turbine expanders is very limited for larger expanders more than $100\,\mathrm{kW}$ and even more for the turbine liquid expanders, and in this sense the expander option seems more appropriate in the future if new technologies will become available on market. However, it is important to emphasize that at the moment several companies and research teams are trying to develop and hydrogen equipment and novel technologies have been emerging constantly. In this work, it will be discussed what is a better option to use for different boil-off gas processes, particularly in terms of energy consumption. Therefore, all processes will be simulated using both alternatives, the Joule-Thomson valve, and the liquid turbine expander, and then compared. Simplified process schemes are presented in Figures 3.1 and 3.2.

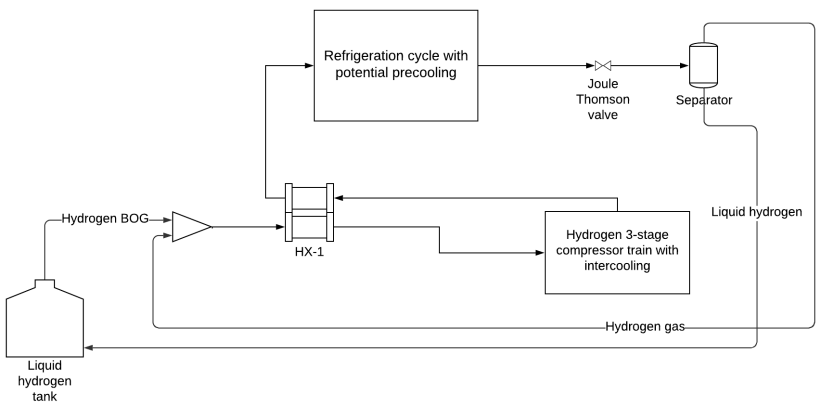

Figure 3.1: Simplified process diagram for reliquefaction of hydrogen boil-off gas with the Joule-Thomson Valve

In the following three subchapters, the designs of each process are presented and described.

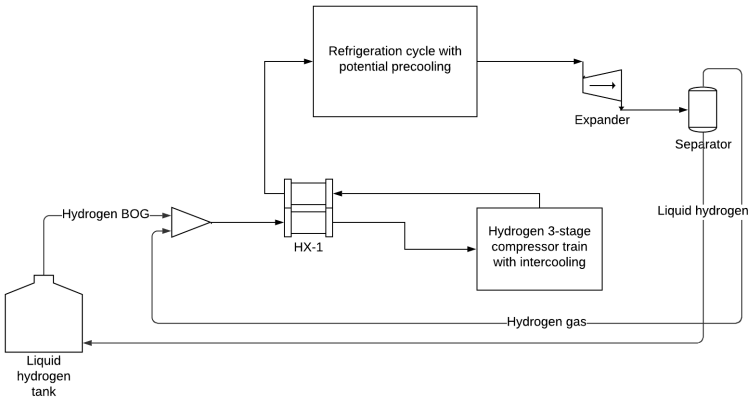

Figure 3.2: Simplified process diagram for reliquefaction of hydrogen boil-off gas with the liquid turbine expander

3.1 Helium reverse Brayton cycle

From the processes analyzed in the literature review part, the simplest is the helium reverse Brayton cycle. It is a very basic process with just one refrigeration cycle, but it can be upgraded by using several expanders, usually two or three, which increase its efficiency. In this case, it was decided to use two expanders.

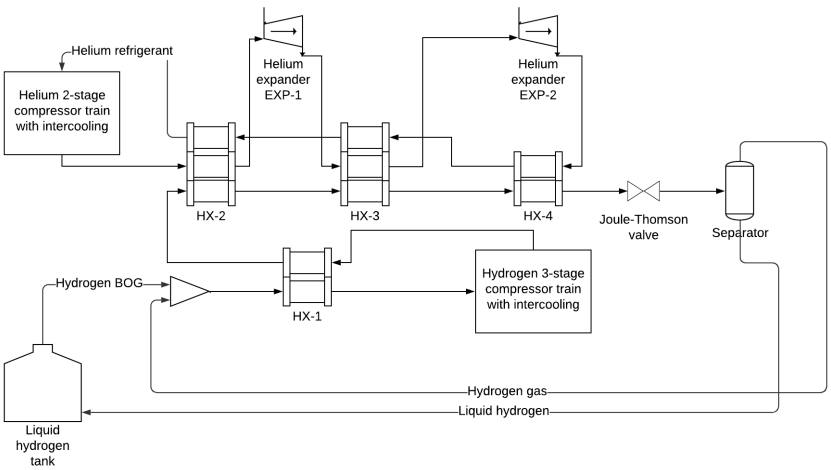

Figure 3.3: Simplified process diagram with the Joule-Thomson valve for helium reverse Brayton cycle with two helium turbine expanders

The reverse helium Brayton cycle is chosen because of its simplicity as a base case in our analysis, and its efficiency and other key performance indicators will be compared to the other two options. The scheme of the process with the Joule-Thomson valve is presented

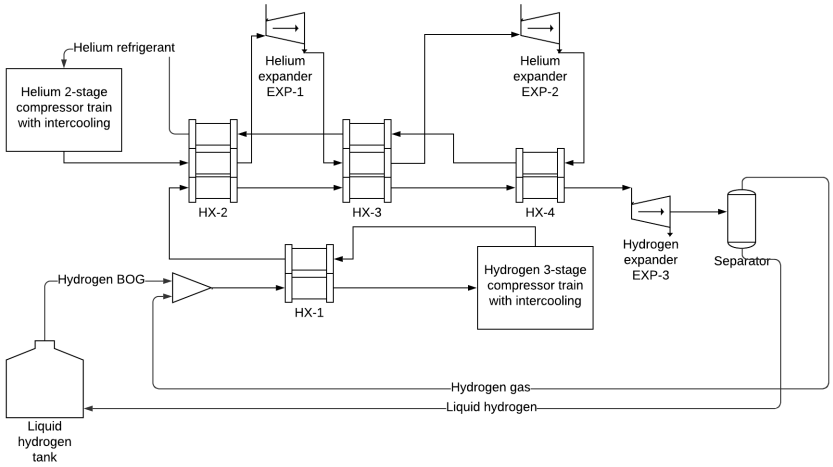

Figure 3.4: Simplified process diagram with the liquid turbine expander for helium reverse Brayton cycle with two helium turbine expanders

in Figure 3.3 and with the liquid turbine expander EXP-3 in Figure 3.4. To decrease the necessary work for liquefaction, the boil-off gas from a tank is initially compressed in a three-stage hydrogen compression train. In this case, hydrogen piston compressors are used. This is done first by heating the cool boil-off gas in a countercurrent heat exchanger HX-1, where heat is exchanged with the warmer compressed gas coming from the hydrogen compressor train. The simplified process flow diagram is presented in Figure 3.5.

Hydrogen compression can be done in several stages, depending on the desired outlet pressure. This means that between two separate compressor stages, there is an intercooler, where the compressed hydrogen gas is cooled with ambient air or cooling water from the environment. After the last compressor stage, compressed gas is cooled to the ambient temperature in an aftercooler. Setting the optimal outlet pressure is part of process optimization, but the pressure ratio should not be higher than 3 according to the literature review of existing hydrogen piston compressors. Afterward, the boil-off gas is compressed and send back to the same heat exchanger HX-1.

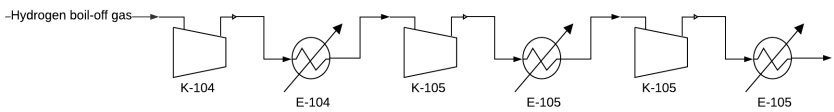

Figure 3.5: Hydrogen boil-off gas compression train with three hydrogen piston compressors and with two intermittent intercoolers and the aftercooler

When hydrogen is compressed to its goal outlet pressure, reverse helium Brayton cycle

with two helium turbine expanders is implemented to cool and liquefy hydrogen. To increase efficiency, two expanders are used instead of just one. At the beginning of the cycle, helium is compressed in the compressor train with two stages The simple process flow diagram is presented in Figure 3.6. The helium refrigerant is compressed in the oil-screw compressors which can obtain pressure ratios up to 10, much higher than piston or turbo compressors, and then cooled by ambient air or cooling water first in the intercooler and then in the aftercooler. The refrigerant then enters the first heat exchanger and it is cooled in the heat exchanger HX-2 together with the hydrogen stream seen in Figures 3.1 and 3.2. After the cooling, the refrigerant stream is then expended in the first expander EXP-1 and it enters the heat exchanger number HX-3, where it is further cooled down at the same time as hydrogen stream. Then helium enters the second expander before it reenters the heat exchanger HX-4 on the cold side, and the heat is transferred from hydrogen to helium. The hydrogen gas is then expanded. Expansion can be done either in the Joule-Thomson valve or in the expander EXP-3. Afterward, the two-phase flow enters the separator, then it follows two-phase hydrogen separation, where the gas phase is returned into the hydrogen reliquefaction process and liquid hydrogen is returned into the liquid hydrogen tank.

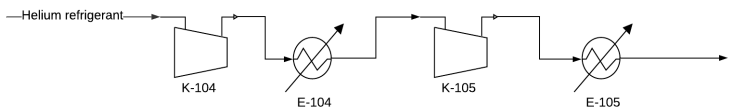

Figure 3.6: Helium compression train with two helium oil-screw compressors with the intermittent intercooler and the aftercooler

3.2 Hydrogen refrigeration cycle

As stated before, all studied processes have the same beginning with compression of hydrogen BOG as shown in Figures 3.1 and 3.2. Identical to the helium reverse Brayton process, the processes with the expander and with the Joule Thomson valve are presented and later simulated. Both alternative processes are presented in Figures 3.7 and 3.8.

First, the hydrogen boil-off gas is compressed in the same way as it is in the case of the helium reverse Brayton cycle. This is presented in Figure 3.5. Then the hydrogen refrigeration cycle is used to cool and reliquefy the hydrogen BOG. In this case, two hydrogen refrigerant streams exit the heat exchanger HX-2 on the cold side. However, these streams have different pressures. Therefore, it is necessary first to compress the hydrogen stream with lower pressure. This first compression is followed by cooling in the intercooler. These two compressors are both hydrogen piston compressors. After that, both streams are mixed and compressed in the second stage, which is followed by aftercooler, where the stream exiting the compressor is cooled to the ambient temperature. This process is presented in Figure 3.9. Afterward, the stream hydrogen refrigerant 3 in the same figure enters the heat exchanger HX-2 on the hot side.

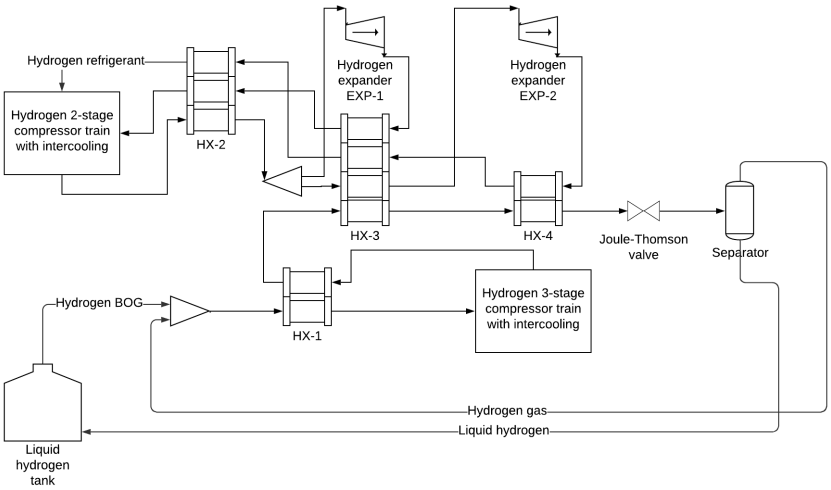

Figure 3.7: Simplified process flow diagram with the Joule-Thomson valve for hydrogen Claude refrigeration cycle with two hydrogen refrigerant turbine expanders

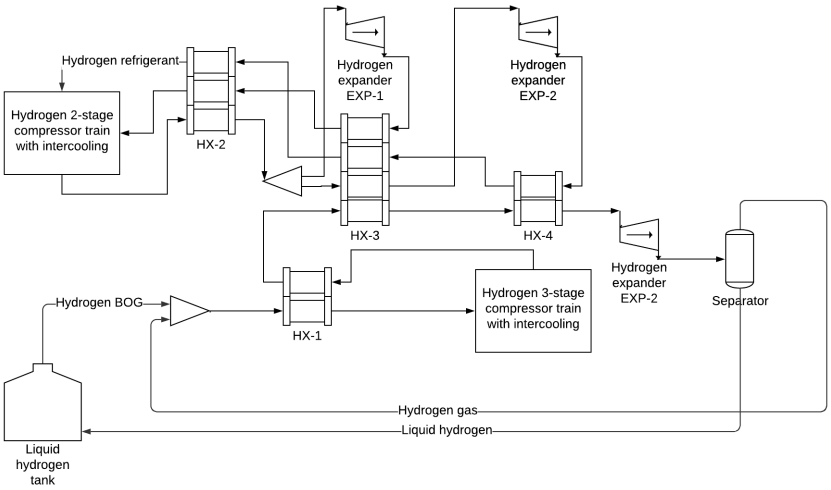

Figure 3.8: Simplified process flow diagram with the liquid turbine expander for hydrogen Claude refrigeration cycle with two hydrogen refrigerant turbine expanders

This stream is now cooled in the heat exchanger HX-2, and it is then separated into two streams. The first stream then enters the hydrogen expander EXP-1 where it is cooled and then comes into the heat exchanger HX-3 on the cold side. The second stream enters the same heat exchanger on the hot side, and here also the compressed hydrogen BOG enters the heat exchanger HX-3 on the hot side. Both streams are then cooled, then hydrogen refrigerant stream is expanded in the hydrogen expander EXP-2 and consequently addi-

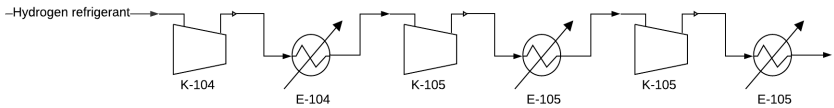

Figure 3.9: Hydrogen refrigerant compression train with two hydrogen piston compressors and with intermittent intercooler and the aftercooler

tionally cooled before it enters the heat exchanger HX-4 on the cold side - at the same time the hydrogen BOG is now cooled in the heat exchanger HX-4 before the expansion in either the Joule-Thomson valve or the last expander. After the expansion, the two-phase hydrogen goes into the separator where liquid hydrogen is returned to the reservoir, while hydrogen gas is recycled into the reliquefaction process.

3.3 Mixed refrigerant cycle

In the case of the mixed refrigerant, the whole process is very similar to the base case, but there are specific differences. The refrigerant is the mixture of neon and helium and not the pure component. The main reason for the introduction of neon is to enable the use of turbo compressors with “nelium”. However, due to significantly lower pressure ratios obtained, it was necessary to implement a compression train with five compressor stages. Otherwise, the rest of the process is identical to the base case. The process flow diagram for the process with the Joule-Thomson valve is presented in Figure 3.10, and with the expander in Figure 3.11.

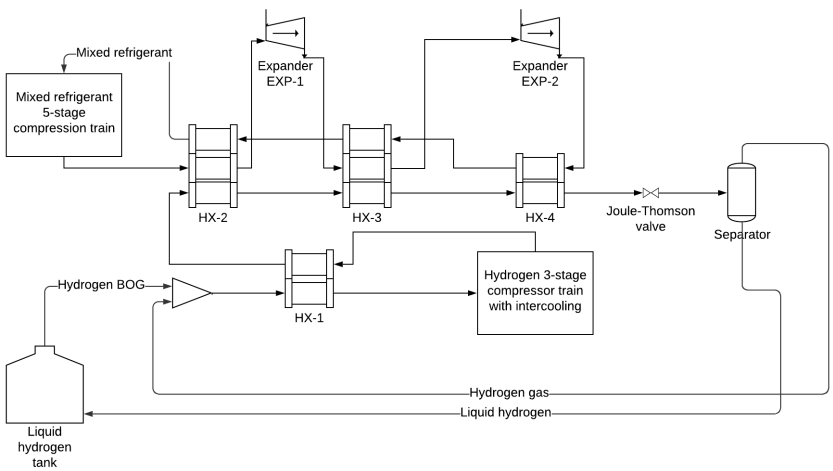

Figure 3.10: Simplified process flow diagram with the Joule-Thomson valve for mixed refrigerant reverse Brayton cycle

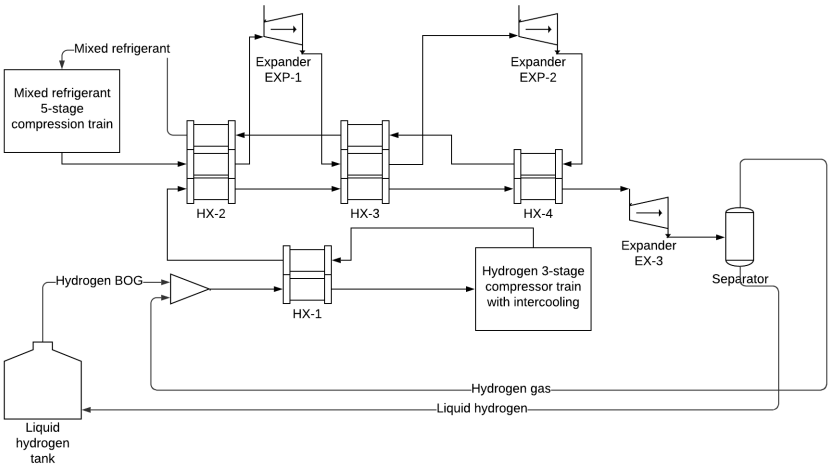

Figure 3.11: Simplified process flow diagram with the liquid expander for mixed refrigerant reverse Brayton cycle

Chapter 4

Process simulation

In this chapter, the simulation procedures of the concepts presented in Chapter 3 are described. For the simulations, Aspen HYSYS simulation software was used. At the first stage of research, static conditions in our simulation setting were considered. This means inputs in small incremental steps are not changed to find its optimal value, but the outcome is analyzed based on the selected static inputs. The goal of this simulation is to compare some of the key performance indicators, advantages, and disadvantages of the following three different concepts:

- Helium reverse Brayton refrigeration cycle with two helium turbine expanders;
- Hydrogen Claude refrigeration cycle with two hydrogen turbine expanders;
- Mixed refrigerant reverse Brayton cycle with two expanders;

The simulation setup has been done consistently for all three cases in the following steps. First, The component lists are based on the specified materials used in the system and then for every material appropriate equation of state was defined. A simulation process flowsheet in the software was set up according to the concept design given in Chapter 3. Properties of process components and material streams, such as temperatures, pressures, mass flows, compositions, process component efficiencies, temperature differences, and others are defined based on assumptions. Then the HYSYS software uses all inputs in computation and provides output results. To obtain the best possible result, the simple optimization procedure was followed.

In the scope of this master's thesis, potential precooling cycles to increase the efficiencies are not included in the simulations as its feasibility depends strongly on the investment and operational cost, availability of industrial gases, utilities and other factors – these should be instead a part of the detailed design for every case separately, and potential precooling processes for hydrogen reliquefaction should be developed and analyzed in the future.

Initially, the idea was to use three different tank volumes for simulation ($50\,\mathrm{m}^3$, $2500\,\mathrm{m}^3$

and $40\,000\,\mathrm{m}^3$). However, due to the steady-state conditions in simulations and the assumptions of constant boil-off rates, this was not part of this thesis. Different applications require additional research to determine real BOR, depending on different reservoir tanks specifications; pressure, temperature, insulations, size, shape, and other factors, and at the moment, there is a lack of research focused on this field. Furthermore, different BOR determine mass flows and distinct mass flows use different equipment with different specifications, but like precooling processes, this should also be a part of the detailed design instead. The initial conditions applied in all cases were chosen to be as following:

- Boil-off rate was $0.2\,\%\,\mathrm{d}^{-1}$ of the stored liquid volume. This was determined based on the experience that BOR is usually in range $0.1\,\%\,\mathrm{d}^{-1}$ to $0.3\,\%\,\mathrm{d}^{-1}$ (Ohlig and Decker, 2019).
- For large reservoir tanks where it is feasible to use BOG reliquefaction systems, storing pressure is usually close to atmospheric pressure. These options are especially larger receiving terminals and large LH_2 carriers shortly. Therefore, it was decided that the reservoir pressure should be $1.16\,\mathrm{bar}$. During detail design, this should also be part of the optimization later on.
- The temperature of the boil-off gas before the first heat exchanger HX-1 in the process is $-235\,°\mathrm{C}$ because at such low temperature there is always a certain heat inleak into pipes due to imperfect insulation. To be able to consistently compare relevant results to the base case, assumptions of identical starting temperatures for all cases were made. This assumption is debatable since it strongly depends on ambient conditions, pipeline insulation, and other factors. However, determining the right temperature should also be part of a detailed design later.

It was assumed that hydrogen boil-off gas consists of pure parahydrogen, while in a real case there would be a mixture with a small amount of orthohydrogen. As it was discussed in Chapter 2, the equilibrium composition at the boiling point of hydrogen at the atmospheric pressure is $99.8\,\%$ parahydrogen, so it seems reasonable to neglect the presence of orthohydrogen traces. Pure components including parahydrogen were simulated using modified Benedict-Webb-Rubin equation of states where empirical data are used to determine numerical parameters, which are relevant just for certain pure components and conditions.

Constant isentropic efficiencies for the same type and same refrigerant of turbine expanders and constant adiabatic efficiencies for compressors were assumed, and heat exchangers had the pinch temperature limited with minimum $0.5\,\mathrm{K}$. All other relevant assumptions are also defined in the Appendix in Tables A.1, B.1 and C.1. Pressure drops in heat exchangers were calculated based on the assumptions given in the Appendix. Pressure drop in the heat exchangers is part of the heat exchanger design, but in this static case, values were set as explained in the following. For hydrogen boil-off gas and hydrogen refrigerant $1.6\,\%$ pressure drop was assumed in heat exchangers with several streams, and $1\,\%$ pressure drop was assumed in air or water coolers. For helium, it was assumed constant pressure drop of $0.1\,\mathrm{bar}$ in all heat exchangers including intercoolers and aftercoolers, and for a mixture of helium and neon it was assumed that pressure drop in every

heat exchanger, intercooler and aftercooler is based on this value; 0.1+0.001 x_{Ne} bar, where x_{Ne} represents the mole concentration of neon. Oil-screw helium compressors and hydrogen piston compressors have adiabatic efficiency 70 %, while turbo compressors for mixed refrigerant have adiabatic efficiency of 75 %. On the other side, it was assumed that the expander isentropic efficiency for every case was 80 %.

4.1 Helium reverse Brayton cycle

This cycle represents the base case for these simulations, and it is the foundation for the other two alternatives. This simulation was done in a steady state. For hydrogen boil-off gas stream, 100 % parahydrogen and modified Benedict – Webb – Rubin (MBWR) equations of state were assumed after some consideration, as they are highly accurate and still reasonably simple and according to the literature review often used for both spin isomers of hydrogen and helium.

The simulation process flow diagram is shown in the Appendix in Figure A.1 with the Joule-Thomson valve and Figure A.2; the assumptions made are stated in Table A.1. The BOG from the hydrogen tank is released from the top and its amount is calculated based on Equation 4.1. It was assumed that hydrogen tank volume is $40\,000\,\mathrm{m}^3$ and the BOR is $0.2\,\%\,\mathrm{d}^{-1}$. From these two parameters and the density of hydrogen liquid at stored pressure $1.16\,\mathrm{bar}$ and corresponding temperature, the mass flow of hydrogen BOG was calculated:

$$\dot{m}_{BOG} = V_{tank} \times BOR \times \rho_{LH_2} \tag{4.1}$$

In the Aspen HYSYS simulation software, the amount of boil-off gas is calculated, and the tee mixer is implemented to use the calculated value of the boil-off gas in the simulation. This stream of BOG is warmed up to the temperature of $-235\,°\mathrm{C}$ in the heat exchanger. As explained above, this is done to simulate the heat inleak from the ambient through pipelines. However, for this heat exchanger, zero pressure drop was assumed, as it was estimated that the real pressure drop would not be significant, and it also depends strongly on ambient temperature, length, and isolation of pipes and similar, and this should be part of additional research. Next, the hydrogen stream from the heat exchanger enters the countercurrent heat exchanger HX-1, where it is additionally warmed up. The estimated pressure drop in the heat exchanger is calculated in the separate spreadsheet according to the assumptions and accounted for in simulation calculations.

Warmed up hydrogen gas enters the three-stage hydrogen compressor train with two intercoolers and an aftercooler, where it is cooled to the temperature of $298.15\,\mathrm{K}$. The intercoolers are used to remove the heat from the compressor stage to minimize compression work, thus trying to follow an isothermal compression curve instead of an adiabatic curve. This means that less energy is needed for compressing the gas. The aftercooler at the end is used to reduce temperature, and it provides consequently necessary cooling energy of the hydrogen stream. The pressure drops in intercoolers and aftercoolers were calculated for each point separately. Hydrogen piston compressors are the most common option in

the industry and possess reliable operation. However, the isentropic efficiency of these piston compressors is not very high for smaller units, and in this thesis, it is assumed to be 70 %. It is assumed that the pressure ratios of different compressor stages are the same. The main reason for this assumption is to minimize the compression work in such a way that the total work is almost equally divided between different stages. Optimum pressure ratio defines high pressure (HP) of hydrogen and it is part of optimization, as it represents one of the parameters that can be changed. After the compression, compressed hydrogen is cooled down in the same countercurrent heat exchanger HX-1 and transfers heat to the gas from the reservoir, which needs to be warmed up. Then this cooled and pressurized hydrogen gas enters the reverse helium Brayton cycle with two expanders.

Helium refrigerant is first compressed in two stages with an intercooler in between and an aftercooler at the end. This is done again to reduce the compression work. However, it could be possible to use just one stage compressors due to significantly higher pressure ratios of oil-screw compressors. For helium compression, oil-injected screw compressors can be used, and they have isentropic efficiencies in the range of 65 % to 75 %, and in this case, it was assumed to be 70 %. Furthermore, it could be possible to use just one stage compressors due to significantly higher pressure ratios of oil-screw compressors, but the main focus was to see a difference, between the helium and hydrogen process. It is assumed that both compressors have the same pressure ratio due to similar required power input, which simplifies the operation and maintenance work. Furthermore, this pressure ratio of helium compressors is one of the parameters considered in process optimization. After the compression, helium gas is cooled down to the ambient temperature (288.15 K) in the aftercooler, and then it enters into the same heat exchanger HX-2 as hydrogen gas where both streams are cooled. The pressure drop in this heat exchanger was calculated in the separated spreadsheet and calculations were implemented into the simulation. It is assumed that the outlet temperatures of the heat exchangers with several outlet streams on one side are the same. The reasoning is that the heat exchanger cooling length of the heat exchanger is long enough to reach temperature equilibrium. However, exact conditions are part of the detailed design for heat exchangers. After that helium stream goes through expansion in the expander EXP-2, where pressure is reduced and consequently temperature drops. The isentropic efficiency of cryogenic expanders is between 70 % to 90 %. In this case, it is assumed to be 80 %. This discharged pressure is also a parameter that was manipulated during the optimization stage. After that cooled helium stream enters the heat exchanger HX-3, into which also the hydrogen boil-off gas stream enters. As with the previous heat exchanger, it is assumed that the temperatures of the outlet streams are the same, and pressure drop is calculated in the same way as for other heat exchangers. At the exit of the heat exchanger HX-3, helium is expanded in the second expander EXP-2, where the low-pressure level of helium refrigerant is determined, and it represents one of the steps of the optimization process. Cooled helium enters the heat exchanger HX-4 on the cold side, while from the hot side the hydrogen BOG from the previous heat exchanger HX-3 enters. In the heat exchanger HX-4, hydrogen BOG is cooled down, while helium is warmed up before it enters the heat exchangers HX-3 and HX-4, where it warms up by cooling down both warm hydrogen and helium streams. Then helium is prepared to reenter the compression train.

Hydrogen from the last heat exchanger is expanded in the Joule-Thomson valve or the expander EXP-3, as stated in the simulation process flow diagrams, to the level of the reservoir pressure. An important part of this thesis is to determine whether it is beneficial to use a more efficient, more complex, and more expensive expander or the valve. After the expansion, two-phase hydrogen goes into the separator, where gas and liquid hydrogen are separated. Liquid hydrogen is returned into the reservoir, while gas is recycled and mixed with hydrogen BOG from the reservoir, where it again enters the reliquefaction process. Due to numerical problems in recycling gas phase where recycle option in the software caused this stream to change the phase from gas to a liquid, we used a pipeline segment where hydrogen gas from the separator is warmed up for $2\,^{\circ}\mathrm{C}$ to ensure that there is no phase change problem in recycling function. Recycle function is an important part of all simulations as it takes time to reach a steady-state. After the recycle, the hydrogen gas stream can enter the mixer and it reenters the refrigeration cycle.

4.2 Hydrogen refrigeration cycle

For hydrogen boil-off gas stream, MBWR equations of state were used and $100\,\%$ parahydrogen was assumed similar to the base case. For hydrogen refrigerant, it was assumed that it is normal hydrogen which consists of $75\,\%$ of orthohydrogen and $25\,\%$ of parahydrogen. MBWR equation of state was used also for the hydrogen refrigerant. The simulation process flow diagrams are shown in Figure B.1 for the Joule-Thomson valve and Figure B.2 for the liquid expander in the Appendix. The main assumptions are summarized in the Appendix in Table B.1. All the process steps before the compressed hydrogen BOG enters the heat exchanger HX-3 were simulated in an identical way as for the helium reverse Brayton cycle. Therefore, its description is omitted here.

The two hydrogen refrigerant streams exit the heat exchanger HX-2 on the cold side. However, these streams have different pressures. In the simulation, it is assumed that the pressure of the stream is approximately in the middle range between the lowest and the highest pressure in the hydrogen refrigeration cycle, while the lowest and the highest pressure are both optimization variables. Due to different pressures, it is necessary to first compress the hydrogen stream with lower pressure. Piston compressors are used for hydrogen compression as they are the most common in the industry and very reliable. Nonetheless, they have rather low efficiency, in this case, it is assumed to be $70\,\%$. Pressure ratios for both compressor stages are the same, and this is also the reason that the higher pressure of those two hydrogen streams is in the middle due to two-stage compression of hydrogen refrigerant. This first compressor K-104 is followed by cooling in the intercooler to the approximately ambient temperature of $288.15\,\mathrm{K}$. After that, both streams are mixed, and in the Aspen HYSYS software, this means that the outlet pressure out of the mixer is set at the lower pressure of inlet streams. The stream exiting the mixer is then compressed in the second stage compressor K-105, which is followed by cooling in the aftercooler to the temperature close to the ambient. This is seen in both process flow simulation diagrams in Figure B.1 and Figure B.2. Afterward, the hydrogen refrigerant stream enters the heat exchanger HX-2 on the hot side, where it is cooled. Pressure drops in all heat exchangers are calculated based on the assumptions and then results are used in the simulation.

Hydrogen at the outlet of the heat exchanger HX-2 is then split into two streams. The ratio of splitting is part of the optimization procedure. The first stream then enters the hydrogen expander EXP-1, where it is expanded to the medium pressure level. Due to expansion, it is also cooled and then comes into the heat exchanger HX-3 on the cold side. The second stream enters the same heat exchanger on the hot side, and here also the compressed hydrogen BOG from the heat exchanger HX-1 enters the heat exchanger HX-3 on the hot side. Both streams are then cooled, and hydrogen refrigerant stream is expanded in the hydrogen expander EXP-2 and consequently additionally cooled. The outlet pressure of the expander EXP-2 is one of the most important optimization variables. It enters the heat exchanger HX-4 on the cold side, while at the same time the hydrogen BOG is now cooled in the heat exchanger HX-4 before the expansion in either the Joule-Thomson valve or the liquid expander EXP-3. After the expansion, the two-phase hydrogen goes into the separator, where liquid hydrogen is returned to the reservoir, while hydrogen gas is recycled into the reliquefaction process. The hydrogen refrigerant from at the outlet of the heat exchanger HX-4 then enters the heat exchanger HX-3, where it is joined by the stream from the expander EXP-1. Both streams are warmed up in the heat exchanger HX-3 and HX-2, and then they can be compressed.

4.3 Mixed refrigerant cycle

The mixed refrigerant simulation will not be explained in detail since it is set up in a similar way to the base case. The simulation process flow diagram is shown in the Appendix in Figure C.1 with the Joule-Thomson valve and Figure C.2; the assumptions made are stated in Table C.1. However, there are a few differences. Due to a mixture of helium and neon, PRSV equations of state were used. It would be possible to use more sophisticated models (Aasen et al., 2020), but it would be time-consuming, thus it has been decided to use PRSV equations of state and verify them with thermodynamic library ThermoPack from SINTEF. However, as explained in the introduction due to coronavirus crisis, it was not possible to do this. Therefore, the results of the mixed refrigerant should be verified. The second difference was that due to higher amounts of neon, it was possible to use turbo compressors, and in this case, the adiabatic efficiency was assumed to be $75\,\%$. Due to the usage of turbo compressors, it is important to determine what is a sufficient amount of neon. Neon is also more expensive than helium, so there is a certain limit at which it is too expensive to introduce a higher concentration of neon. Therefore, it was assumed that neon molar concentration is constant at $20\,\%$. Furthermore, it was assumed that the pressure ratio of turbo compressors is constant at 1.3. Therefore, it was assumed that we will use five compressor stages. In this case, the result was based solely on the trial and error approach.

4.4 Optimization approach

The optimization objective was to minimize the specific energy of the process, thus also increasing the exergy efficiency of the process. According to the literature, when dealing with the liquefaction of hydrogen, the energy needed for compression of hydrogen is not

included in the reported results. However, in the scope of this thesis where it is needed to deal with the reliquefaction of hydrogen boil-off gas, precompression plays an important part in the specific energy consumption. Therefore, total specific energy consumption consists of two parts: hydrogen boil-off gas compression and refrigerant compression. The objective function was total specific energy consumption which is defined as it follows:

$$e_{total} = \frac{W_{net}}{\dot{m}_{LH_2}} \tag{4.2}$$

In Equation 4.2, W_{net} is defined as the sum of work produced from the hydrogen and refrigerants expander subtracted from the sum of work needed for compression of hydrogen and refrigerants:

$$W_{net} = \sum W_{comp} - x \sum W_{exp} \tag{4.3}$$

In the upper equation, x represents the share of power which can be utilized from the expanders. It is assumed that the maximum value of x can be $80\,\%$. However, it is not very common to have turbo compounder which could utilize the power, thus first reported results are without recovery of turbine power where it is not possible to utilize the power, meaning that x equals zero in Equation 4.3. Furthermore, exergy efficiency is defined as the ratio between the minimum specific energy and a total specific energy for the given process.

$$\psi_{total} = \frac{e_{min}}{e_{total}} \tag{4.4}$$

As explained in Chapter 2, minimum liquefaction work is derived from the second law of thermodynamics. In this case, 2.6 is transformed into the next equation:

$$e_{min} = h_{LH_2} - h_{BOG} - T_{amb}(s_{LH_2} - s_{BOG}) \tag{4.5}$$

In the equation above, BOG represents properties of boil-off gas at the point after the heat exchanger, which simulates heat inleak into the pipes and other equipment for BOG transfer from the tank, and LH_2 represents properties of liquid hydrogen after the two-phase separation.

As stated above, the main goal was to minimize the specific energy of the process. To do so, it was necessary to obtain low logarithmic mean temperature difference LMTD and to minimize the pinch point temperature, which is the minimum temperature difference between the cooling and heating curve, to temperature between $0.5\,\mathrm{K}$ to $3\,\mathrm{K}$ for this cryogenic process. This ensures a good fit between hot and cold composite curves. Another important part of optimization is that the pinch point is at the cold end of heat exchangers due to higher exergy loss at a lower temperature. This means that the temperature difference should be higher at a warmer end. Furthermore, reducing irreversibilities is also intrinsically connected to minimizing the transferred heat as explained in the literature review.

Initially, the plan was to use Aspen HYSYS optimizer, which is integrated into the software, but it is not the most suitable for complicated liquefaction processes with several

degrees of freedom. Therefore, in the scope of this thesis, the optimization process was simplified and was done in steps as described below. The optimization was done using the case study option in Aspen HYSYS software, and it will be further explained for every individual case. However, for better results in the future, more sophisticated optimization models should be used in external numerical computing environments such as Python, MATLAB, and similar.

4.4.1 Optimization procedure of the base case

For the reverse helium Brayton cycle, parameters that can be manipulated were defined to minimize the specific energy consumption for this selected case, and then the case study tool provides different results depending on the input parameters. These parameters are:

- Mass flow rate of the helium refrigerant $\dot{m}_{He}$:
- Pressure ratios of helium compressor stages to determine helium refrigerant high pressure;
- Outlet pressures of both helium expanders p_{exp1} and p_{exp2};
- Pressure ratios of hydrogen compressor stages to determine high pressure of hydrogen boil-off gas.

First, the simulation was based on the trial and error method. This means that based on initial and boundary conditions and predefined assumptions from Table A.1, values of the parameters were determined and adjusted until reasonable results were obtained. From that point on, the optimization procedure in the following steps started.

The first optimization step was to determine the optimum pressure ratio of hydrogen compressor stages. The too high-pressure ratio resulted in the large energy consumption for compression of hydrogen. On the other side, too low pressure leads to more energy needed to liquefy hydrogen. As mentioned before, it is beneficial to use the identical pressure ratio for all hydrogen compressor stages. The case study for changing the pressure ratio within a certain range was set up. Therefore, this step plays a crucial role in this process. To find the optimum value, the pressure ratio of helium compressor stages and both outlet helium expanders outlet pressures were fixed, while adjust function was used to adjust the mass flow of the helium refrigerant to obtain minimum temperature approach of $0.5\,\mathrm{K}$ temperature in the heat exchanger HX-4.

After determining the best pressure ratio for hydrogen compressors, it was possible to proceed to the next step. At this step, the goal was to determine the optimum high and low pressure of the helium refrigeration cycle. High pressure of helium was defined by the pressure ratio of helium compressor stages, which were again assumed to be identical. On the other side, helium low pressure was defined by the outlet pressure of the second expander. However, during this stage also the outlet pressure of the first expander was manipulated. The case study was defined for this case. At the same time, the adjust function to adjust the mass flow rate of the helium refrigerant was still running to reach the specified temperature.

4.4.2 Optimization procedure of the hydrogen refrigeration case

For the hydrogen Claude process, the whole optimization procedure was very similar to the base case. Parameters for manipulation were defined to minimize the specific energy consumption for this selected case, and then the case study tool provides different results depending on the input parameters. These parameters are:

- Mass flow rate of the hydrogen refrigerant $\dot{m}_{RH_2}$;
- Pressure ratios of hydrogen refrigerant compressor stages to determine hydrogen refrigerant high pressure;
- Outlet pressures of the second hydrogen refrigerant expander p_{exp2};
- Pressure ratios of hydrogen boil-off gas compressor stages to determine the pressure of BOG before entering the reliquefaction process;
- The split ratio of the streams in the TEE.

Identically as in the base case, the simulation was based on a trial and error method to obtain reasonable results. From there, the optimization procedure followed similar steps to the base case.

4.5 Exergy analysis and key performance indicators

In terms of exergy analysis, first exergy flows in kW of every stream were determined according to Equation 4.6, and then for every process equipment, the exergy efficiency and exergy destruction or irreversibility were determined according to other equations.

$$\dot{E}x_{flow} = \dot{m}((h - h_{amb}) - T_{amb}(s - s_{amb})) \tag{4.6}$$

For heat exchangers, the exergy efficiencies were calculated according to Equation 4.7 and irreversiblities according to Equation 4.8

$$\psi_{HX} = \frac{\sum(\dot{E}x_{out,h} - \dot{E}x_{in,h})}{\sum(\dot{E}x_{in,c} - \dot{E}x_{out,c})} \tag{4.7}$$

$$\dot{E}x_{dest} = \frac{\sum \dot{E}x_{out,h} - \dot{E}x_{in,h}}{\sum \dot{E}x_{in,c} - \dot{E}x_{out,c}} \tag{4.8}$$

In the case of compressors, because there was only one inlet and one outlet flow, the exergy efficiency is calculated according to Equation 4.9 and irreversibilities are calculated according to Equation 4.10.

$$\psi_{comp} = \frac{\dot{E}x_{out} - \dot{E}x_{in}}{W_{comp}} \tag{4.9}$$

$$\dot{E}x_{dest} = \dot{E}x_{in} + W_{comp} - \dot{E}x_{out} \tag{4.10}$$

On the other side in terms of turbines, there were also only one inlet and one outlet stream. Therefore, exergy efficiencies were determined according to Equation 4.11 and irreversibilities according to Equation 4.12.

$$\psi_{turb} = \frac{W_{turb}}{\dot{E}x_{in} - \dot{E}x_{out}} \tag{4.11}$$

$$\dot{E}x_{dest} = \dot{E}x_{in} - W_{turb} - \dot{E}x_{out} \tag{4.12}$$

For coolers and Joule-Thomson valves with only one outlet and one inlet stream, exergy efficiencies were defined according to Equation 4.13 and irreversibilities according to Equation 4.14

$$\psi = \frac{\dot{E}x_{in}}{\dot{E}x_{out}} \tag{4.13}$$

$$\dot{E}x_{dest} = \dot{E}x_{in} - \dot{E}x_{out} \tag{4.14}$$

However, at the end irreversibilities are converted into specific irreversibilities according to Equation 4.15. In this case specific irreversibility is defined as a ratio between irreversibility and mass flow of produced liquid hydrogen from the process.

$$ex_{dest} = \frac{\dot{E}x_{dest}}{\dot{m}_{LH_2}} \tag{4.15}$$

Then considering the calculated irreversibilities, it is possible to determine the total liquefaction specific energy as in Equation 4.2 according to Equation 4.16. Total liquefaction specific energy is a sum of minimum liquefaction energy and specific irreversibilities:

$$e_{total} = ex_{dest} + e_{min} \tag{4.16}$$

Apart from the specific exergy and exergy efficiency, there are certain other key performance indicators to determine the process. Because part of this thesis was to determine also which process components are needed, some other parameters could help with the future economic analysis. It is very important to determine the type of heat exchangers used, and only then it is possible to make a detailed design. Furthermore, it is very important to determine the size defined by area A and the heat transfer coefficient U, which is defined by properties of fluids in the heat exchanger. However, in this case, only the product UA results will be presented and from there it is possible to determine the size of a heat exchanger. The most important factor to determine the fit between the cooling and heating curve is the logarithmic mean temperature difference (LMTD), and the relation between UA and LMTD is given in Equation 4.17, where Q represents heat exchanger duty.

$$Q = UA \times LMTD \tag{4.17}$$

Other important performance indicators, which are not included in the analysis in the scope of this thesis include available space for heat exchangers, manufacturing technologies,

capital expenditures, operational expenditures, and other characteristics that define the final performance of a heat exchanger.

For coolers in the scope of this thesis, only two key performance indicators are presented: cooler duty Q and capacity. The size is determined based on the cooling medium and ambient conditions for air or water.

For compressors, key performance indicators are power consumption, efficiencies (isentropic, polytropic), capacities, and type of a compressor. In the case of piston compressors, also displacement volume will be reported.

Similar for expanders: it is important to report power consumption, efficiencies and capacities. Capacity is also an important parameter for Joule-Thomson valves.

Chapter 5

Final results and analysis

In this chapter, the simulation results of helium, hydrogen, and nelium processes and their alternatives are presented, compared, and discussed. The detailed process and flow diagrams of the main reliquefaction concept are included in the Appendix Figures A.1, A.2, B.1, B.2, C.1, C.2, including mass and energy balance of all streams and composite and splitting curves of certain simulations.

To calculate minimum necessary liquefaction work, values from Table 5.1 were used. These values were acquired from Aspen HYSYS software for $100\,\%$ parahydrogen with MBWR equations of state. In this table, H_{BOG} represents the hydrogen BOG stream after the first heat exchanger E-100 as seen from Figure A.1 in the Appendix, which simulates the heat inleak into the pipes from the reservoir to reliquefaction part, while H_{LH_2} is the liquid hydrogen stream after the separator V-101 in the same figure. In Figure 5.1 the comparison is given for how does the minimum liquefaction energy change with temperature of the boil-off gas for $100\,\%$ parahydrogen at pressure $1.16\,\mathrm{bar}$, which is assumed storage pressure in these simulations.

Using Equation 4.5 and data from Table 5.1, calculated minimum liquefaction work for these simulations with these assumptions is $2.078\,\mathrm{kW\,h\,kg^{-1}}$.

Stream	**p** [bar]	**T** [°C]	**h** [$\mathrm{kJ\,kg^{-1}}$]	**s** [$\mathrm{kJ\,kg^{-1}\,K}$]
$\mathrm{Hydrogen_{BOG}}$	-235	1.16	385.1	36.39
$\mathrm{Hydrogen_{LH_2}}$	-252.4	1.16	-251.3	8.21

Table 5.1: Pressure, temperature, specific enthalpy and specific entropy of hydrogen streams used to define the minimum liquefaction energy.

Figure 5.2 shows how minimum specific energy necessary to reliquefy hydrogen boil-off gas depends on hydrogen boil-off gas pressure at the outlet of heat exchanger HX-1 in Figure 3.1 before it enters additional liquefaction process. The blue curve is calculated

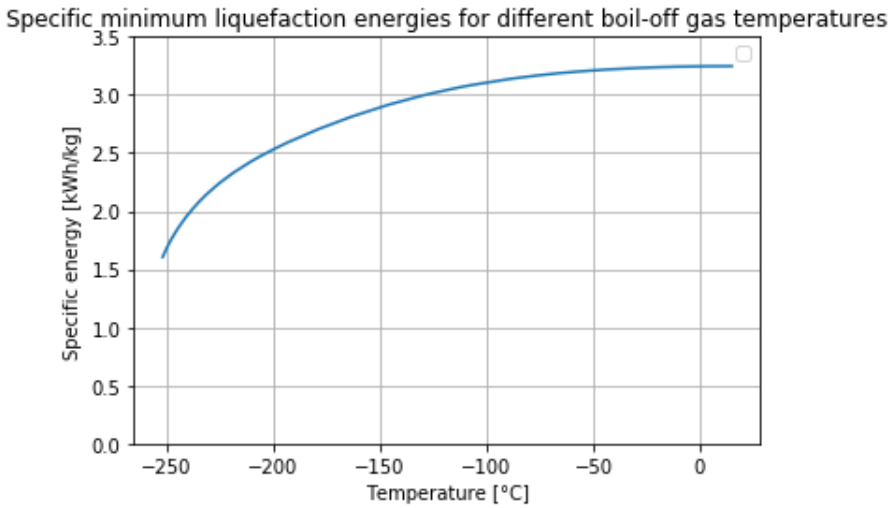

Figure 5.1: Theoretical minimum specific energy for boil-off gas reliquefaction depending on different boil-off gas temperatures at pressure $1.16\,\mathrm{bar}$.

based on Equation 2.6, where specific enthalpy and specific entropy for stream denoted with number 2 in that equation are values of $\mathrm{Hydrogen}_{\mathrm{LH}_2}$ from Table 5.1, and number 1 represents specific enthalpy and entropy of hydrogen boil-off gas stream out of HX-1 as presented in Figure 3.1 and 3.2. From this curve, it is obvious that minimum liquefaction energy is lower for compressed hydrogen boil-off gas. However, as can be seen, this relation is not linear for the simulations with given assumptions. These can be partially explained by a larger absolute pressure drop at higher pressures.

On the other side, the specific energy needed for compression, the green curve, is based on simulations with realistic assumptions explained in Chapter 4. According to the assumptions, specific energy needed for compression increases with higher outlet pressure. The red curve is a sum of both curves and represents theoretical minimum reliquefaction for this set up with the assumptions used. As seen from Figure 5.2, theoretically is not beneficial to compress hydrogen boil-off gas before reliquefaction in this case, but of course, real liquefaction energy depends strongly also on other factors and simulation results will be presented on following pages. As explained in Chapter 2, most liquefaction processes use hydrogen pressure at $21\,\mathrm{bar}$ and up to $80\,\mathrm{bar}$. However, compression work in these cases is usually smaller, because natural gas steam reforming, autothermal reforming, and electrolysis as the most common ways of producing hydrogen all deliver hydrogen at elevated pressures. In the applications related to boil-off gas, this is not the case. Therefore, it is not straightforward that higher hydrogen pressure would lead to lower liquefaction work. On the contrary, in this case, energy consumption increases with hydrogen pressure.

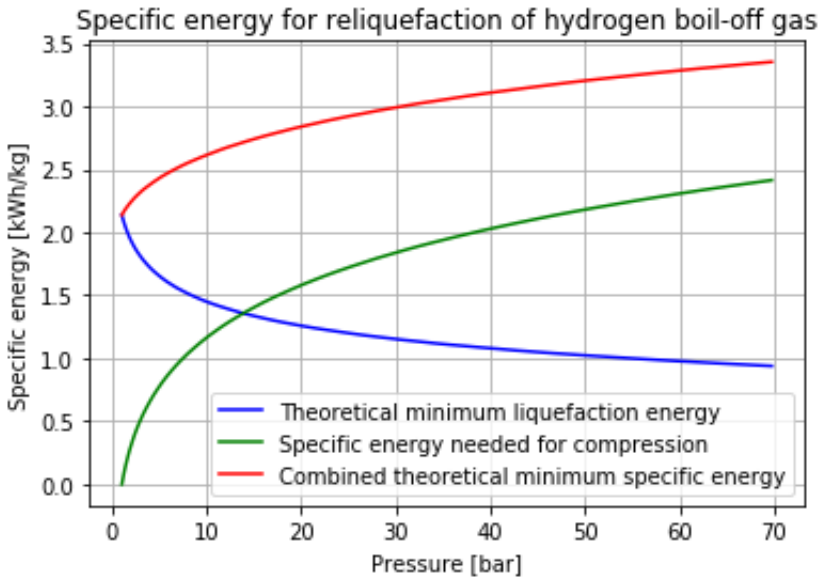

Figure 5.2: Theoretical specific energy to reliquefy hydrogen boil-off gas based on theoretical minimum specific liquefaction energy, specific energy for compression dependency on hydrogen boil-off gas outlet pressure from precooling process.

5.1 Results for the helium refrigeration cycle

This cycle was used as the base case for the master's thesis. This means that certain findings from the base case helped to design and evaluate the simulations of other alternatives. The initial result was based on the trial and error approach, where values were manipulated to get a reasonable result. For a reasonable pressure ratio for hydrogen piston compressors, our starting pressure ratio was set at 2.7, which resulted in the hydrogen pressure at the outlet of the third compressor stage set at around $22\,\mathrm{bar}$. Due to the pressure drop in the aftercooler and the next heat exchanger, this means that hydrogen enters the helium reverse Brayton cycle with two helium expanders at the pressure of $21.5\,\mathrm{bar}$ and temperature of $-223\,^{\circ}\mathrm{C}$. As explained before, this starting pressure was chosen because most of the liquefaction processes start at elevated pressure. Helium high pressure was at $10.1\,\mathrm{bar}$ and low pressure of helium cycle was at $3\,\mathrm{bar}$. This means that the specific energy consumption and exergy efficiency are $7.299\,\mathrm{kW\,h\,kg^{-1}}$ and $28.47\,\%$, respectively.

5.1.1 First simulation result

In this section, the detailed results of the first successful simulation are presented. The same labels of the equipment are used as they are presented in the process flow diagram made from Aspen HYSYS software, which is shown in the Appendix, Figure A.1. For comparison, split and composite temperature-heat flow diagrams for every heat exchanger are reported, but due to easier comparison, they are all put in the Appendix. in Table 5.2

results are given for simple weighted LMTD and UA, which are calculated separately for each interval on a heat curve and summed together to calculate an overall heat exchanger UA. Heat exchanger duties Q and minimum temperature difference ΔT_{min} for every heat exchanger are also included. Other performance indicators will be presented in the next section when all alternative processes will be compared. Heat splitting and composite curves for every heat exchanger are presented in Figure A.3a, Figure A.3b, Figure A.4a and Figure A.4b in the Appendix. Furthermore, mass balance with the main streams and corresponding properties is included as well in Table 5.3. At the end of this section, the results of the compressors and the expanders are given in Table 5.4 and Table 5.5.

In Table 5.2, basic results for every heat exchanger are presented. From the table, it is obvious the most heat is transferred in the HX-2 heat exchanger, and the least heat is transferred in the last one between helium refrigerant and hydrogen stream - as expected. Figure A.3a, Figure A.3b, Figure A.4a and Figure A.4b represent all main heat exchangers and they are available in the Appendix. In these figures, the red line presents the hot composite curve, which consists of hot streams that are cooled down by transferring the heat to cold streams that are warmed up, and these streams are combined into the cold composite curve, the blue line. These figures present how good is the fit between cold and warm streams. However, Figures A.3a and A.3b refer to a much larger temperature scale, and for this reason, the fit appears to be better. However, according to the results from Table 5.2, it can be seen that actually, the last heat exchanger has the best fit according to LMTD and ΔT_{min}, although this is at first not obvious from the figures due to scaling perspective.

Specification	**HX-1**	**HX-2**	**HX-3**	**HX-4**
LMTD [K]	2.40	2.05	3.49	1.5
Δ**T$_{min}$**[K]	1.50	0.83	2.50	0.5
Q [kW]	261.7	1310	37.7	2.7
UA [kW K^{-1}]	109	639.4	10.8	1.8

Table 5.2: Main results for heat exchangers for the first simulation result of helium reverse Brayton cycle with the Joule-Thomson valve.

In Table 5.3, data for the main material streams of hydrogen and helium refrigerant are given. As explained before, the stream H-RCY is used to prevent a phase change when recycling the stream back to the reliquefaction process. In Tables 5.4 and 5.5, the main properties of compressors and expanders are given. As we see from the tables, the power consumption of helium compressors was significantly higher than hydrogen compressors.

5.1.2 Process optimization

After obtaining the first reasonable result from the trial and error method, simple optimization began. As it was described in Chapter 4, optimization started by manipulating the pressure ratio of hydrogen compressor stages. As emphasized in Chapter 4, the adjust function was used to set the mass flow rate of the helium refrigerant to get the minimum

Name		H-2	H-4	H-10	H-11	H-12
Vapour Fraction		1.0000	1.0000	1.0000	1.0000	1.0000
Temperature	(C)	-235.0 *	13.50 *	15.00 *	-223.0	-236.0 *
Pressure	(kPa)	116.0	114.1	2180	2145	2111
Mass Flow	(kg/h)	234.2	259.4	259.4	259.4	259.4
Mass Enthalpy	(kJ/kg)	385.1	4001	4033	401.2	97.27
Mass Entropy	(kJ/kg-C)	36.39	63.61	51.51	25.71	18.51
Name		H-13	H-14	H-15	H-16	H-17
Vapour Fraction		0.0000	0.0000	0.0969	0.0000	1.0000
Temperature	(C)	-246.7	-249.9	-252.4	-252.4	-252.4
Pressure	(kPa)	2077	2044	116.0 *	116.0	116.0
Mass Flow	(kg/h)	259.4	259.4	259.4	234.2	25.12
Mass Enthalpy	(kJ/kg)	-171.1	-208.3	-208.3	-251.2	192.0
Mass Entropy	(kJ/kg-C)	10.39	8.915	10.28	8.211	29.58
Name		H-RCY	He-1	He-5	He-7	He-10
Vapour Fraction		1.0000	1.0000	1.0000	1.0000	1.0000
Temperature	(C)	-250.0 *	13.00 *	15.00 *	-243.2	-250.4
Pressure	(kPa)	116.0 *	270.0	997.2	493.6	300.0 *
Mass Flow	(kg/h)	25.16	3549 *	3549	3549	3549
Mass Enthalpy	(kJ/kg)	220.9	1487	1499	154.7	116.9
Mass Entropy	(kJ/kg-C)	30.90	27.34	24.66	14.31	13.91

Table 5.3: Material balance of the main hydrogen and helium streams for the first simulation result of helium reverse Brayton cycle with the Joule-Thomson valve.

Property	**K-101**	**K-102**	**K-103**	**K-104**	**K-105**
Power [kW]	139.4	140.4	141.1	641.7	647.1
Inlet pressure [bar]	1.14	3.05	8.16	2.70	5.17
Outlet pressure [bar]	3.08	8.24	22.02	5.27	10.07
Adiabatic efficiency [%]	70	70	70	70	70
Polytropic efficiency [%]	74	74	74	74	74

Table 5.4: Power, inlet and outlet pressures, adiabatic and polytropic efficiencies of hydrogen and helium compressors for the first simulation result of helium reverse Brayton cycle with the Joule-Thomson valve.

Property	**EXP-101**	**EXP-102**
Power [kW]	37.52	18.93
Inlet pressure [bar]	9.87	4.84
Outlet pressure [bar]	4.94	3.00
Isentropic efficiency [%]	80	80
Polytropic efficiency [%]	78	78

Table 5.5: Power, inlet and outlet pressures, isentropic and polytropic efficiencies of hydrogen and helium expanders for the first simulation result of helium reverse Brayton cycle with the Joule-Thomson valve.

temperature approach in the HX-4 close to $0.5\,\mathrm{K}$. Furthermore, temperatures of certain streams were manipulated to lower the minimum approach and LMTD in the heat exchangers at lower temperature levels, thus reducing irreversibilities in the process and decreasing power consumption. For this reason, there are several results for every hydrogen pressure level depending on a different temperature assumption combination. Temperature values consequently influenced the vapor fraction at the outlet of the Joule-Thomson valve, and how much gas it is needed to recycle back into the reliquefaction process. The results of this approach are shown in Figure 5.3 in terms of pressure ratio of hydrogen

compressors, and in Figure 5.4 in terms of hydrogen high pressure. As we see from the figures, the optimum value of compressor ratio for hydrogen boil-off gas is 2, and outlet pressure of hydrogen before the helium liquefaction process, in this case, is 8.72 bar. Low pressure is expected for these cases, as seen from Figure 5.2. However, it is interesting that this pressure is still a bit higher than the ambient. With the defined pressure level of hydrogen, it is possible to proceed with the second step of the optimization procedure.

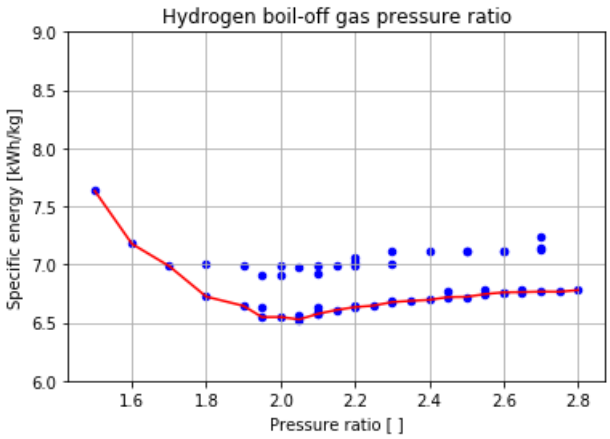

Figure 5.3: The results of specific energy consumption depending on the hydrogen outlet pressure for the simulation of helium reverse Brayton cycle with the Joule-Thomson valve.

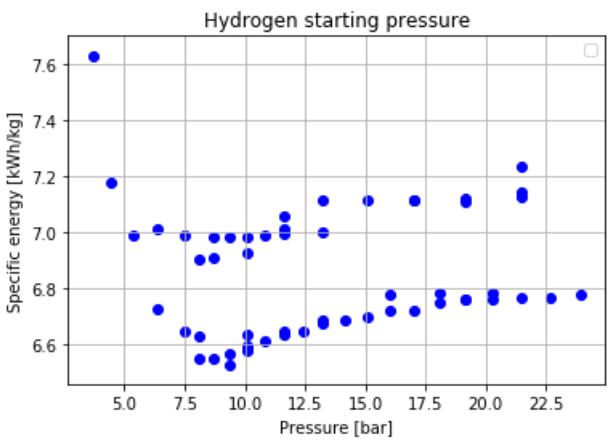

Figure 5.4: The results of specific energy consumption depending on the hydrogen outlet pressure for the simulation of helium reverse Brayton cycle with the Joule-Thomson valve.

At this step, the low and high pressure of helium refrigerant was determined. High pressure was determined by the pressure ratio of helium compressors. Identical to the previous step, the adjust function was used to get the low-temperature ΔT_{min}. Besides this, also values

of certain temperature streams were manipulated. Figures 5.5 and 5.6 present how the specific power consumption depends on different pressure ratios of helium compressors which define HP on the helium refrigerant side, and how it depends on the low pressure (LP) of helium. As we see from the figures, the optimum value for pressure ratio for helium compressors is 1.9 and helium outlet pressure is 10 bar.

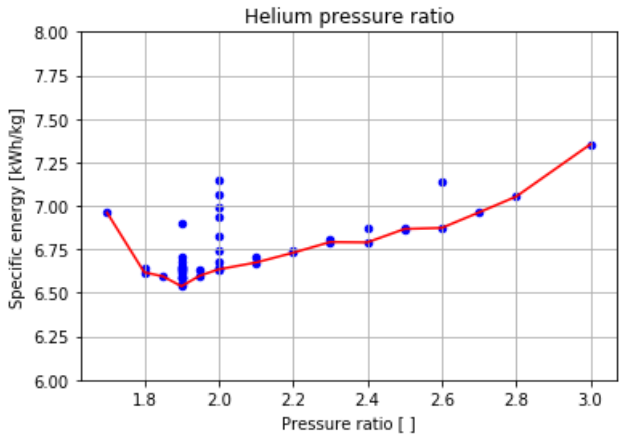

Figure 5.5: The results of specific energy consumption depending on the pressure ratio of helium compressors for the simulation of helium reverse Brayton cycle with the Joule-Thomson valve.

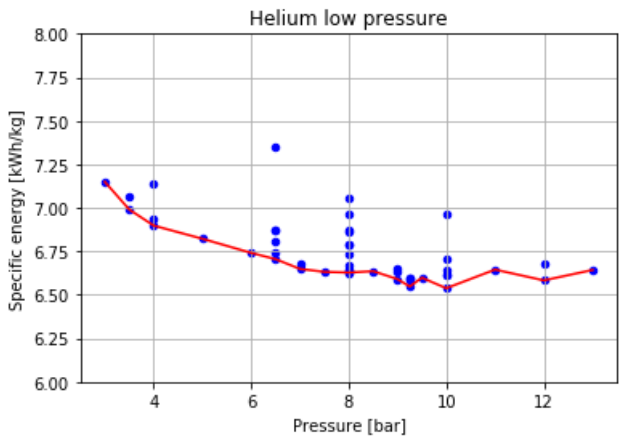

Figure 5.6: The results of specific energy consumption depending on the outlet pressure of the second expander in the helium cycle for the simulation of helium reverse Brayton cycle with the Joule-Thomson valve.

The combination of values for helium compressors pressure ratio and low pressure of helium also defined the high pressure of hydrogen. High pressure of helium influence on the efficiency of the process is illustrated by Figure 5.7 which presents the dependence

of the specific energy consumption on helium high pressure. From this figure, it can be seen that there is a certain range of high helium pressures where the specific energy consumption is low, and the goal is to find the combination of the pressure ratio of helium compressors and helium outlet pressure of the second expander which gives us the high pressure in the certain range.

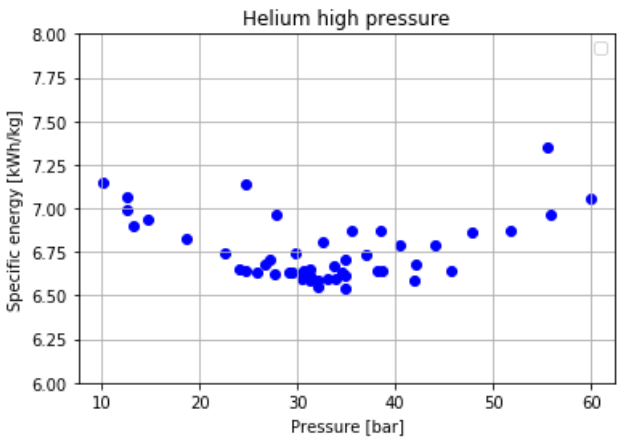

Figure 5.7: The results of specific energy consumption depending on the high pressure in the helium cycle for the simulation of helium reverse Brayton cycle with the Joule-Thomson valve.

5.1.3 The best simulation results

Based on the optimization results, the settings leading to the best result were identified. The hydrogen pressure ratio, in this case, was set at 2, which resulted in the hydrogen pressure at the outlet of the third compressor stage set at around $8.95\,\mathrm{bar}$. Due to pressure drop in the aftercooler and the next heat exchanger HX-1, this means that hydrogen enters the helium reverse Brayton cycle with two expanders at the pressure of $8.72\,\mathrm{bar}$ and temperature of $-229.4\,°\mathrm{C}$. Helium compressor ratio was set at 1.9 and low pressure of helium cycle was at $10\,\mathrm{bar}$ resulting in high pressure at $34.83\,\mathrm{bar}$. This resulted in the values of the specific energy consumption and exergy efficiency of $6.528\,\mathrm{kW\,h\,kg^{-1}}$ and $31.8\,\%$, respectively. However, with potential utilization of $80\,\%$ of the power from helium expanders, the specific energy consumption drops by $6.317\,\mathrm{kW\,h\,kg^{-1}}$, and the exergy efficiency, in this case, is $32.9\,\%$.

The detailed results of the best case for the process design are given in the Appendix, and the simulation process flow diagram is presented in Figure A.1. The results, in this case, are presented identically as for the first case. The heat exchangers' results are presented in Table 5.7. Heat splitting and composite curves for every heat exchanger are presented in Figures A.5a, A.5b, A.6a and A.6b in the Appendix. The mass balance with the main streams and corresponding properties is included in Table 5.8. At the end of this section, results for the compressors and the expanders are presented in Tables 5.8 and 5.9.

Specification	HX-1	HX-2	HX-3	HX-4
LMTD [K]	1.94	2.06	1.93	1.71
$\Delta \mathbf{T_{min}}$[K]	1.50	0.50	0.51	0.50
Q [kW]	262.6	1318	37.0	4.1
UA [kW K^{-1}]	135.5	639.4	19.1	2.4

Table 5.6: Heat exchangers for the best simulation case of helium reverse Brayton cycle with the Joule-Thomson valve.

In Table 5.6, results for the heat exchangers are given. As seen from the table, the results show lower LMTD and lower minimum approach in comparison to the starting case. This leads to a better fit between the cooling and heating curves and lower energy consumption in comparison to the base case. In Table 5.7, the main material streams of hydrogen and helium refrigerant are given, while the rest are in the Appendix, Table A.2. Tables 5.8 and 5.9 show the main properties of compressors and expanders. Compared to the starting simulation, significantly lower power is needed to run hydrogen compressors (K-101 to K-103), while there is also a small reduction in helium compressors' power. These two things result in a significantly smaller specific power consumption.

Name		H-2	H-4	H-10	H-11	H-12
Vapour Fraction		1.0000	1.0000	1.0000	1.0000	1.0000
Temperature	(C)	-235.0 *	13.50 *	15.00 *	-229.4	-237.1
Pressure	(kPa)	116.0	114.1	886.0	871.9	857.9
Mass Flow	(kg/h)	234.2	260.2	260.2	260.2	260.2
Mass Enthalpy	(kJ/kg)	385.1	4001	4027	394.6	292.0
Mass Entropy	(kJ/kg-C)	36.39	63.61	55.23	28.76	26.23
Name		H-13	H-14	H-15	H-16	H-17
Vapour Fraction		0.0000	0.0000	0.0997	0.0000	1.0000
Temperature	(C)	-245.0	-248.9	-252.4	-252.4	-252.4
Pressure	(kPa)	844.2	830.7	116.0 *	116.0	116.0
Mass Flow	(kg/h)	260.2	260.2	260.2	234.3	25.94
Mass Enthalpy	(kJ/kg)	-150.1	-207.0	-207.0	-251.2	192.0
Mass Entropy	(kJ/kg-C)	11.87	9.714	10.34	8.212	29.58
Name		H-RCY	He-1	He-5	He-7	He-10
Vapour Fraction		1.0000	1.0000	1.0000	1.0000	1.0000
Temperature	(C)	-250.0 *	13.00 *	15.00 *	-244.1	-249.4
Pressure	(kPa)	116.0 *	970.0	3473	1731	1000 *
Mass Flow	(kg/h)	26.01 *	3574 *	3574	3574	3574
Mass Enthalpy	(kJ/kg)	220.9	1489	1507	148.4	119.9
Mass Entropy	(kJ/kg-C)	30.90	24.68	22.07	11.43	11.52

Table 5.7: Material balance of the main hydrogen and helium streams for the best simulation case of helium reverse Brayton cycle with the Joule-Thomson valve.

As explained before, the important goal of this thesis is to estimate, whether it is beneficial to implement the liquid turbine expander instead of the Joule-Thomson valve. Therefore, in Figure 5.8, expansion in the valve, and the expander are compared. Based on the assumptions final expansion is done to the pressure of 1.16 bar. It is important to enter the two-phase region of liquid and gas, and the amount of corresponding phases is defined based on the phase fraction. In this case, 1 means that this is only a gas phase, and 0 means that this is only a liquid phase. Any number between 0 to 1 represents the two-phase region. With the lower number, meaning that a higher relative amount was liquefied. To see the difference in expansions in the Joule-Thomson valve and the turbine expander results for different pressures and temperatures at the inlet were compared in the figure. As seen from the figure, in the expander, there is always a higher amount of liquid phase in

Property	K-101	K-102	K-103	K-104	K-105
Power [kW]	93.4	94.0	94.2	620.2	627.7
Inlet pressure [bar]	1.14	2.26	4.48	9.70	18.33
Outlet pressure [bar]	2.28	4.52	8.95	18.43	34.83
Adiabatic efficiency [%]	70	70	70	70	70
Polytropic efficiency [%]	73	73	73	73	73

Table 5.8: Power, inlet and outlet pressures, adiabatic and polytropic efficiencies of hydrogen and helium compressors for the best simulation case of helium reverse Brayton cycle with the Joule-Thomson valve.

Property	EXP-101	EXP-102
Power [kW]	38.6	23.3
Inlet pressure [bar]	34.63	17.21
Outlet pressure [bar]	17.31	10
Isentropic efficiency [%]	80	80
Polytropic efficiency [%]	78	78

Table 5.9: Power, inlet and outlet pressures, isentropic and polytropic efficiencies of hydrogen and helium expanders for the best simulation case of helium reverse Brayton cycle with the Joule-Thomson valve.

comparison to the Joule-Thomson valve, if the inlet conditions are the same. However, the difference becomes smaller with lower temperatures as seen from Figure 5.9. As seen from Figure 5.8, it is not beneficial to expand at a temperature higher than $-246\,°\mathrm{C}$ as the gas fraction, in this case, is higher than $20\,\%$ and at these temperatures, the difference is not so large. Furthermore, it is worth noticing higher inlet pressure results in larger differences in gas fractions for expansions in the Joule-Thomson valve and the turbine expander. However, as seen from the results for the base case, it is not beneficial to compress boil-off gas to higher pressures with these assumptions.

Therefore, the implementation of a liquid expander, in this case, is not automatically a better solution. In a detailed design, the economic analysis would determine if benefits outweigh the drawbacks and whether it is worth it to implement it. Based on the trial and error approach, the best result was found. Hydrogen boil-off gas pressure ratio was set on 2, which resulted in the hydrogen pressure at the outlet of the third compressor stage set at around $8.95\,\mathrm{bar}$. Due to pressure drop in the aftercooler and the next heat exchanger, this means that hydrogen enters the helium reverse Brayton cycle with two expanders at the pressure of $8.72\,\mathrm{bar}$ and temperature of $-229.2\,°\mathrm{C}$. Helium compressor ratio and pressure at the outlet of the second expander was equivalent to the values as determined in the best case. These assumptions resulted in the values of the specific energy consumption and exergy efficiency of $6.343\,\mathrm{kW\,h\,kg^{-1}}$ and $32.8\,\%$ respectively, and with potential utilization of $80\,\%$ of the power from helium expanders, the specific energy consumption drops by $6.134\,\mathrm{kW\,h\,kg^{-1}}$, and the exergy efficiency, in this case, is $33.9\,\%$.

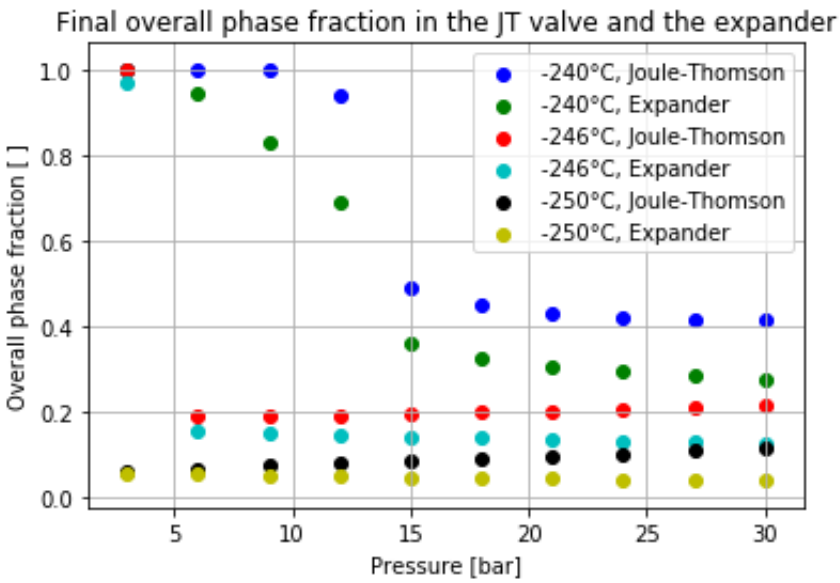

Figure 5.8: Theoretical specific energy to reliquefy hydrogen boil-off gas based on theoretical minimum specific liquefaction energy and specific compression work dependency on hydrogen boil-off gas outlet pressure from precooling process.

The detailed results of the best case for the process design are given in the Appendix, and the simulation process flow diagram is presented in Figure A.2. The heat exchangers results are presented in Table 5.10. Heat splitting and composite curves for heat exchangers are very similar to Figures A.5a, A.5b, A.6a and A.6b and are not presented here. The mass balance with the main streams and corresponding properties is included in Table 5.11. The full material balance including exergy flows is in the Appendix in table A.3. At the end of this section, results for the compressors and the expanders are presented in Tables 5.12 and 5.13.

Specification	**HX-1**	**HX-2**	**HX-3**	**HX-4**
LMTD [K]	1.94	2.05	1.86	1.73
Δ**T**$_{\mathbf{min}}$[K]	1.50	0.5	0.5	0.5
Q [kW]	258.4	1276	33.6	4.3
UA [kW K^{-1}]	133.4	622.1	18.1	2.5

Table 5.10: Heat exchangers results for the best simulation case of helium reverse Brayton cycle with the liquid turbine expander.

As seen from the table above, the LMTD and minimum approach are even lower in this case, but this was expected due to lower specific energy consumption. In Table 5.11, the main hydrogen and helium streams are presented, but the whole material balance is

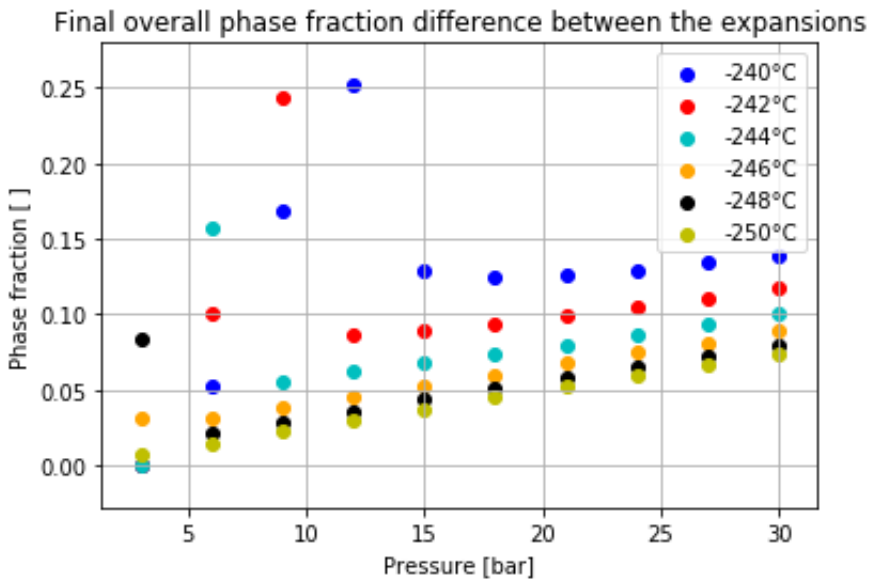

Figure 5.9: Theoretical specific energy to reliquefy hydrogen boil-off gas based on theoretical minimum specific liquefaction energy and specific compression work dependency on hydrogen boil-off gas outlet pressure from precooling process.

presented in the Appendix in Table A.3. As seen from Table 5.12, the required power for all compressors was lower and this was the main reason for the better results in this case. On the other side, liquid expander EXP-103 of hydrogen for such a low pressure does not produce a lot of power, as seen from Table 5.13. In conclusion, the utilization of this power from the expander does not have a significant impact on the overall performance results, if included or not.

Name		H-2	H-4	H-10	H-11	H-12
Vapour Fraction		1.0000	1.0000	1.0000	1.0000	1.0000
Temperature	(C)	-235.0 *	13.50 *	15.00 *	-229.2	-237.0
Pressure	(kPa)	116.0	114.1	886.0	871.9	857.9
Mass Flow	(kg/h)	234.2	256.3	256.3	256.3	256.3
Mass Enthalpy	(kJ/kg)	385.1	4001	4027	396.9	293.2
Mass Entropy	(kJ/kg-C)	36.39	63.61	55.23	28.82	26.27
Name		H-13	H-14	H-15	H-16	H-17
Vapour Fraction		0.0000	0.0000	0.0860	0.0000	1.0000
Temperature	(C)	-244.5	-248.5	-252.4	-252.4	-252.4
Pressure	(kPa)	844.2	830.7	116.0 *	116.0	116.0
Mass Flow	(kg/h)	256.3	256.3	256.3	234.2	22.03
Mass Enthalpy	(kJ/kg)	-141.6	-202.1	-213.1	-251.2	192.0
Mass Entropy	(kJ/kg-C)	12.17	9.916	10.05	8.212	29.58
Name		H-RCY	He-1	He-5	He-7	He-10
Vapour Fraction		1.0000	1.0000	1.0000	1.0000	1.0000
Temperature	(C)	-250.0 *	13.00 *	15.00 *	-244.0	-249.0
Pressure	(kPa)	116.0 *	970.0	3473	1731	1000 *
Mass Flow	(kg/h)	22.07 *	3461 *	3461	3461	3461
Mass Enthalpy	(kJ/kg)	220.9	1489	1507	148.8	122.1
Mass Entropy	(kJ/kg-C)	30.90	24.68	22.07	11.44	11.61

Table 5.11: Material balance of the main hydrogen and helium streams for the best simulation case of helium reverse Brayton cycle with the liquid turbine expander.

Property	K-101	K-102	K-103	K-104	K-105
Power [kW]	92.0	92.6	92.8	600.6	607.7
Inlet pressure [bar]	1.14	2.26	4.48	9.70	18.33
Outlet pressure [bar]	2.28	4.52	8.95	18.43	34.83
Adiabatic efficiency [%]	70	70	70	70	70
Polytropic efficiency [%]	73	73	73	73	73

Table 5.12: Power, inlet and outlet pressures, adiabatic and polytropic efficiencies of hydrogen and helium compressors for the best simulation case of helium reverse Brayton cycle with the liquid turbine expander.

Property	EXP-101	EXP-102	EXP-103
Power [kW]	37.42	22.98	0.78
Inlet pressure [bar]	34.63	17.21	8.31
Outlet pressure [bar]	17.31	10.0	1.16
Isentropic efficiency [%]	80	80	80
Polytropic efficiency [%]	78	78	78

Table 5.13: Power, inlet and outlet pressures, isentropic and polytropic efficiencies of hydrogen and helium expanders for the best simulation case of helium reverse Brayton cycle with the liquid turbine expander.

5.2 Results for hydrogen Claude refrigeration cycle

Different than to the helium process, in this case, the first simulation results are not included because the process simulation was set up based on the findings from the helium reverse Brayton cycle and these results do not provide any important new insights. Therefore, first, the results of the optimization will be presented, and then detailed results of the best case are reported. Like process optimization for the helium refrigerant cycle, manipulation of certain temperature parameters was needed to get the lowest specific energy consumption. As it was explained before, the adjust function was used to reach the pinch temperature in the last heat exchanger at $0.5\,\mathrm{K}$. To find the best hydrogen boil-off gas pressure for this reliquefaction process, the first step was to optimize this value. The results are presented in Figure 5.10 in terms of hydrogen boil-off gas compressors pressure ratio, and in Figure 5.11 in terms of hydrogen boil-off gas outlet pressure.

As seen from these figures, in this case, it is beneficial to have slightly higher pressure. It was possible to get a better fit with higher pressure when using hydrogen refrigerant. Based on the results, the optimum pressure was around $15\,\mathrm{bar}$ corresponding to the pressure ratio of 2.4.

After this first optimization step, the optimization focus was on the hydrogen refrigerant side. The outlet pressure of the second hydrogen expander determined the inlet temper-

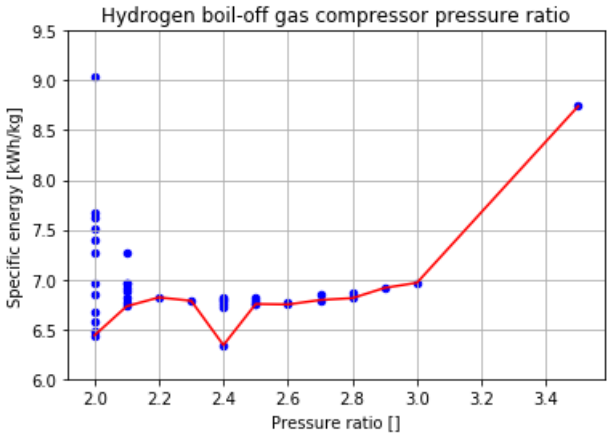

Figure 5.10: The results of specific energy consumption depending on the hydrogen boil-off gas pressure ratio for the hydrogen Claude process with the Joule-Thomson valve.

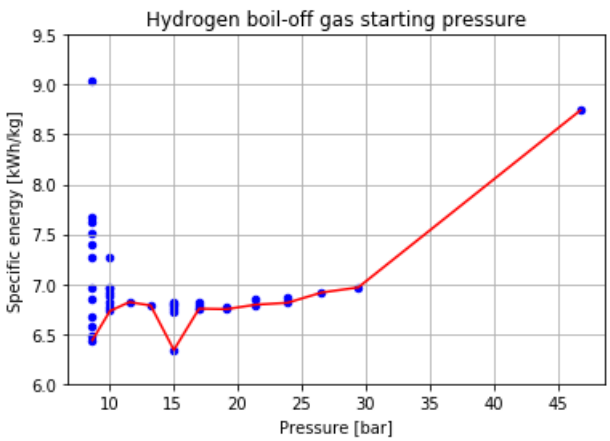

Figure 5.11: The results of specific energy consumption depending on the hydrogen boil-off gas pressure entering the reliquefaction cycle for the hydrogen Claude process with the Joule-Thomson valve.

ature of the refrigerant into the final expander, consequently determining the final liquid fraction after the expansion in the Joule-Thomson valve. Liquid fraction also determined how much boil-off gas needs to be recycled back into the reliquefaction process. The results of the low hydrogen pressure are presented in Figure 5.12, while the results for a pressure ratio of hydrogen refrigerant compressors and consequently high pressure of hydrogen are presented in Figure 5.13 and Figure 5.14.

As seen from the figures, the best setting is the pressure ratio of 2.65 and low pressure of

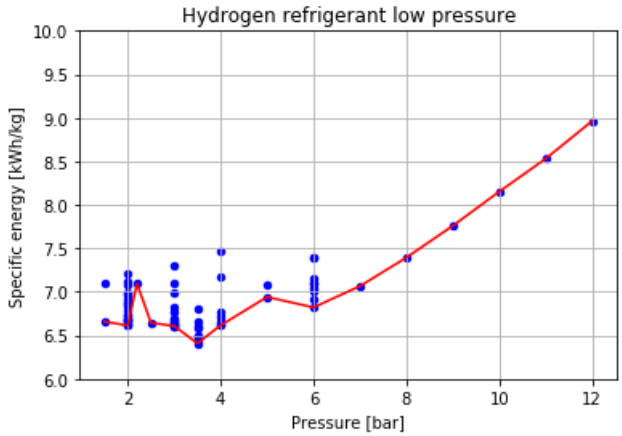

Figure 5.12: The results of specific energy consumption depending on the hydrogen refrigerant second expander outlet pressure for the hydrogen Claude process with the Joule-Thomson valve.

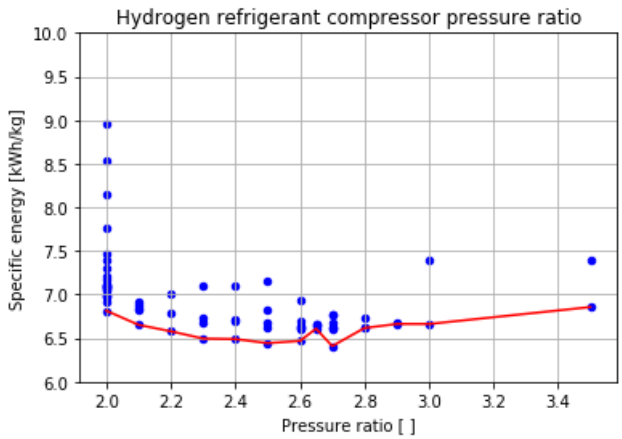

Figure 5.13: The results of specific energy consumption depending on the hydrogen refrigerant compressors pressure ratio for the hydrogen Claude process with the Joule-Thomson valve.

hydrogen refrigerant at $3.5\,\mathrm{bar}$.

5.2.1 The best simulation result

Using the values from the optimization part, the best case for hydrogen is defined. Hydrogen boil-off gas pressure ratio was set on 2.4 and thus the pressure out of the third compressor stage is $15.47\,\mathrm{bar}$ Due to pressure drops in the heat exchangers, hydrogen enters the hydrogen Claude cycle at the pressure of $15.07\,\mathrm{bar}$ and temperature of $-226.6\,°\mathrm{C}$. Hydrogen refrigerant compressors pressure ratio 2.65 and low pressure at the outlet of the second expander is at $3.5\,\mathrm{bar}$. This means that hydrogen refrigerant high pressure was

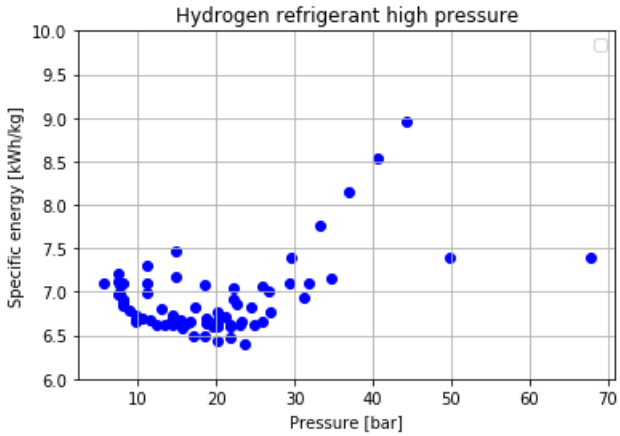

Figure 5.14: The results of specific energy consumption depending on the hydrogen refrigerant high pressure for the hydrogen Claude process with the Joule-Thomson valve

set at $22.7\,\mathrm{bar}$ The result of the specific energy consumption and exergy efficiency was of $6.337\,\mathrm{kW\,h\,kg^{-1}}$ and $32.8\,\%$ respectively, and with potential utilization of $80\,\%$ of the power from hydrogen refrigerant expanders, the specific energy consumption drops by $6.140\,\mathrm{kW\,h\,kg^{-1}}$, and the exergy efficiency, in this case, is $33.9\,\%$.

Hydrogen process is expected to be more efficient than the helium process. This is due to the better fit between the BOG and the refrigerant. The process flow diagram of the hydrogen Claude process with the Joule-Thomson valve is presented in Figure B.1. The main results of the heat exchanger for this process are reported in Table 5.14. The split and composite curves for heat-temperature for every heat exchanger are presented in Figures B.3a, B.3b, B.4a and B.4b in the Appendix. The material balance of the most important streams is given in Table 5.15, while compressors and expanders are given in Table 5.16 and 5.17.

Specification	**HX-1**	**HX-2**	**HX-3**	**HX-4**
LMTD [K]	2.19	2.94	2.03	1.66
$\Delta\mathbf{T_{min}}$[K]	1.50	2	0.51	0.5
Q [kW]	280	1106	62.5	42.9
UA [$\mathrm{kW\,K^{-1}}$]	127.7	376.4	30.8	25.8

Table 5.14: Heat exchangers results for the hydrogen Claude process with the Joule-Thomson valve

In Table 5.15, the main streams and their properties are presented. Other material streams are presented in the Appendix in Table B.2. The results for the compressors and expanders are presented below in Table 5.16 and 5.17. The required power for hydrogen boil-off gas compression was higher due to higher outlet pressure in comparison to the helium refrig-

eration cycle. However, in this case, there was quite a significant decrease in consumption power on the refrigerant side, and this is the main reason that the hydrogen process is more efficient than helium.

Name		H-2	H-4	H-10	H-11	H-12
Vapour Fraction		1.0000	1.0000	1.0000	1.0000	1.0000
Temperature	(C)	-235.0 *	13.50 *	15.00 *	-226.6	-227.7
Pressure	(kPa)	116.0	114.1	1531	1507	1482
Mass Flow	(kg/h)	234.2	276.8	276.8	276.8	276.8
Mass Enthalpy	(kJ/kg)	385.1	4001	4030	388.8	374.8
Mass Entropy	(kJ/kg-C)	36.39	63.61	52.97	26.68	26.43
Name		H-13	H-14	H-15	H-16	H-RCY
Vapour Fraction		0.0000	0.1536	0.0000	1.0000	1.0000
Temperature	(C)	-247.3	-252.4	-252.4	-252.4	-250.0 *
Pressure	(kPa)	1459	116.0 *	116.0	116.0	116.0 *
Mass Flow	(kg/h)	276.8	276.8	234.3	42.52	42.59 *
Mass Enthalpy	(kJ/kg)	-183.2	-183.2	-251.3	192.0	220.9
Mass Entropy	(kJ/kg-C)	10.29	11.49	8.211	29.58	30.90
Name		Hyd-1	Hyd-4	Hyd-5	Hyd-7	Hyd-8
Vapour Fraction		1.0000	1.0000	1.0000	1.0000	1.0000
Temperature	(C)	13.00 *	13.00	14.00	15.00 *	-204.3
Pressure	(kPa)	333.5	855.6	855.6	2245	2209
Mass Flow	(kg/h)	687.7	687.7	1375	1375 *	1375
Mass Enthalpy	(kJ/kg)	4024	4026	4041	4061	1166
Mass Entropy	(kJ/kg-C)	65.02	61.12	61.17	57.23	38.90
Name		Hyd-11	Hyd-13			
Vapour Fraction		1.0000	0.9459			
Temperature	(C)	-222.1	-247.8			
Pressure	(kPa)	883.7	350.0 *			
Mass Flow	(kg/h)	687.7	687.7			
Mass Enthalpy	(kJ/kg)	1003	703.8			
Mass Entropy	(kJ/kg-C)	39.72	34.57			

Table 5.15: Material balance of the main hydrogen boil-off gas and hydrogen refrigerant streams for the hydrogen Claude process with the Joule-Thomson valve

Property	**K-101**	**K-102**	**K-103**	**K-104**	**K-105**
Power [kW]	128.9	129.8	130.2	363.4	733.0
Inlet pressure [bar]	1.14	2.71	6.44	3.33	8.55
Outlet pressure [bar]	2.74	6.51	15.47	8.83	22.67
Adiabatic efficiency [%]	70	70	70	70	70
Polytropic efficiency [%]	73	73	73	74	74

Table 5.16: Power, inlet and outlet pressures, adiabatic and polytropic efficiencies of hydrogen compressors for the hydrogen Claude process with the Joule-Thomson valve

Property	**EXP-101**	**EXP-102**
Power [kW]	30.99	26.85
Inlet pressure [bar]	22.09	21.74
Outlet pressure [bar]	8.83	3.5
Isentropic efficiency [%]	80	80
Polytropic efficiency [%]	77	77

Table 5.17: Power, inlet and outlet pressures, isentropic and polytropic efficiencies of hydrogen refrigerant expanders for the hydrogen Claude process with the Joule-Thomson valve

For comparison, the turbine expander substituted the Joule-Thomson valve. In this case, the best result was based similar to the helium reverse Brayton refrigeration cycle with the liquid expander on the trial and error approach. For the best setting, the hydrogen boil-off gas pressure ratio was set on 2.4 and hydrogen enters the hydrogen Claude cycle at the pressure of $15.07\,\mathrm{bar}$ and temperature of $-226.1\,°\mathrm{C}$. Hydrogen refrigerant compressors pressure ratio and low pressure at the outlet of the second expander were the same as for the case with the Joule-Thomson valve. The result of the specific energy consumption and exergy efficiency was of $6.123\,\mathrm{kW\,h\,kg^{-1}}$ and $33.9\,\%$ respectively, and with potential utilization of $80\,\%$ of the power from hydrogen refrigerant expanders, the specific energy consumption drops by $5.927\,\mathrm{kW\,h\,kg^{-1}}$, and the exergy efficiency, in this case, is $35.06\,\%$.

The results for the heat exchangers are given in Table 5.18. In this case, composite and split curves are not included, because they do not provide any additional relevant information. The main streams are presented in Table 5.19, and other streams are presented in the Appendix in Table B.3. The main results for hydrogen compressors and expanders are given in Table 5.20 and Table 5.21.

The results of the power for the compressors show that in this case, the compression power is smaller for all compressors, and this can be explained by a more efficient polytropic expansion in the turbine expander in comparison to isenthalpic expansion in the Joule-Thomson valve, as shown in Figure 5.8 and Figure 5.9. More efficient expansion results in a lower amount of recycled hydrogen boil-off gas, and consequently, also the compression energy is lower.

Specification	**HX-1**	**HX-2**	**HX-3**	**HX-4**
LMTD [K]	2.19	2.94	2.05	2.46
$\Delta\mathbf{T_{min}}$[K]	1.50	2	0.52	0.51
Q [kW]	265.2	1074	62.8	40.3
UA [$\mathrm{kW\,K^{-1}}$]	121.2	365.6	30.7	16.4

Table 5.18: Results for heat exchangers for the hydrogen Claude process with the expander

5.3 Mixed refrigerant results

As explained in Chapter 4, the mixed refrigerant result in the scope of this thesis was based on the error and trial approach. The hydrogen pressure ratio, in this case, was set at 2, which resulted in the hydrogen pressure at the outlet of the third compressor stage set at around $8.95\,\mathrm{bar}$. Due to pressure drop in the aftercooler and the next heat exchanger HX-1, this means that hydrogen enters the mixed refrigerant reverse Brayton cycle with two expanders at the pressure of $8.72\,\mathrm{bar}$ and temperature of $-229.9\,°\mathrm{C}$. Nelium compressor ratio was set at 1.3 according to assumptions, and low pressure of the cycle was at $7\,\mathrm{bar}$ resulting in high pressure at $23.6\,\mathrm{bar}$. This setting resulted in the values of the specific energy consumption and exergy efficiency of $6.222\,\mathrm{kW\,h\,kg^{-1}}$ and $33.4\,\%$, respectively.

Name		H-2	H-4	H-10	H-11	H-12
Vapour Fraction		1.0000	1.0000	1.0000	1.0000	1.0000
Temperature	(C)	-235.0 *	13.50 *	15.00 *	-226.1	-228.1
Pressure	(kPa)	116.0	114.1	1531	1507	1482
Mass Flow	(kg/h)	234.2	262.8	262.8	262.8	262.8
Mass Enthalpy	(kJ/kg)	385.1	4001	4030	396.2	369.4
Mass Entropy	(kJ/kg-C)	36.39	63.61	52.97	26.83	26.31
Name		H-13	H-14	H-15	H-16	H-RCY
Vapour Fraction		0.0000	0.1086	0.0000	1.0000	1.0000
Temperature	(C)	-247.3	-252.4	-252.4	-252.4	-250.0 *
Pressure	(kPa)	1459	116.0 *	116.0	116.0	116.0 *
Mass Flow	(kg/h)	262.8	262.8	234.2	28.54	28.56 *
Mass Enthalpy	(kJ/kg)	-183.1	-203.1	-251.2	192.0	220.9
Mass Entropy	(kJ/kg-C)	10.29	10.53	8.212	29.58	30.90
Name		Hyd-1	Hyd-4	Hyd-5	Hyd-7	Hyd-8
Vapour Fraction		1.0000	1.0000	1.0000	1.0000	1.0000
Temperature	(C)	13.00 *	13.00	14.00	15.00 *	-204.2
Pressure	(kPa)	333.5	855.6	855.6	2245	2209
Mass Flow	(kg/h)	667.9	667.9	1336	1336 *	1336
Mass Enthalpy	(kJ/kg)	4024	4026	4041	4061	1166
Mass Entropy	(kJ/kg-C)	65.02	61.12	61.17	57.23	38.90
Name		Hyd-11	Hyd-13			
Vapour Fraction		1.0000	0.9351			
Temperature	(C)	-222.0	-247.8			
Pressure	(kPa)	883.7	350.0 *			
Mass Flow	(kg/h)	667.9	667.9			
Mass Enthalpy	(kJ/kg)	1004	699.5			
Mass Entropy	(kJ/kg-C)	39.72	34.40			

Table 5.19: Material balance of the main hydrogen boil-off gas and hydrogen refrigerant streams for the best simulation of the hydrogen Claude process with the liquid expander.

Property	**K-101**	**K-102**	**K-103**	**K-104**	**K-105**
Power [kW]	122.4	123.2	123.6	353.0	711.9
Inlet pressure [bar]	1.14	2.71	6.44	3.33	8.56
Outlet pressure [bar]	2.74	6.51	15.47	8.83	22.67
Adiabatic efficiency [%]	70	70	70	70	70
Polytropic efficiency [%]	73	73	73	74	74

Table 5.20: Power, inlet and outlet pressures, adiabatic and polytropic efficiencies of hydrogen compressors for the best simulation of the hydrogen Claude process with the liquid expander.

Property	**EXP-101**	**EXP-102**	**EXP-103**
Power [kW]	30.11	25.64	1.46
Inlet pressure [bar]	21.74	22.09	14.59
Outlet pressure [bar]	8.83	3.5	1.16
Isentropic efficiency [%]	80	80	80
Polytropic efficiency [%]	77	77	77

Table 5.21: Power, inlet and outlet pressures, isentropic and polytropic efficiencies of hydrogen refrigerant expanders for the best simulation of the hydrogen Claude process with the liquid expander.

However, with potential utilization of $80\,\%$ of the power from helium expanders, the specific energy consumption drops by $6.043\,\mathrm{kW\,h\,kg^{-1}}$, and the exergy efficiency, in this case, is $34.4\,\%$.

These results are presented in the same way as it was before for the other two cases. In

Table 5.22, the results for heat exchangers are presented. Heat splitting and composite curves for every heat exchanger are presented in Figure C.3a, Figure C.3b, Figure C.4a and Figure C.4b in the Appendix. Furthermore, mass balance with the main streams and corresponding properties are included in Table 5.23, while the whole material balance with exergy flows is included in the Appendix in Table C.2. At the end of this section, the results of the compressors and the expanders are given in Table 5.24 and Table 5.25.

Specification	**HX-1**	**HX-2**	**HX-3**	**HX-4**
LMTD [K]	1.94	2.52	1.83	1.01
$\Delta \mathbf{T_{min}}$[K]	1.50	1.42	0.56	0.5
Q [kW]	280.9	1399	70.6	1.02
UA [kW K^{-1}]	144.6	554.7	38.5	1.5

Table 5.22: Main results for heat exchangers for the simulation of mixed refrigerant with the Joule-Thomson valve.

As seen from Table 5.22, pure helium refrigerant is more efficient in terms of heat transfer based on the results. However, it is beneficial for adding neon to reduce compression energy. Figure C.3a, Figure C.3b, Figure C.4a and Figure C.4b all represent fit, which is worse than for helium Brayton cycle. From Table 5.24 it is possible to see that the efficiency of the nelium compressors is higher and the compressor energy consumption is significantly lower in comparison to helium reverse Brayton cycle and hydrogen Claude process.

Name		H-2	H-3	H-7	H-10	H-12
Vapour Fraction		1.0000	1.0000	1.0000	1.0000	1.0000
Temperature	(C)	-235.0 *	-237.4	103.3	15.00 *	-235.8
Pressure	(kPa)	116.0	116.0	452.0	886.0	857.9
Mass Flow	(kg/h)	234.2	277.7	277.7	277.7	277.7
Mass Enthalpy	(kJ/kg)	385.1	359.4	5324	4027	311.9
Mass Entropy	(kJ/kg-C)	36.39	35.69	61.95	55.23	26.78
Name		H-16	H-RCY	HeNe-1	HeNe-11	HeNe-12
Vapour Fraction		0.0000	1.0000	1.0000	1.0000	1.0000
Temperature	(C)	-252.4	-250.0 *	13.00 *	15.00 *	-235.8
Pressure	(kPa)	116.0	116.0 *	664.0	2357	2345
Mass Flow	(kg/h)	234.2	43.49	6834 *	6834	6834
Mass Enthalpy	(kJ/kg)	-251.3	220.9	-35.03	-30.53	-764.3
Mass Entropy	(kJ/kg-C)	8.211	30.90	10.36	8.923	2.868
Name		HeNe-13	HeNe-14	HeNe-15	HeNe-16	HeNe-17
Vapour Fraction		1.0000	0.9469	0.9135	0.9162	1.0000
Temperature	(C)	-243.5	-245.7	-247.5 *	-247.5	-241.7
Pressure	(kPa)	1172	1160	700.0 *	688.0	676.0
Mass Flow	(kg/h)	6834	6834	6834	6834	6834
Mass Enthalpy	(kJ/kg)	-781.9	-799.8	-809.8	-809.0	-771.8
Mass Entropy	(kJ/kg-C)	3.019	2.393	2.491	2.538	3.913

Table 5.23: Material balance of the main hydrogen and helium streams for the simulation of mixed refrigerant with the Joule-Thomson valve.

In the same way as for the other alternatives, also the case with the liquid expander is presented. The best case was also based on trial and error approach and results are presented later on. The hydrogen pressure ratio, in this case, was set at 2, which resulted in the hydrogen pressure at the outlet of the third compressor stage set at around $8.95\,\mathrm{bar}$. Due to pressure drop in the aftercooler and the next heat exchanger HX-1, this means that hydrogen enters the mixed refrigerant reverse Brayton cycle with two expanders at the pressure of $8.72\,\mathrm{bar}$ and temperature of $-229.7\,°\mathrm{C}$. Nelium compressor ratio was set at

Property	K-101	K-102	K-103	K-104	K-105	K-106	K-107	K-108
Power [kW]	99.7	100.3	100.5	230.7	231.7	231.7	231.7	220.7
Inlet pressure [bar]	1.14	2.26	4.48	6.64	8.51	10.95	14.11	18.22
Outlet pressure [bar]	2.28	4.52	8.95	8.63	11.07	14.23	18.34	23.69
Adiabatic efficiency [%]	70	70	70	75	75	75	75	75
Polytropic efficiency [%]	73	73	73	76	76	76	76	76

Table 5.24: Power, inlet and outlet pressures, adiabatic and polytropic efficiencies of hydrogen and nelium compressors for the simulation of mixed refrigerant with the Joule-Thomson valve.

Property	EXP-101	EXP-102
Power [kW]	33.3	19.0
Inlet pressure [bar]	23.45	11.6
Outlet pressure [bar]	11.7	37.00
Isentropic efficiency [%]	80	80
Polytropic efficiency [%]	78	79

Table 5.25: Power, inlet and outlet pressures, isentropic and polytropic efficiencies of hydrogen and nelium expanders for the simulation of mixed refrigerant with the Joule-Thomson valve.

1.3 according to assumptions, and low pressure of the cycle was at 7 bar resulting in high pressure at 23.6 bar. This resulted in the values of the specific energy consumption and exergy efficiency of $5.985\,\mathrm{kW\,h\,kg^{-1}}$ and 34.8 %, respectively. However, with potential utilization of 80 % of the power from helium expanders, the specific energy consumption drops by $5.804\,\mathrm{kW\,h\,kg^{-1}}$, and the exergy efficiency, in this case, is 35.8 %.

Presentation of results is done in the same way as it was before for other cases. In Table 5.26, the results for heat exchangers are presented. Also, mass balance with the main streams and corresponding properties are included as well in Table 5.27. The whole material balance is presented in Table C.3. At the end of this section, the results of the compressors and the expanders are given in Table 5.28 and Table 5.29.

Specification	HX-1	HX-2	HX-3	HX-4
LMTD [K]	1.94	2.53	1.80	1.01
ΔT_{min}[K]	1.50	1.49	0.5	0.5
Q [kW]	270.5	1357	68.9	1.44
UA [$\mathrm{kW\,K^{-1}}$]	139.4	537.1	38.4	1.4

Table 5.26: Heat exchangers results for the simulation of mixed refrigerant with the liquid expander.

Name		H-2	H-3	H-7	H-10	H-12
Vapour Fraction		1.0000	1.0000	1.0000	1.0000	1.0000
Temperature	(C)	-235.0 *	-237.4	103.3	15.00 *	-235.8
Pressure	(kPa)	116.0	116.0	452.0	886.0	857.9
Mass Flow	(kg/h)	234.2	277.7	277.7	277.7	277.7
Mass Enthalpy	(kJ/kg)	385.1	359.4	5324	4027	311.9
Mass Entropy	(kJ/kg-C)	36.39	35.69	61.95	55.23	26.78
Name		H-16	H-RCY	HeNe-1	HeNe-11	HeNe-12
Vapour Fraction		0.0000	1.0000	1.0000	1.0000	1.0000
Temperature	(C)	-252.4	-250.0 *	13.00 *	15.00 *	-235.8
Pressure	(kPa)	116.0	116.0 *	664.0	2357	2345
Mass Flow	(kg/h)	234.2	43.49	6834 *	6834	6834
Mass Enthalpy	(kJ/kg)	-251.3	220.9	-35.03	-30.53	-764.3
Mass Entropy	(kJ/kg-C)	8.211	30.90	10.36	8.923	2.868
Name		HeNe-13	HeNe-14	HeNe-15	HeNe-16	HeNe-17
Vapour Fraction		1.0000	0.9469	0.9135	0.9162	1.0000
Temperature	(C)	-243.5	-245.7	-247.5 *	-247.5	-241.7
Pressure	(kPa)	1172	1160	700.0 *	688.0	676.0
Mass Flow	(kg/h)	6834	6834	6834	6834	6834
Mass Enthalpy	(kJ/kg)	-781.9	-799.8	-809.8	-809.0	-771.8
Mass Entropy	(kJ/kg-C)	3.019	2.393	2.491	2.538	3.913

Table 5.27: Material balance of the main hydrogen and helium streams for the simulation of mixed refrigerant with the liquid expander.

Property	**K-101**	**K-102**	**K-103**	**K-104**	**K-105**	**K-106**	**K-107**	**K-108**
Power [kW]	96.2	96.8	96.9	223.3	224.8	224.8	224.8	224.9
Inlet pressure [bar]	1.14	2.26	4.48	6.64	8.51	10.95	14.11	18.22
Outlet pressure [bar]	2.28	4.52	8.95	8.63	11.07	14.23	18.34	23.69
Adiabatic efficiency [%]	70	70	70	75	75	75	75	75
Polytropic efficiency [%]	73	73	73	76	76	76	76	76

Table 5.28: Power, inlet and outlet pressures, adiabatic and polytropic efficiencies of hydrogen and nelium compressors for the simulation of mixed refrigerant with the liquid expander

Property	**EXP-101**	**EXP-102**	**EXP-103**
Power [kW]	32.4	18.5	1.0
Inlet pressure [bar]	23.45	11.6	8.31
Outlet pressure [bar]	11.72	7.00	1.16
Isentropic efficiency [%]	80	80	80
Polytropic efficiency [%]	78	78	78

Table 5.29: Power, inlet and outlet pressures, isentropic and polytropic efficiencies of hydrogen and nelium expanders for the simulation of mixed refrigerant with the liquid expander

5.4 Exergy analysis

For exergy analysis, only processes with the Joule-Thomson valve and without turbine expander energy utilization are compared, because it is especially important to directly contrast process alternatives. This means that processes that use the liquid expander instead are not included in this part of the analysis. As explained before, the minimum liquefaction energy for these processes was $2.078\,\mathrm{kW\,h\,kg^{-1}}$. In Table 5.30 and in Table 5.31, the main three process alternatives are presented; helium reverse Brayton cycle, hydrogen Claude cycle, and nelium reverse Brayton cycle. The results needed for calculation of irreversibilities are given in the Appendix for every case separately in Table A.2, Table B.2 and Table C.2.

As seen from Table 5.30, the most efficient is the nelium process and the least efficient is

Specifications	Helium process	Hydrogen process	Nelium process
SEC [$\mathrm{kW\,h\,kg^{-1}}$]	6.528	6.337	6.222
ψ [%]	31.8	32.8	33.4
$\mathbf{ex_{dest,cum}}$ [$\mathrm{kW\,h\,kg^{-1}}$]	4.430	4.244	4.136

Table 5.30: Comparison of main alternatives in terms of specific energy consumption, exergy efficiency and cumulative specific irreversibilities.

the helium process. Therefore, most irreversibilities are accumulated in the helium process, followed by the hydrogen process, while the most efficient is the nelium process. There is a small difference between cumulative irreversibilities and the result obtained if minimum liquefaction specific energy is subtracted from the total specific energy consumption. This is due to exergy destruction in the pipe - the pipe was installed before the recycle to avoid a phase change in the recycle and in the recycle itself, as there was a slight difference between inlet and outlet mass flows.

In Table 5.31, specific irreversibilities, or specific exergy destruction per mass of produced liquid hydrogen are presented for every part of the process. These results enable comparison and detection wherein the process improvements can be made. To graphically compare them, it is possible to use Figure 5.15. The detailed results of irreversibilities and exergy efficiencies of every part of the equipment are presented in Tables 5.33, 5.34 and 5.35, 5.36, 5.37 and 5.38 and the exergy flows of the stream are in the Appendix Table A.2, Table A.2 and Table C.2.

Specifications	Helium process	Hydrogen process	Nelium process
Ref turbines	0.992	0.795	0.833
Ref compressors	1.184	1.024	1.095
Ref coolers	0.878	0.841	0.447
BOG compressors	0.287	0.373	0.306
BOG coolers	0.162	0.271	0.173
Heat exchangers	0.871	0.826	1.202
JT valve	0.056	0.114	0.080
Cumulative	4.430	4.244	4.136

Table 5.31: Comparison of specific irreversibilities for different parts of the process in $\mathrm{kW\,h\,kg^{-1}}$ of liquid hydrogen

As seen from Figure 5.15, the largest exergy destruction is related to heat exchangers and refrigerant compressors. Nelium cycle has the largest exergy destruction related to heat exchangers. Probably, the main reason for this is that the result is based only on the trial and error approach. Therefore, the fit between the hot and cold composite curves is the worst. This means that the nelium refrigeration cycle even in the existing form has a larger room for improvements in comparison to helium and hydrogen refrigeration cycles. However, according to the results for individual heat exchanger, the largest amount of

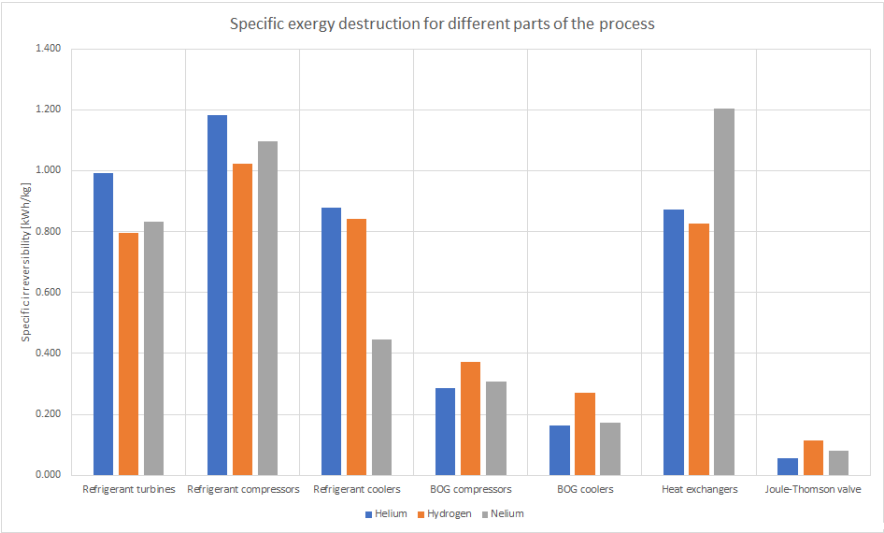

Figure 5.15: Comparison of irreversibilities for all three different parts of the process

exergy destruction comes from cooling in the heat exchanger HX-2 where the refrigerant is cooled from the ambient temperature. This means that it is possible to significantly improve the process by implementing the precooling cycle, and this is valid for every alternative.

On the other side, for the processes with helium refrigerant and hydrogen refrigerant, the largest irreversibilities are related to refrigerant compressors and coolers and refrigerant turbines. To reduce the irreversibilities in the refrigerant compressors, it is necessary to increase the efficiency of the compressors. For coolers, it would be possible to reduce irreversibilities by using heat from the refrigerant to warm up water needed for district heating, but the system would become more complex and for a limited scale, it is most likely not viable. On the other side, an example of an alternative way of irreversibility reduction would be to lower the temperature of an inlet to the first stage of hydrogen and helium compressors, thus reducing irreversibilities. This would be particularly effective for helium compression because it would be possible to use just one compressor stage instead of two. The reason behind this is that oil-screw compressors can have a significantly higher-pressure ratio. However, in this case, compression work would be higher and it is questionable, whether the benefits would outweigh the drawbacks. Anyway, this kind of challenge should be left to a detailed design study, which needs to be done for every real case separately. On the other side, exergy destruction related to turbine expanders would be lower, if the produced energy from the expanders would be used. However, in this case, it would be necessary to use the turbo compound engine, but this is most likely feasible only for large amounts of boil-off gas, and this should also part of the detailed design.

It can be observed that utilizing at the same time hydrogen boil-off gas compression and

coolers are not related to significant irreversibilities. The main reason for this is that hydrogen boil-off gas mass flow is significantly lower than refrigerant. The second reason is that the outlet pressure after the compression train is not very high. However, hydrogen boil-off gas compression has an indirect impact also on other components. Therefore, it is important to develop more efficient ways of hydrogen compression, which would possibly reduce irreversibilities.

5.5 Comparison of processes

To summarize results, in these section key performance indicators and process flow diagrams with the most important temperatures, pressure and mass flows are presented. Only process flow diagrams of alternatives with the Joule-Thomson valve are provided, while key performance indicators of all options are given in Table 5.32. Furthermore, data of the three alternatives with pressures, temperatures and mass flows of main streams are presented in Figures 5.16, 5.17, 5.18. In the end, there are data on selected crucial components for every of the main three cases with the Joule-Thomson valve. Key performance indicators are stated for every compressor stage, turbine expander, Joule-Thomson valve, and, the last but not the least, heat exchangers. Data for heat exchangers are given in Table 5.33 to 5.34 and 5.35. For compressors, data is given in Tables 5.36, 5.37 and 5.38.

Specifications	**Helium process**	**Hydrogen process**	**Nelium process**
Joule-Thomson valve without utilization			
SEC [$\mathrm{kW\,h\,kg^{-1}}$]	6.528	6.337	6.222
ψ [%]	31.8	32.8	33.4
Joule-Thomson valve with utilization			
SEC [$\mathrm{kW\,h\,kg^{-1}}$]	6.317	6.140	6.043
ψ [%]	32.9	33.9	34.4
Liquid expander without utilization			
SEC [$\mathrm{kW\,h\,kg^{-1}}$]	6.343	6.123	6.027
ψ [%]	32.8	33.9	34.5
Liquid expander with utilization			
SEC [$\mathrm{kW\,h\,kg^{-1}}$]	6.134	5.927	5.850
ψ [%]	33.9	35.0	35.5

Table 5.32: Comparison of specific energy consumption and exergy efficiencies of all alternatives

As seen from Table 5.32, the most efficient process for all alternatives is the nelium process, and even this one has still significant room for improvement especially related to heat exchangers, as discussed in the Exergy analysis part. On the other side, the hydrogen refrigerant process is more efficient than the one with helium as a refrigerant. From the energy point of view, it is beneficial to utilize generated power from turbine expanders, but in reality, this depends on the economic analysis. On the other side, the usage of turbine liquid expanders instead of the Joule-Thomson valve is beneficial from the energy point of view. However, there have yet to be developed liquid expanders for liquid hydrogen, and

at this point, this would be simply too expensive. Furthermore, the benefits in BOG reliquefaction are smaller than for hydrogen liquefaction processes due to the lower pressure of hydrogen feed. This means that at this point it is most likely not economically viable to use liquid expanders at all, but this might change in the future with standardization of the liquid expanders for pure hydrogen. Even more: if hydrogen compression becomes more efficient, it will be even more beneficial to increase pressure in the BOG reliquefaction cycles.

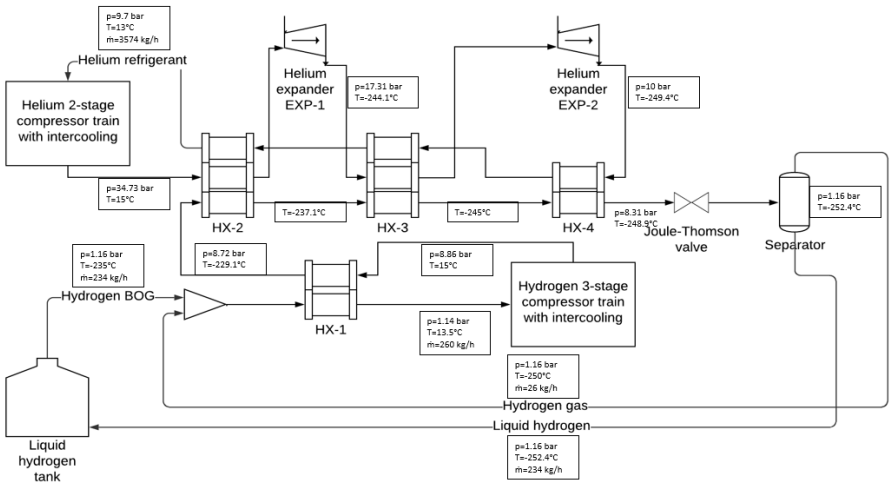

Figure 5.16: Helium refrigeration cycle process flow diagram with pressures, temperatures and mass flows of main streams

Tables for heat exchangers are Table 5.33 to 5.34 and 5.35. For compressors Tables 5.36, 5.37 and 5.38. For compressors, it is worth noticing that for nelium process the number of required compressors is significantly larger than for helium and hydrogen. This means that, several compressor stages are needed increasing investment costs and also operational costs. On the other side, it is important to emphasize that only one helium compressor stage could be used instead of two. This would reduce investment costs and also operational cost. In general for compression, there are only three different compressors; piston compressors, oil-screw compressors and turbo compressors. While, piston compressors are state of the art component for hydrogen compression and oil-screw compressors are state of the art component for helium compression, turbo compressors are relatively expensive to use with mixtures of helium and neon. In comparison liquid neon is significantly more expensive than helium, but they are both significantly more expensive than hydrogen and also harder to get. Therefore, it seems that hydrogen process is the best option. From heat exchangers results it is possible to see that high HX-1 and HX-2 have significantly higher UA product, which determines the size based on the fluid properties. In this case, it is necessary to do a detail design of all heat exchangers to estimate cost of these processes.

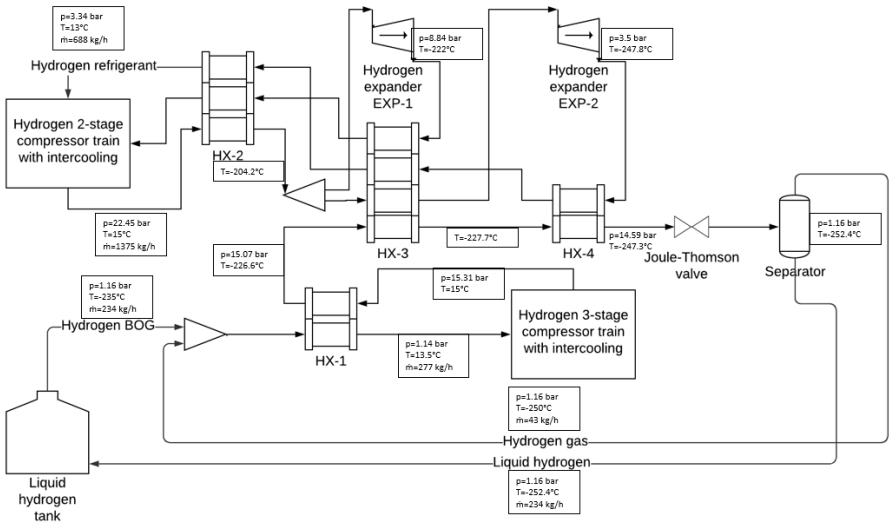

Figure 5.17: Hydrogen refrigeration cycle process flow diagram with pressures, temperatures and mass flows of main streams

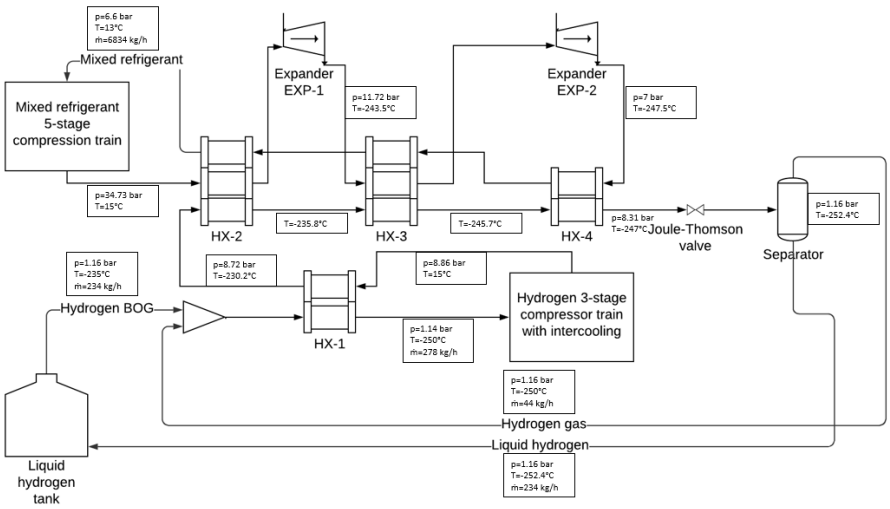

Figure 5.18: Nelium refrigeration cycle process flow diagram with pressures, temperatures and mass flows of main streams

Specification	**HX-1**	**HX-2**	**HX-3**	**HX-4**
Type	PFHX	PFHX	PFHX	PFHX
No. Sides	2	3	3	2
LMTD [K]	1.9	2.1	1.9	1.7
UA [$\mathrm{kW\,K^{-1}}$]	135.5	639.4	19.1	2.4
Δ**T$_{\mathbf{min}}$** [K]	1.5	0.5	0.5	0.5
Q[kW]	262.6	1318.0	36.9	4.1
ψ [percent]	92.0	93.8	87.3	79.9
$\dot{\mathbf{E}}\mathbf{x}_{\mathbf{dest}}$[kW]	25.0	123.9	44.8	10.3

Table 5.33: Heat exchangers for the process with helium refrigerant.

Specification	**HX-1**	**HX-2**	**HX-3**	**HX-4**
Type	PFHX	PFHX	PFHX	PFHX
No. Sides	2.0	3.0	4.0	2.0
LMTD [K]	2.2	2.9	2.0	1.7
UA [$\mathrm{kW\,K^{-1}}$]	127.8	376.4	31.2	25.9
Δ**T$_{\mathbf{min}}$** [K]	1.5	2.0	0.5	0.5
Q[kW]	280.1	1105.9	62.6	42.9
ψ [percent]	89.4	91.0	89.6	89.3
$\dot{\mathbf{E}}\mathbf{x}_{\mathbf{dest}}$[kW]	35.9	90.1	30.0	37.6

Table 5.34: Heat exchangers for the process with hydrogen refrigerant

Specification	**HX-1**	**HX-2**	**HX-3**	**HX-4**
Type	PFHX	PFHX	PFHX	PFHX
No. Sides	2	3	3	2
LMTD	1.9	2.5	1.8	1.0
UA [$\mathrm{kW\,K^{-1}}$]	144.6	554.7	38.5	1.5
Δ**T$_{\mathbf{min}}$** [K]	1.5	1.4	0.6	0.5
Q[kW]	280.9	1398.6	70.6	1.5
ψ [percent]	91.9	91.7	90.0	59.1
$\dot{\mathbf{E}}\mathbf{x}_{\mathbf{dest}}$[kW]	27.6	175.7	68.4	9.9

Table 5.35: Heat exchangers for the process with nelium refrigerant

Specification	**K-101**	**K-102**	**K-103**	**K-104**	**K-105**
Fluid	Hydrogen	Hydrogen	Hydrogen	Helium	Helium
Type	Piston	Piston	Piston	Oil-screw	Oil-screw
P [kW]	93.4	94.0	94.2	620.2	627.6
$\dot{\mathbf{m}}$ [$\mathrm{kg\,h^{-1}}$]	260.2	260.2	260.2	3573.6	3573.6
ψ [%]	76.1	76.2	76.2	77.7	77.9
$\dot{\mathbf{E}}\mathbf{x}_{\mathbf{dest}}$[kW]	22.4	22.4	22.4	138.3	139.0

Table 5.36: Compressors for the process with helium refrigerant

Specification	**K-101**	**K-102**	**K-103**	**K-104**	**K-105**
Fluid	Hydrogen	Hydrogen	Hydrogen	Hydrogen	Hydrogen
Type	Piston	Piston	Piston	Piston	Piston
P [kW]	128.9	129.8	130.3	363.4	732.9
$\dot{\mathbf{m}}$ [$\mathrm{kg\,h^{-1}}$]	276.9	276.9	276.9	687.6	1375.0
ψ [%]	77.4	77.6	77.6	78.3	78.3
$\dot{\mathbf{E}}\mathbf{x}_{\mathbf{dest}}$[kW]	29.1	29.1	29.2	79.0	158.7

Table 5.37: Compressors for the process with hydrogen refrigerant

Unit	**Fluid**	**Type**	**P** [kW]	$\dot{\mathbf{m}}$ [$\mathrm{kg\,h^{-1}}$]	ψ [%]	$\dot{\mathbf{E}}\mathbf{x}_{\mathbf{dest}}$[kW]
K-101	Hydrogen	Piston	99.7	277.7	76.1	23.9
K-102	Hydrogen	Piston	100.3	277.7	76.2	23.9
K-103	Hydrogen	Piston	100.5	277.7	76.6	23.9
K-104	nelium	Turbo	230.1	6834.0	77.7	51.3
K-105	nelium	Turbo	231.7	6834.0	77.9	51.3
K-106	nelium	Turbo	231.7	6834.0	77.9	51.3
K-107	nelium	Turbo	231.7	6834.0	77.9	51.3
K-108	nelium	Turbo	231.7	6834.0	77.9	51.3

Table 5.38: Compressors for the process with nelium refrigerant

Specifications	**EXP-101**	**EXP-102**	**JT valve**
Fluid	Helium	Helium	Hydrogen
P [kW]	38.6	23.3	\
Polytropic η	77.6	78.2	\
$\dot{\mathbf{m}}$ [$\mathrm{kg\,h^{-1}}$]	3573.6	3573.6	260.2
ψ [%]	28.1	24.4	98.4
$\dot{\mathbf{E}}\mathbf{x}_{\mathbf{dest}}$[kW]	137.0	95.5	13.1

Table 5.39: The Turbine expanders and the Joule-Thomson valve for the process with helium refrigerant

Specifications	**EXP-101**	**EXP-102**	**JT valve**
Fluid	Hydrogen	Hydrogen	Hydrogen
P [kW]	31.0	26.8	\
Polytropic η	76.8	76.8	\
$\dot{\mathbf{m}}$ [$\mathrm{kg\,h^{-1}}$]	687.6	687.6	276.9
ψ [%]	40.7	35.2	96.9
$\dot{\mathbf{E}}\mathbf{x}_{\mathbf{dest}}$[kW]	76.2	103.3	26.6

Table 5.40: The Turbine expanders and the Joule-Thomson valve for the process with hydrogen refrigerant

Specifications	**EXP-101**	**EXP-102**	**JT valve**
Fluid	Nelium	Nelium	Hydrogen
P [kW]	33.3	19.0	\
Polytropic η	77.9	79.4	\
$\dot{\mathbf{m}}$	6834.0	6834.0	277.7
ψ [%]	28.6	26.2	97.8
$\dot{\mathbf{E}}\mathbf{x}_{\mathbf{dest}}$[kW]	116.2	72.7	18.7

Table 5.41: The Turbine expanders and the Joule-Thomson valve for the process with nelium refrigerant

Chapter 6

Conclusion

In this master's thesis, based on preliminary elimination, three alternative processes for hydrogen boil-off gas reliquefaction were simulated, analyzed, and compared. These selected processes, helium Brayton refrigeration cycle with two helium turbine expanders, hydrogen Claude refrigeration cycle with two hydrogen expanders, and Brayton refrigeration cycle with two expanders for the mixture of helium and neon called "nelium", are considered the most promising basic concepts. While the simulation analysis was focused on lowering energy consumption, the relevant theoretical framework is laid out, the literature overview is presented, and practical implementation aspects are considered beyond this analytical goal.

From an exclusively energy related perspective, the Brayton refrigeration process involving nelium proves to be the most efficient option for hydrogen boil-off gas reliquefaction. In the version with using the Joule-Thomson valve, the specific energy consumption is $6.222\,\mathrm{kW\,h\,kg^{-1}}$ and exergy efficiency of $33.4\,\%$. The second most efficient option is the hydrogen Claude refrigeration cycle, with $6.337\,\mathrm{kW\,h\,kg^{-1}}$ and an exergy efficiency of $32.8\,\%$. The least efficient among three options considered is the helium reverse Brayton refrigeration process, with $6.528\,\mathrm{kW\,h\,kg^{-1}}$ and exergy efficiency of $33.4\,\%$.

These results, however, should be taken as first assessment values only within the specific context of the relevant assumptions. The results also present numerous uncertainties. The main uncertainties are connected to compressor and turbine expander efficiencies. Furthermore, results are obtained through equations of state that require verification and validation. Energy consumption is not the only relevant key performance indicator, and it is also unlikely to be the most important one. Energy efficiency must be weighted with investment efficiency, but this ambitious task was not possible within this master thesis due to the many uncertainties that need to be addressed in a detailed study. Regardless, this thesis provides a systematic approach to energy efficiency evaluation of optional solutions for the increasingly relevant BOG challenge. Moreover, the thesis provides a helpful framework for open issues to be considered for a possible detailed study and economic

analysis.

One of the most interesting conclusions based on the results is that, theoretically, it is not beneficial to compress hydrogen boil-off gas prior the reliquefaction cycle, specifically in cases involving state of the art hydrogen compressors. This is due to a relatively low efficiency of hydrogen compression in piston compressors. Based on the simulation, certain pressure increases were beneficial, but these values were still significantly lower than for most hydrogen liquefaction processes with pressure at the inlet of refrigeration process, from around $21\,\mathrm{bar}$ and up to $80\,\mathrm{bar}$. Compression work in these cases is usually smaller because natural gas steam reforming, autothermal reforming, and electrolysis, the most common ways of producing hydrogen, all deliver hydrogen at elevated pressures. It is also important to emphasize that specific energy consumption for these liquefaction processes is calculated without necessary hydrogen compression.

An important goal of this thesis was to estimate whether it is beneficial to implement the liquid turbine expander instead of the Joule-Thomson valve. Based on the results obtained, it can be concluded that the difference in the ratio between the gas and liquid phase was not substantial at the combination of a relatively low pressure of compressed hydrogen boil-off and the temperatures needed to reliquefy a sufficient part of the boil-off gas. Furthermore, liquid expanders for hydrogen are not yet standardized components, and they are not only much more expensive, but also more complex to operate. Therefore, at this moment, processes with liquid expanders are not believed to be economically viable. However, this may change in the future with emerging new technologies.

From exergy analysis, it was concluded that potential precooling cycles could significantly improve the performance of these processes. However, these precooling processes were not included in the simulations as their feasibility depends strongly on investment and operational cost, availability of industrial gases, utilities, and other factors that are beyond the scope of this master thesis. From the exergy analysis, it was also concluded that the nelium cycle has the largest exergy destruction related to heat exchangers. The most probable reason for this is that the result is based only on a trial and error approach. Therefore, the fit between the hot and cold composite curves is the worst. This means that the nelium refrigeration cycle even in the existing form has significant room for improvement, which is not the case for helium and hydrogen processes.

Although the economic analysis was not done within this thesis, it is important to emphasize that the nelium mixed refrigerant process has the largest number of required compressors. This is to say that several compressor stages are needed, leading to increased investment and operational costs. It is important to emphasize, however, that a single helium compressor stage could be used instead of two. This would potentially reduce investment costs. Another important aspect is the price of these refrigerants. While liquid neon is more expensive than helium, they are both significantly more expensive than hydrogen because of their relative rarity. Therefore, it seems that the hydrogen process may be the best value-for-money option. In general, hydrogen liquefaction processes require larger investment costs, but they have lower operational costs in comparison to helium

liquefaction processes.

Based on the results from this thesis, it is not possible to simply conclude which are the best options for BOG reliquefaction, because this strongly depends on a variety of factors including the different applications, the liquid hydrogen market, prices of electricity and natural gas, available utilities at the location, available space, among others. However, it is possible to present some guidelines. For example, for large scale storage tanks, it is appropriate to use the hydrogen Claude refrigeration process or mixed refrigerant Brayton refrigeration process with neon and helium as a mixture. Perhaps soon hydrogen should also be included within this mix. For small scale storage tanks that require boil-off gas reliquefaction, the helium cycle is the best option with the lowest investment costs, the lowest number of equipment and with less complex safety measures in comparison to hydrogen.

The topic of this thesis is boil-off gas handling, therefore it is necessary to consider also other possibilities besides reliquefaction. Which option is the best for any given situation depends mostly on the price of hydrogen in comparison to electricity and natural gas prices. If hydrogen price is significantly higher than electricity and natural gas, it is likely a better option to reliquefy boil-off gas. If the difference is smaller, however, it should be primarily utilized only if there are available consumers for hydrogen itself or for electric and heat energy. At the moment, it is believed that the best way to handle hydrogen BOG at large receiving terminals is to use a combination of refrigeration cycles with hydrogen or mixed refrigerant with potential precooling of liquid nitrogen or LNG or similar as well as a heat generation and power system on-site, via fuel cells. In the future, as the number of pipeline networks connected to these receiving terminals increases, and if there is clear demand, the easiest way to handle BOG may be to send it directly through the pipeline to the consumers. In the small-sized receiving terminals, the best primary option is to use fuel cells to generate power on-site, with the best additional option would be to use a simpler reverse Brayton helium refrigeration cycle to reliquefy boil-off gas. If liquid hydrogen carriers can utilize BOG, a less complex reliquefaction cycle can then be used. If, though, the carriers use other fuel for propulsion and ancillary services, the more complex reliquefaction cycle needs to be installed. For other vehicles such as trains, buses, and trucks, it would hardly be feasible to use any BOG handling systems. In this case, BOG should be exchanged at hydrogen stations and different reliquefaction cycles or utilization alternatives should be designed there to handle BOG, depending, of course, on the size and demand for hydrogen gas in the area.

The addressed research topic is interesting, indisputably relevant, applicable, complex, and challenging – from both a research and industry perspective. While research typically opens more questions than provides definite answers, this thesis hopefully also provides some useful insights for future research steps.

Chapter 7

Proposal for future research

At this point, there is a scarcity of research focused on hydrogen boil-off gas. This can partially be explained by only relatively small liquid hydrogen plants currently being in operation. However, this is likely to change soon as the public, industry, and research community are intensively searching for the best options to answer looming eco-energy challenges.

Within the scope of this thesis and design, certain topics could not be covered and, thus, future work is needed. Foremost among these topics, it is crucially important to verify and validate thermodynamic data obtained from Aspen HYSYS software with the thermodynamic library called ThermoPack from SINTEF resarch organization. It is especially important to verify which equations of state give results with enough accuracy to feasibly be used in process simulation design and optimization.

Furthermore, while this thesis does not provide an economic assessment of design options, it covers an important research aspect that should be addressed in the future. For this step, a detailed design of the entire process equipment is necessary, as well as detailed studies of all main process components. These include oil-screw compressors, which, in this case, it is particularly important to investigate the influence on performance by fluid properties, such as temperature, pressure, and mass flows , and so on. Additionally, the same investigative studies need to be done for the performance of hydrogen piston compressors and turbo compressor under different concentrations of mixtures of helium, neon, and hydrogen with changing fluid properties, heat exchangers, turbines and air or water coolers. All these details are also necessary to provide a relevant cost analysis. While this thesis provides general concepts and a systematic assessment of their energy efficiency, cost analysis should be based on specific equipment options. Even if, in general, more expensive equipment is expected to yield better energetic results, the relevant question for the industry is marginal investment analysis, when additional investment outweighs additional financial savings from a better and more expensive design setting. In this view, the detailed design must assess the specific contribution in the energy efficiency of each element versus its

financial cost in terms of procurement and the whole life cycle expenses.

Different reliquefaction concepts must be developed for different specific needs, such as different sizes of reservoir tanks, different applications such as storage tanks at the receiving terminals, liquid hydrogen carriers, and so on. It is very important to dedicate research to the influence of different sizes, shapes, and other properties of storage tanks on the amount of boil-off gas. Also, ambient conditions influencing boil-off gas must be considered. Properties of equilibrium boil-off gas differ, e.g. from the reservoir tank, and this further changes energy consumption of the process.

This thesis provides general concepts and their analysis as needed for general comparisons. For this purpose, the applied simulation algorithms served well. In future research, it is necessary to develop and implement more sophisticated algorithms in an external numerical computing environment to optimize these processes for every process application and concept.

It was not part of this thesis, but it is both interesting and necessary to futurely develop and analyze the reliquefaction process with the mixed refrigerant of neon, hydrogen, and helium, to explore mixtures, and to give best results from energy and economic point of view. There are still uncertainties regarding the performance of turbo compressors in the case of mixtures, and also in the conditions when it would be beneficial to use them. Regarding hydrogen boil-off gas, the possibility of additional buffer tanks should be explored, as short-term storage options for boil-off gas could be a promising research field with important practical implementation consequences. These buffer tanks should be able to stand higher pressures, so that hydrogen boil-off gas compression would not be so energy-intensive to reliquefy boil-off.

Another important research aspect outside the scope of this thesis is the development of the precooling process concepts for reservoir tanks at receiving terminals, liquid hydrogen carriers, and hydrogen filling stations. These are all likely to be the only viable alternatives where boil-off gas reliquefaction processes are feasible. In this case, it is important to consider which compounds are available and suitable for different alternatives.

In the end, it is important to stress that all applications of possible BOG handling must be systematically reviewed and addressed in the research and development field. In this thesis, the focus was solely on the BOG total reliquefaction process, but other alternatives must be considered systematically and comparably, including heat and power generation in fuel cells, partial reliquefaction, which is the case for LOPEX process from Linde, and other options.

This thesis addresses a small subset of the relevant research questions from the field of BOG and its reliquefaction, but this is a promising and rich scientific area, and future intensive activities and advances can be expected.

Bibliography

Aasen, A., Hammer, M., Müller, E.A., Wilhelmsen, Ø., 2020. Equation of state and force fields for feynman–hibbs-corrected mie fluids. II. application to mixtures of helium, neon, hydrogen, and deuterium. The Journal of Chemical Physics 152, 074507.

Airproducts, 2013. Large LNG plant capabilities for capacity ¿ 2 MTPA. Technical Report. Air products and chemicals, Inc.

Alekseev, A., 2015. Basics of Low-temperature Refrigeration , 111–139. 20.

Ashour, I., Al-Rawahi, N., Fatemi, A., Vakili-Nezh, G., 2011. Applications of equations of state in the oil and gas industry, in: Thermodynamics - Kinetics of Dynamic Systems. InTech.

Bacquart, T., Murugan, A., Carre, M., Gozlan, B., Aupretre, F., Haloua, F., Aarhaug, T., 2018. Probability of occurrence of 14687-2 contaminants in hydrogen: Principles and examples from steam methane reforming and electrolysis (water and chlor-alkali) production processes model. International Journal of Hydrogen Energy 43, 11872–11883.

Berstad, D., Skaugen, G., Wilhelmsen, Ø., 2019. Concepts for efficient hydrogen liquefaction. Technical Report. SINTEF.

Berstad, D.O., Stang, J., Nekså, P., 2010. Large-scale hydrogen liquefier utilising mixed-refrigerant pre-cooling. International Journal of Hydrogen Energy 35, 4512–4523.

Bloch, H.P., Soares, C., 2001. Turboexpanders and Process Applications. Elsevier.

Bracha, M., Lorenz, G., Patzelt, A., Wanner, M., 1994. Large-scale hydrogen liquefaction in germany. International Journal of Hydrogen Energy 19, 53–59.

Brun, A. (Ed.), 1997. Spectra and Pulse Shapes of a Decoupled Liquid Hydrogen Moderator.

Burckhardt, 2019. Compressor solutions for BOG handling. Technical Report. Burckhardt Compression.

Cardella, U.F., 2018. Large-scale hydrogen liquefaction under the aspect of economic viability. Ph.D. thesis. Die Fakultät für Maschinenwesen der Technischen Universität München.

Cardella, U.F., Decker, L., Klein, H., 2017a. Aspects of hydrogen liquefier scale-up - process and equipment design. Proceedings of the 14th Cryogenics 2017 IIR International Conference .

Cardella, U.F., Decker, L., Sundberg, J., Klein, H., 2017b. Process optimization for large-scale hydrogen liquefaction. International Journal of Hydrogen Energy 42, 12339–12354.

ConocoPhillips, L.N.G., 2013. Optimized Cascade Process. Technical Report. ConocoPhillips.

Ding, H., H., S., Sun, S., Chen, C., 2017. Analysis and optimisation of a mixed fluid cascade (MFC) process. Cryogenics 83, 35–49.

Eifler, W., Schlücker, E., Spicher, U., Will, G., 2009. Küttner Kolbenmaschinen: Kolbenpumpen, Kolbenverdichter, Brennkraftmaschinen. Springer DE.

Fahmy, M.F.M., Nabih, H.I., El-Aziz, M.R.A., 2016a. Enhancement of the efficiency of the open cycle phillips optimized cascade lng process. Energy Conversion and Management 112, 308–318.

Fahmy, M.F.M., Nabih, H.I., El-Aziz, M.R.A., 2016b. Investigation and performance improvement of the propane precooling cycle in the propane precooled mixed refrigerant cycle liquefaction process. Industrial & Engineering Chemistry Research 55, 2769–2783.

Fernandez, I.A., Gomez, M., Gomez, J., Insua, A.B., 2017. Review of propulsion systems on lng carriers. Renewable and Sustainable Energy Reviews 67, 1395–1411.

Ghorbani, B., Mehrpooya, M., Aasadnia, M., Niasar, M.S., 2019. Hydrogen liquefaction process using solar energy and organic rankine cycle power system. Journal of Cleaner Production 235, 1465–1482.

Grote, K.H., Feldhusen, J., 2014. DUBBEL: Taschenbuch für den Maschinenbau. Springer DE.

Gunnarsson, L., Heland, E., 2015. How to Handle Boil-off Gases from LNG Trucks. Master's thesis. Linköping University.

Hammad, A., Dincer, I., 2018. Analysis and assessment of an advanced hydrogen liquefaction system. International Journal of Hydrogen Energy 43, 1139–1151.

Häring, H., 2007. Industrial Gases Processing. Wiley.

Huang, C., Zhi, X., Cao, R., Liang, K., Qiu, L., X., X., 2020. A stirling type pulse tube cryocooler working at liquid hydrogen temperatures with a precooled transmission tube. International Journal of Refrigeration 111, 29–38.

Hyunyong, L., Yude, S., Seunghun, L., 2019. Analysis and assessment of partial re-liquefaction system for liquefied hydrogen tankers using liquefied natural gas (lng) and h2 hybrid propulsion. International Journal of Hydrogen Energy 44, 15056–15071.

IRENA, 2019. Hydrogen: A renewable energy perspective. Technical Report. International Renewable Energy Agency.

Jang, N., Wook, M.S., Choi, S.H., Yoon, E.S., 2011. Dynamic simulation and optimization of the operation of boil-off gas compressors in a liquefied natural gas gasification plant. Korean Journal of Chemical Engineering 28, 1166–1171.

Kaviani, S., Feyzi, F., Khosravi, B., 2015. Modification of the peng–robinson equation of state for helium in low temperature regions. Physics and Chemistry of Liquids 54, 542–551.

Khan, M., Karimi, I., Lee, M., 2016. Evolution and optimization of the dual mixed refrigerant process of natural gas liquefaction. Applied Thermal Engineering 96, 320–329.

Kim, D., Hwang, C., Gundersen, T., Lim, Y., 2019. Process design and economic optimization of boil-off-gas re-liquefaction systems for lng carriers. Energy 173, 1119–1129.

Krasae-in, S., Stang, J.H., Nekså, P., 2010. Simulation on a proposed large-scale liquid hydrogen plant using a multi-component refrigerant refrigeration system. International Journal of Hydrogen Energy 35, 12531–12544.

Kuendig, A., Loehlein, K., Kramer, G.K., Huijsmans, J., 2008. Large scale hydrogen liquefaction in combination with LNG re-gasification. Technical Report. Linde Kryotechnik AG and Shell hydrogen B.V.

Kuzmenko, I.F., Morkovkin, I.M., Gurov, E.I., 2004. Concept of building medium-capacity hydrogen liquefiers with helium refrigeration cycle. Chemical and Petroleum Engineering 40, 94–98.

Leachman, J.W., Jacobsen, R.T., Lemmon, E.W., Penoncello, S.G., 2017. Hydrogen, in: Thermodynamic Properties of Cryogenic Fluids. Springer International Publishing, pp. 41–71.

Leachman, J.W., Jacobsen, R.T., Penoncello, S.G., Lemmon, E.W., 2009. Fundamental equations of state for parahydrogen, normal hydrogen, and orthohydrogen. Journal of Physical and Chemical Reference Data 38, 721–748.

Leclercq, N., Desrumaux, P., 2018. Design solutions to minimize Boil-off. Technical Report. European Commision.

Lee, M., 2017. Innovative Way to Recondense Boil-Off Gas. Technical Report. Sulzer Ltd.

Linde, 2019a. LNG Technology: Optimised solutions for small- to world-scale plants. Technical Report. Linde Engineering.

Linde, G.d., 2019b. The cleanest energy ever: Hydrogen Solutions from Linde Gas. Technical Report. Linde AG.

Liquide, A., 2017. Boil-off gas management: LNG terminal technologies. Technical Report. Air Liquide S.A.

solutions MAN, E., 2020. Marine Engine Program: MAN Energy solutions. Technical Report. MAN SE.

Marmolejo-Correa, D., Gundersen, T., 2012. A comparison of exergy efficiency definitions with focus on low temperature processes. Energy 44, 477–489.

Matthews, M.J., Petitpas, G., Aceves, S.M., 2011. A study of spin isomer conversion kinetics in supercritical fluid hydrogen for cryogenic fuel storage technologies. Applied Physics Letters 99, 81–90.

McCoy, G.A., Douglass, J.G., 2014. PREMIUM EFFICIENCY MOTOR SELECTION AND APPLICATION GUIDE: A HANDBOOK FOR INDUSTRY. Technical Report. The U.S. Department of Energy (DOE) Office of Energy Efficiency.

McIntosh, G.E., 2015. Applications of ortho-para hydrogen catalyst. IOP Conference Series: Materials Science and Engineering 101, 12–79.

Moein, P., Sarmad, M., Ebrahimi, M., Zare, M., Pakseresht, S., Vakili, S., 2015. Apci-lng single mixed refrigerant process for natural gas liquefaction cycle: Analysis and optimization. Journal of Natural Gas Science and Engineering 26, 470–479.

MWConsulting, G., 2007. Report 2002–2007. Technical Report. Clean Energy Partnership.

Myhre, G., Shindell, D., Breon, F.M., Collins, W., Fuglestvedt, J., Huang, J., Koch, D., Lamarque, J.F., Lee, D., Mendoza, B., Nakajima, T., Robock, A., Stephens, G., Takemura, T., Zhang, H., 2013. Anthropogenic and Natural Radiative Forcing. Cambridge University Press. chapter 8. p. 659–740.

Nakano, A., Maeda, T., Ito, H., Masuda, M., Kawakami, Y., Kato, A., Tange, M., Takahashi, T., Matsuo, M., 2010. Small-scale hydrogen liquefaction with a two-stage gifford–mcmahon cycle refrigerator. International Journal of Hydrogen Energy 35, 9088–9094.

NCE, 2016. Norwegian future value chains for liquid hydrogen. Technical Report. Norwegian Centres of Experties.

Niu, L., Hou, Y., Sun, W., Chen, S., 2015. The measurement of thermodynamic performance in cryogenic two-phase turbo-expander. Cryogenics 70, 76–84.

Numazawa, T., Kamiya, K., Utaki, T., Matsumoto, K., 2014. Magnetic refrigerator for hydrogen liquefaction. Cryogenics 62, 185–192.

Ohlig, K., Decker, L., 2014. The latest developments and outlook for hydrogen liquefaction technology, AIP Publishing LLC.

Ohlig, K., Decker, L., 2019. Industrial Cryogenic Plants. Technical Report. Linde Kryotechnik AG.

Parker, S., 2019. Don't waste a drop – how frugal LNG engines are cracking emissions limits. Technical Report. Riviera.

Pearsall, R., Schmidt, W., 2012. Proceedings of the 3rd Gas Processing Symposium. Elsevier.

Plachta, D., Stephens, J., Johnson, W., Zagarola, M., 2018. Nasa cryocooler technology developments and goals to achieve zero boil-off and to liquefy cryogenic propellants for space exploration. Cryogenics 94, 95–102.

Programme, U.N.E., 2019. Emissions Gap Report. Technical Report. INTERNATIONAL GAS UNION.

Quack, H., Haberstroh, C., Seemann, I., Klaus, M., 2015. Nelium, a refrigerant with high potential for the temperature range between 27 and 70 k. Physics Procedia 67, 176–182.

Rant, Z., 2001. Termodinamika - knjiga za uk in prakso. Fakulteta za strojništvo, Univerza v Ljubljani.

Roder, H.M., 1975. A MODIFIED BENEDICT WEBB-RUBIN EQUATION OF STATE FOR PARAHYDROGEN-II. Technical Report. National Bureau of Standards, Institute for basic standards, Cryogenics division.

Romero, J., Orosa, J., Oliveira, A.C., 2012. Research on the brayton cycle design conditions for reliquefaction cooling of LNG boil off. Journal of Marine Science and Technology 17, 532–541.

Rowlinson, J.S., 2014. History of Artificial Cold, Scientific, Technological and Cultural Issues. Springer Netherlands. chapter James Dewar and His Route to the Liquefaction of Hydrogen. pp. 53–64.

Sadaghiani, M.S., Mehrpooya, M., 2017. Introducing and energy analysis of a novel cryogenic hydrogen liquefaction process configuration. International Journal of Hydrogen Energy 42, 6033–6050.

Shimko, M.A., Gardiner, M.R., Bakke, P., 2008. Innovative hydrogen liquefaction cycle. Technical Report. U.S. Department of Energy.

Skaugen, G., Berstad, D., Wilhelmsen, Ø., 2020. Comparing exergy losses and evaluating the potential of catalyst-filled plate-fin and spiral-wound heat exchangers in a large-scale claude hydrogen liquefaction process. International Journal of Hydrogen Energy 45, 6663–6679.

Stryjek, R., Vera, J.H., 1986. PRSV: An improved peng-robinson equation of state for pure compounds and mixtures. The Canadian Journal of Chemical Engineering 64, 323–333.

Thomas, R.J., Ghosh, P., Chowdhury, K., 2011. Exergy analysis of helium liquefaction systems based on modified claude cycle with two-expanders. Cryogenics 51, 287–294.

Ubaid, S., Xiao, J., Zacharia, R., Chahine, R., Bernard, P., 2014. Effect of para–ortho conversion on hydrogen storage system performance. International Journal of Hydrogen Energy 39, 11651–11660.

UNION, I.G., 2019. 2019 WORLD LNG REPORT. Technical Report. INTERNATIONAL GAS UNION.

Valenti, G., Macchi, E., 2008. Proposal of an innovative, high-efficiency, large-scale hydrogen liquefier. International Journal of Hydrogen Energy 33, 3116–3121.

Vaudolon, A., 2000. LIQUEFIED GASES: Marine Transportation and Storage. Whiterby Company limited.

Vikse, M., Watson, H., Gundersen, T., Barton, P., 2018. Simulation of dual mixed refrigerant natural gas liquefaction processes using a nonsmooth framework. Processes 6, 193.

Wilhelmsen, Ø., Berstad, D., Aasen, A., Nekså, P., Skaugen, G., 2018. Reducing the exergy destruction in the cryogenic heat exchangers of hydrogen liquefaction processes. International Journal of Hydrogen Energy 43, 5033–5047.

Yang, C., Ogden, J.M., 2007. Determining the lowest-cost hydrogen delivery mode. International Journal of Hydrogen Energy 32, 268–286.

Yuksel, Y.E., Ozturk, M., Dincer, I., 2017. Analysis and assessment of a novel hydrogen liquefaction process. International Journal of Hydrogen Energy 42, 11429–11438.

Zhang, P., Zhou, L., Zeng, W., Xiong, G., Huang, H., Cai, L., Ye, H., Qu, S., 2020. Hydrocarbon dew point measurement and model evaluation of synthetic and real natural gases. ACS Omega 5, 8463–8473.

Zhuzhgov, A.V., Krivoruchko, O.P., Isupova, L.A., Martyanov, O.N., Parmon, V.N., 2018. Low-temperature conversion of ortho-hydrogen into liquid para-hydrogen: Process and catalysts. review. Catalysis in Industry 10, 9–19.

Appendices

Appendix A

Helium reverse Brayton cycle

Parameter	Value	Unit
Hydrogen boil-off gas		
Reservoir volume	40 000	m^3
Boil-off rate	0.2	$\% \, d^{-1}$
Storage pressure	1.16	bar
Starting temperature	-235	°C
Mass flow	234.2	$kg \, h^{-1}$
Para-hydrogen concentration	100	mol %
Expander isentropic efficiency	80	%
Piston compressor adiabatic efficiency	70	%
Pressure drop in a heat exchanger	1.6	%
Pressure drop in an inter/aftercooler	1	%
Helium refrigerant		
Expander isentropic efficiency	80	%
Oil-screw helium compressor adiabatic efficiency	70	%
Pressure drop in a heat exchanger	0.1	bar

Table A.1: Reverse helium Brayton assumptions

Stream No.	T [°C]	p [kPa]	$\dot{m}$ [kg h^{-1}]	h [kJ kg^{-1}]	s [kJ kg^{-1} K]	$\dot{E}x$ [kW]
BOG	-252.4	116.0	0.0	192.0	29.6	0.0
H-1	-252.4	116.0	234.2	192.0	29.6	399.4
H-2	-235.0	116.0	234.2	385.1	36.4	284.4
H-3	-236.5	116.0	260.2	368.7	35.9	323.9
H-4	13.5	114.1	260.2	4001.0	63.6	10.3
H-5	101.3	228.3	260.2	5293.5	64.7	81.3
H-6	15.0	226.0	260.2	4023.9	60.9	69.0
H-7	103.3	452.0	260.2	5324.5	61.9	140.6
H-8	15.0	447.5	260.2	4025.0	58.1	127.8
H-9	103.3	895.0	260.2	5327.9	59.1	199.5
H-10	15.0	886.0	260.2	4027.0	55.2	186.7
H-11	-229.4	871.9	260.2	394.6	28.8	475.4
H-12	-237.1	857.9	260.2	292.0	26.2	520.7
H-13	-245.0	844.2	260.2	-150.1	11.9	787.8
H-14	-248.9	830.7	260.2	-207.0	9.7	828.7
H-15	-252.4	116.0	260.2	-207.0	10.3	815.6
H-16	-252.4	116.0	234.3	-251.2	8.2	771.4
H-17	-252.4	116.0	25.9	192.0	29.6	44.2
H-18	-250.0	116.0	25.9	220.9	30.9	41.7
H-RCY	-250.0	116.0	26.0	220.9	30.9	41.8
He-1	13.0	970.0	3573.6	1489.0	24.7	1344.7
He-2	132.8	1843.0	3573.6	2113.8	25.2	1826.6
He-3	15.0	1833.0	3573.6	1502.2	23.4	1725.3
He-4	135.8	3482.7	3573.6	2134.4	23.9	2213.9
He-5	15.0	3472.7	3573.6	1507.5	22.1	2109.5
He-6	-237.1	3462.7	3573.6	187.3	11.1	3941.3
He-7	-244.1	1731.3	3573.6	148.4	11.4	3804.4
He-8	-245.0	1721.3	3573.6	143.4	11.3	3846.0
He-10	-249.4	1000.0	3573.6	119.9	11.5	3750.5
He-11	-248.7	990.0	3573.6	124.1	11.7	3699.3
He-12	-241.9	980.0	3573.6	161.3	13.1	3345.8

Table A.2: Material balance with exergy flows for helium refrigeration process with the Joule-Thomson valve

Stream No.	T [°C]	p [kPa]	$\dot{m}$ [$kg\,h^{-1}$]	h [$kJ\,kg^{-1}$]	s [$kJ\,kg^{-1}\,K$]	$\dot{E}x$ [kW]
H-1	-252.4	116.0	234.2	192.0	29.6	399.4
H-2	-235.0	116.0	234.2	385.1	36.4	284.4
H-3	-236.3	116.0	256.3	370.9	36.0	317.9
H-4	13.5	114.1	256.3	4001.0	63.6	10.1
H-5	101.3	228.3	256.3	5293.5	64.7	80.1
H-6	15.0	226.0	256.3	4023.9	60.9	68.0
H-7	103.3	452.0	256.3	5324.5	61.9	138.5
H-8	15.0	447.5	256.3	4025.0	58.1	125.9
H-9	103.3	895.0	256.3	5327.9	59.1	196.5
H-10	15.0	886.0	256.3	4027.0	55.2	183.9
H-11	-229.2	871.9	256.3	396.9	28.8	467.3
H-12	-237.0	857.9	256.3	293.2	26.3	512.2
H-13	-244.5	844.2	256.3	-141.6	12.2	770.3
H-14	-248.5	830.7	256.3	-202.1	9.9	812.3
H-15	-252.4	116.0	256.3	-213.1	10.0	808.8
H-16	-252.4	116.0	234.2	-251.2	8.2	771.2
H-17	-252.4	116.0	22.0	192.0	29.6	37.6
H-18	-250.0	116.0	22.0	220.9	30.9	35.4
H-RCY	-250.0	116.0	22.1	220.9	30.9	35.5
He-1	13.0	970.0	3460.6	1489.0	24.7	1302.2
He-2	132.8	1843.0	3460.6	2113.8	25.2	1768.9
He-3	15.0	1833.0	3460.6	1502.2	23.4	1670.7
He-4	135.8	3482.7	3460.6	2134.4	23.9	2143.9
He-5	15.0	3472.7	3460.6	1507.5	22.1	2042.8
He-6	-237.0	3462.7	3460.6	187.7	11.1	3813.6
He-7	-244.0	1731.3	3460.6	148.8	11.4	3680.9
He-8	-244.5	1721.3	3460.6	146.0	11.4	3701.4
He-10	-249.0	1000.0	3460.6	122.1	11.6	3608.5
He-11	-248.2	990.0	3460.6	126.6	11.8	3556.3
He-12	-241.8	980.0	3460.6	161.6	13.1	3237.5

Table A.3: Material balance with exergy flows for helium refrigeration process with the liquid turbine expander

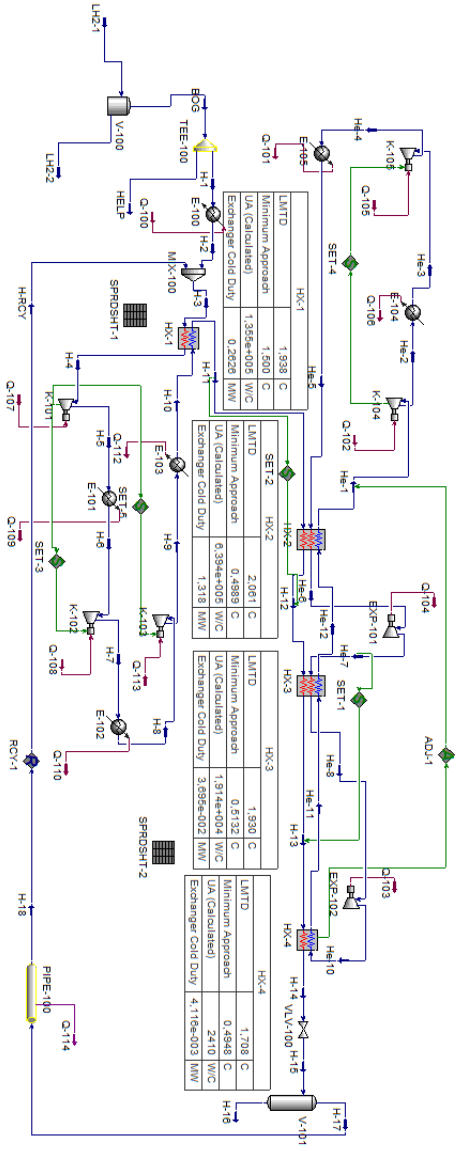

Figure A.1: Simplified process flow diagram for the simulation of helium reverse Brayton process with the Joule-Thomson valve

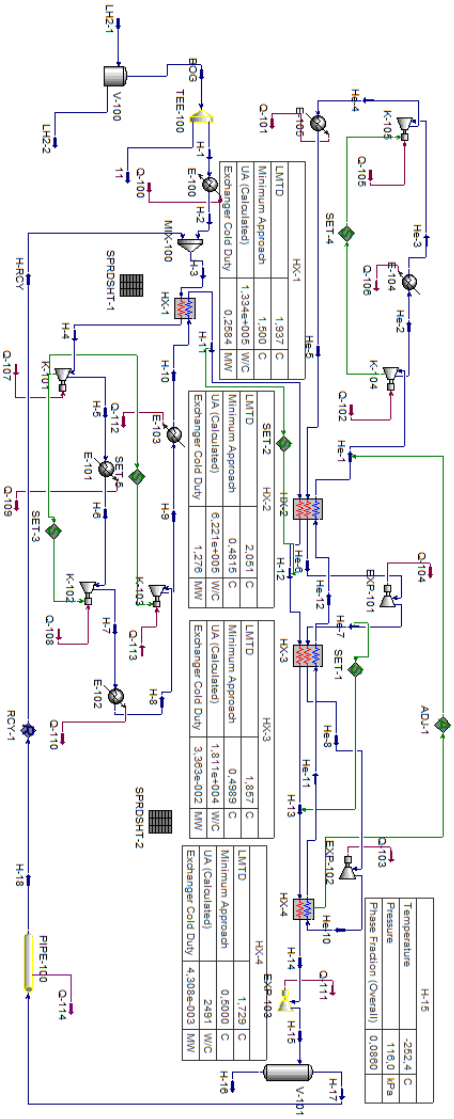

Figure A.2: Simplified process flow diagram for the simulation of helium reverse Brayton process with the liquid expander

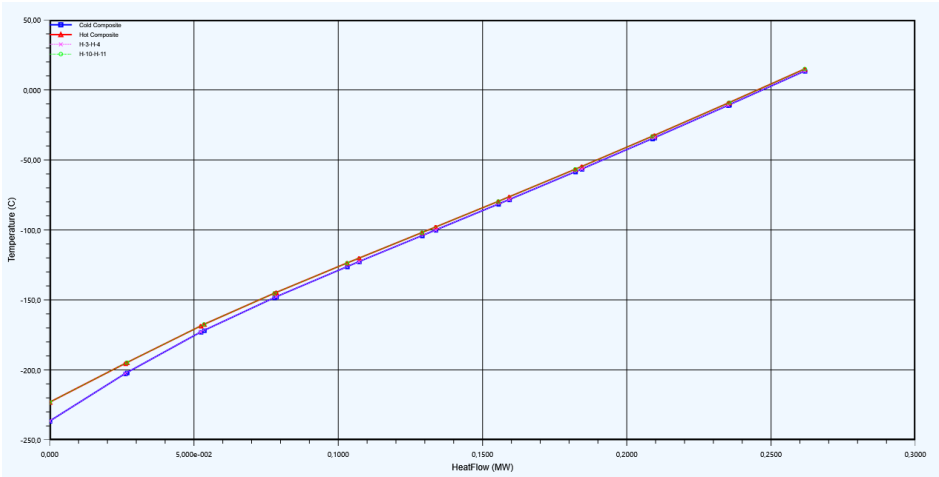

(a) Heating curves for the first heat exchanger HX-1

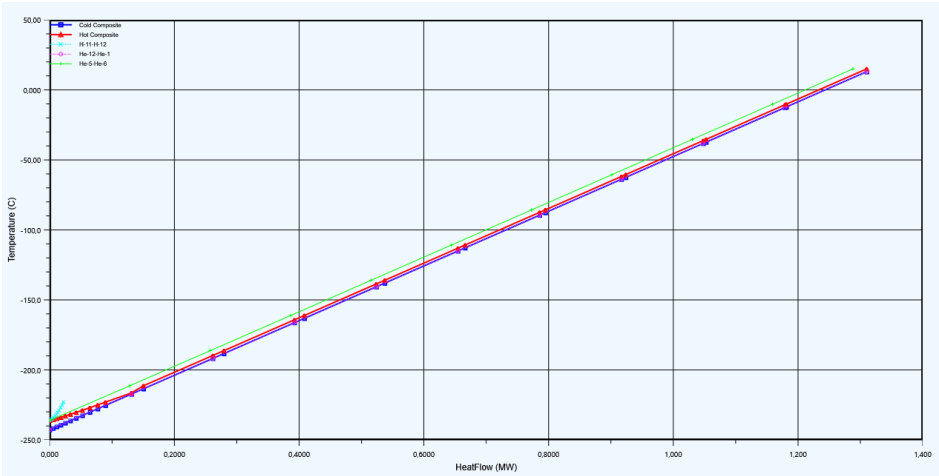

(b) Heating curves for the second heat exchanger HX-2

Figure A.3: Heating curves for the first and second heat exchanger for the first simulation result of helium reverse Brayton cycle with the Joule-Thomson valve.

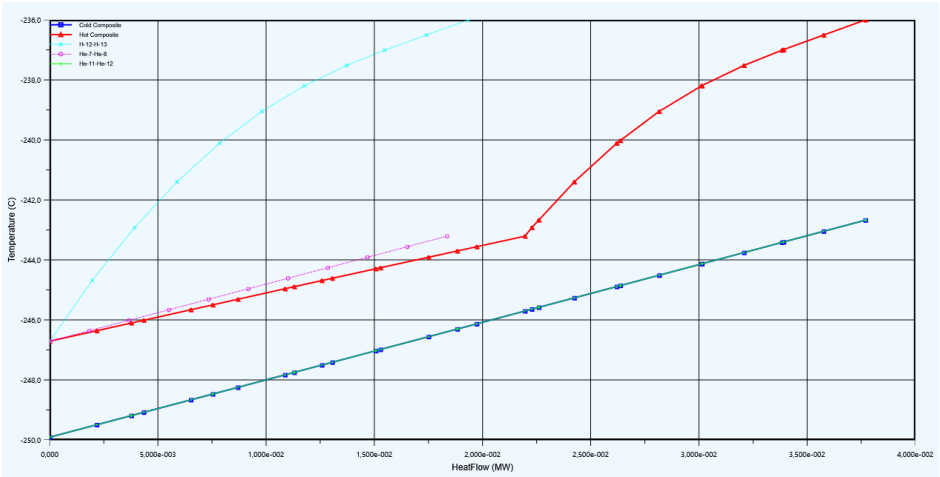

(a) Heating curves for the third heat exchanger HX-3

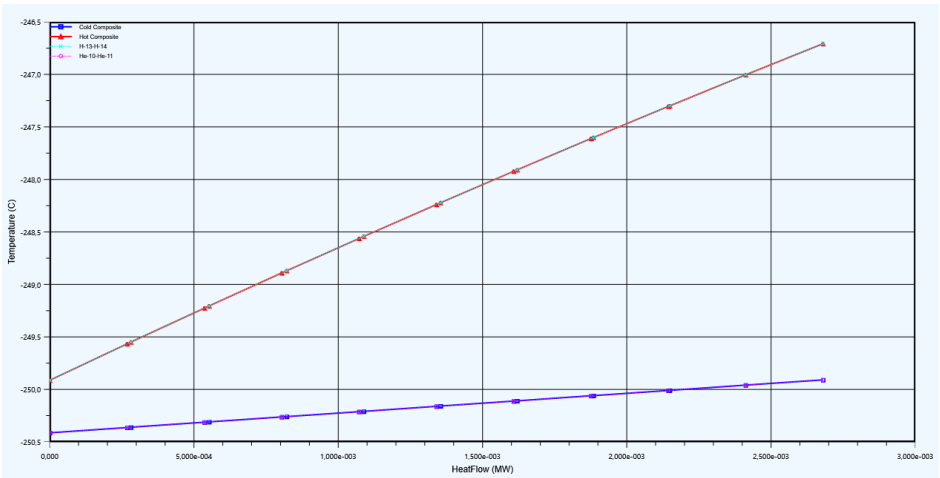

(b) Heating curves for the last heat exchanger HX-4

Figure A.4: Heating curves for the third and fourth heat exchanger for the first simulation result of helium reverse Brayton cycle with the Joule-Thomson valve.

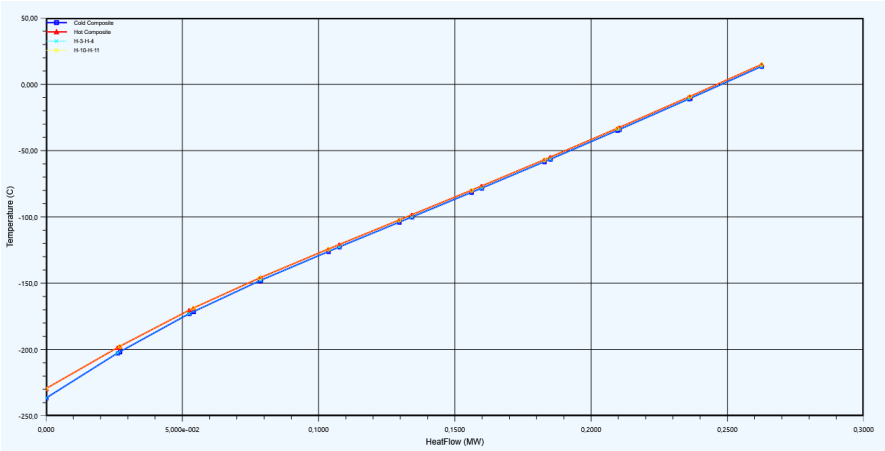

(a) Heating curves for the first heat exchanger HX-1

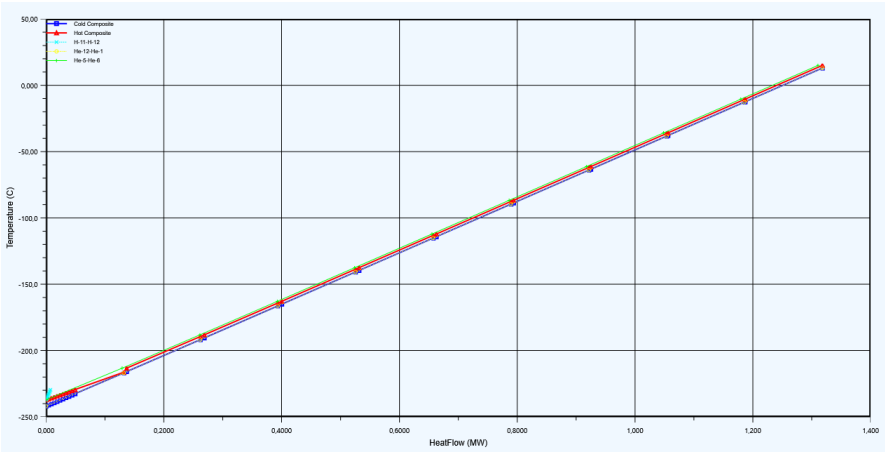

(b) Heating curves for the second heat exchanger HX-2

Figure A.5: Heating curves for the first and second heat exchanger for the best simulation result of helium reverse Brayton cycle with the Joule-Thomson valve.

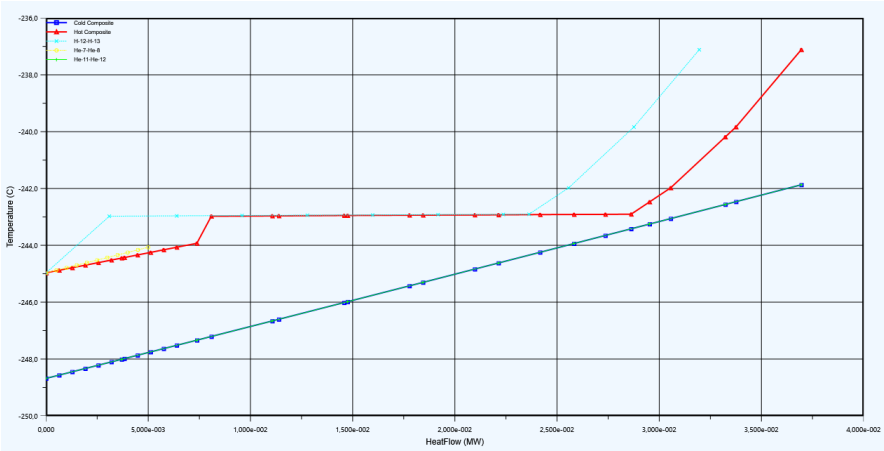

(a) Heating curves for the third heat exchanger HX-3

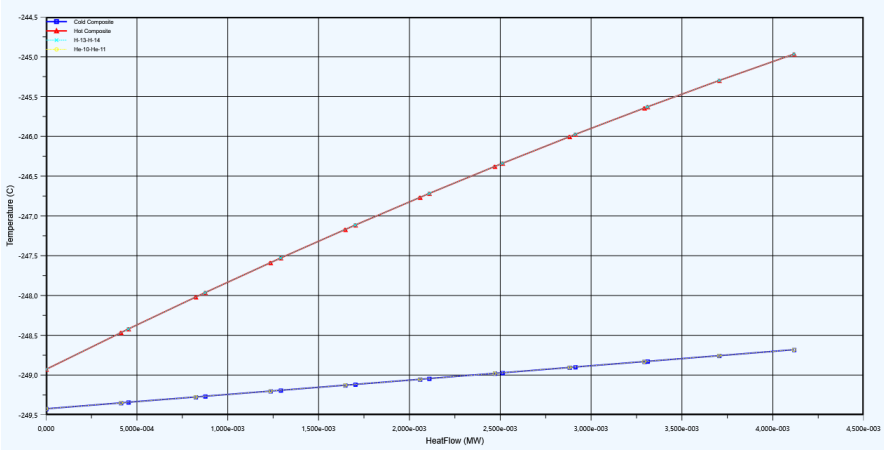

(b) Heating curves for the last heat exchanger HX-4

Figure A.6: Heating curves for the third and fourth heat exchanger for the best simulation result of helium reverse Brayton cycle with the Joule-Thomson valve.

Appendix B

Hydrogen Claude process

Parameter	Value	Unit
Hydrogen boil-off gas		
Reservoir volume	40 000	m^3
Boil-off rate	0.2	$\% \, d^{-1}$
Storage pressure	1.16	bar
Starting temperature	-235	°C
Mass flow	234.2	$kg \, h^{-1}$
Para-hydrogen concentration	100	mol %
Expander isentropic efficiency	80	%
Hydrogen piston compressor adiabatic efficiency	70	%
Pressure drop in a heat exchanger	1.6	%
Pressure drop in an inter/aftercooler	1	%
Hydrogen refrigerant		
Expander isentropic efficiency	80	%
Hydrogen piston compressor adiabatic efficiency	70	%
Pressure drop in a heat exchanger	1.6	%
Pressure drop in an inter/aftercooler	1	%

Table B.1: Hydrogen Claude refrigeration cycle assumptions

Stream No.	T [°C]	p [kPa]	$\dot{m}$ [$kg\,h^{-1}$]	h [$kJ\,kg^{-1}$]	s [$kJ\,kg^{-1}\,K$]	$\dot{E}x$ [kW]
BOG	-252.4	116.0	0.0	192.0	29.6	0.0
H-1	-252.4	116.0	234.2	192.0	29.6	399.4
H-2	-235.0	116.0	234.2	385.1	36.4	284.4
H-3	-237.4	116.0	276.9	359.8	35.7	349.4
H-4	13.5	114.1	276.9	4001.0	63.6	10.9
H-5	127.6	273.9	276.9	5677.5	64.9	110.8
H-6	15.0	271.2	276.9	4024.1	60.1	90.1
H-7	129.8	650.9	276.9	5711.9	61.4	190.8
H-8	15.0	644.4	276.9	4025.9	56.5	169.4
H-9	129.9	1546.5	276.9	5719.4	57.9	270.5
H-10	15.0	1531.1	276.9	4030.0	53.0	249.0
H-11	-226.6	1506.6	276.9	388.8	26.7	551.7
H-12	-227.7	1482.5	276.9	374.8	26.4	556.1
H-13	-247.3	1458.7	276.9	-183.2	10.3	870.8
H-14	-252.4	116.0	276.9	-183.2	11.5	844.2
H-15	-252.4	116.0	234.4	-251.3	8.2	771.7
H-16	-252.4	116.0	42.5	192.0	29.6	72.5
H-17	-250.0	116.0	42.5	220.9	30.9	68.4
H-RCY	-250.0	116.0	42.7	220.9	30.9	68.6
Hyd-1	13.0	333.5	687.6	4023.8	65.0	270.8
Hyd-2	144.7	883.7	687.6	5926.2	66.4	555.2
Hyd-3	15.0	874.9	687.6	4054.9	61.1	490.5
Hyd-4	13.0	855.6	687.6	4026.2	61.1	485.4
Hyd-5	14.0	855.6	1375.2	4040.5	61.2	970.8
Hyd-6	146.3	2267.4	1375.2	5959.1	62.6	1545.0
Hyd-7	15.0	2244.8	1375.2	4061.3	57.2	1412.6
Hyd-8	-204.2	2208.8	1375.2	1166.2	38.9	2324.0
Hyd-9	-204.2	2208.8	687.6	1166.2	38.9	1162.0
Hyd-10	-204.2	2208.8	687.6	1166.2	38.9	1162.0
Hyd-11	-222.0	883.7	687.6	1003.9	39.7	1085.8
Hyd-12	-227.7	2173.5	687.6	844.3	33.2	1415.4
Hyd-13	-247.8	350.0	687.6	703.7	34.6	1312.1
Hyd-14	-231.4	344.4	687.6	928.4	41.8	959.8
Hyd-15	-211.9	338.9	687.6	1140.0	46.0	767.4
Hyd-16	-211.9	869.5	687.6	1119.9	41.9	990.4

Table B.2: Material balance with exergy flows for hydrogen refrigeration process with the Joule-Thomson valve

Stream No.	T [°C]	p [kPa]	$\dot{m}$ [$kg\,h^{-1}$]	h [$kJ\,kg^{-1}$]	s [$kJ\,kg^{-1}\,K$]	$\dot{E}x$ [kW]
BOG	-252.4	116.0	0.0	192.0	29.6	0.0
H-1	-252.4	116.0	234.2	192.0	29.6	399.4
H-2	-235.0	116.0	234.2	385.1	36.4	284.4
H-3	-236.7	116.0	262.8	367.2	35.9	327.8
H-4	13.5	114.1	262.8	4001.0	63.6	10.4
H-5	127.6	273.9	262.8	5677.5	64.9	105.1
H-6	15.0	271.2	262.8	4024.1	60.1	85.5
H-7	129.8	650.9	262.8	5711.9	61.4	181.1
H-8	15.0	644.4	262.8	4025.9	56.5	160.8
H-9	129.9	1546.5	262.8	5719.4	57.9	256.7
H-10	15.0	1531.1	262.8	4030.0	53.0	236.3
H-11	-226.1	1506.6	262.8	396.2	26.8	520.8
H-12	-228.1	1482.5	262.8	369.4	26.3	529.8
H-13	-247.3	1458.7	262.8	-183.1	10.3	826.4
H-14	-252.4	116.0	262.8	-203.1	10.5	819.8
H-15	-252.4	116.0	234.2	-251.2	8.2	771.2
H-16	-252.4	116.0	28.5	192.0	29.6	48.7
H-17	-250.0	116.0	28.5	220.9	30.9	45.9
H-RCY	-250.0	116.0	28.6	220.9	30.9	45.9
Hyd-1	13.0	333.5	667.9	4023.8	65.0	263.1
Hyd-2	144.7	883.7	667.9	5926.2	66.4	539.3
Hyd-3	15.0	874.9	667.9	4054.9	61.1	476.5
Hyd-4	13.0	855.6	667.9	4026.2	61.1	471.6
Hyd-5	14.0	855.6	1335.9	4040.5	61.2	943.1
Hyd-6	146.3	2267.4	1335.9	5959.1	62.6	1500.9
Hyd-7	15.0	2244.8	1335.9	4061.3	57.2	1372.2
Hyd-8	-204.2	2208.8	1335.9	1166.0	38.9	2257.8
Hyd-9	-204.2	2208.8	667.9	1166.0	38.9	1128.9
Hyd-10	-204.2	2208.8	667.9	1166.0	38.9	1128.9
Hyd-11	-222.0	883.7	667.9	1003.7	39.7	1054.9
Hyd-12	-228.1	2173.5	667.9	837.7	33.0	1381.5
Hyd-13	-247.8	350.0	667.9	699.5	34.4	1282.9
Hyd-14	-232.5	344.4	667.9	916.8	41.5	945.2
Hyd-15	-212.0	338.9	667.9	1139.8	46.0	745.6
Hyd-16	-212.0	869.5	667.9	1119.7	41.9	962.2

Table B.3: Material balance with exergy flows for hydrogen refrigeration process with the liquid turbine expander

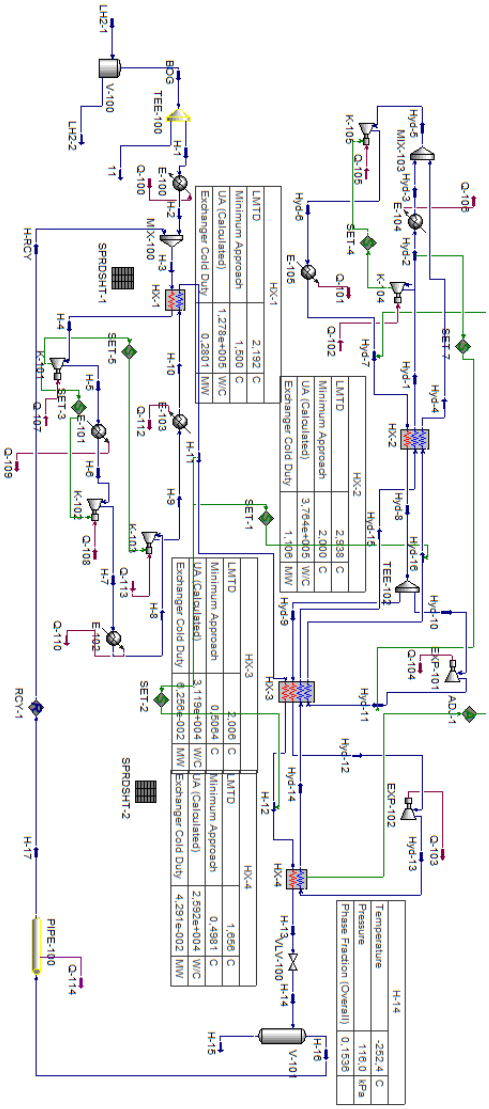

Figure B.1: Simplified process flow diagram for the simulation of hydrogen Claude process with the Joule-Thomson valve

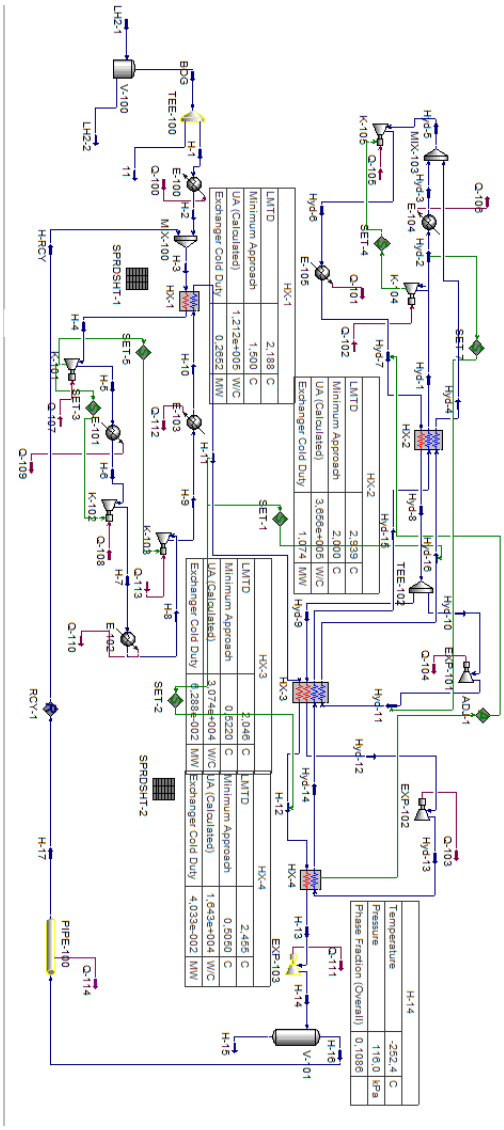

Figure B.2: Simplified process flow diagram for the simulation of hydrogen Claude process with the liquid expander

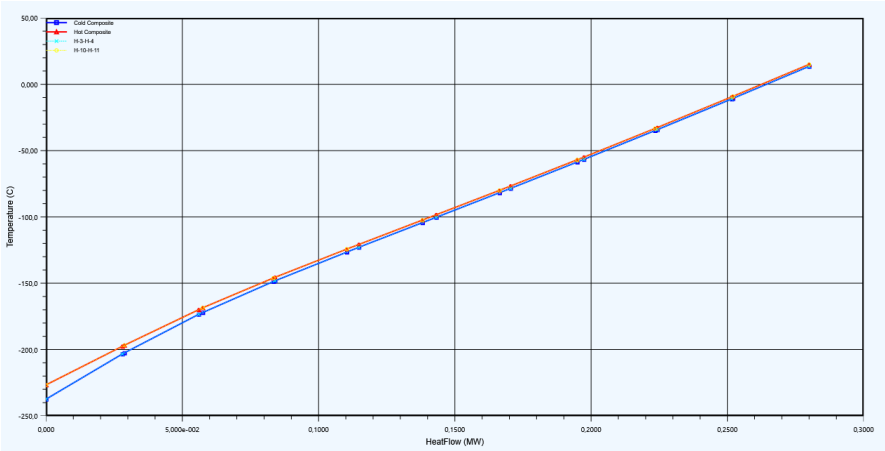

(a) Heating curves for the first heat exchanger HX-1

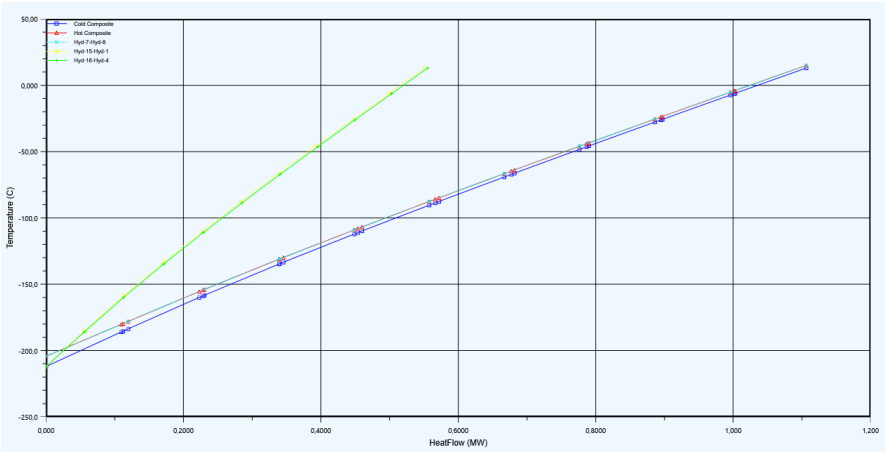

(b) Heating curves for the second heat exchanger HX-2

Figure B.3: Heating curves for the first and second heat exchanger for the hydrogen Claude process with the Joule-Thomson valve

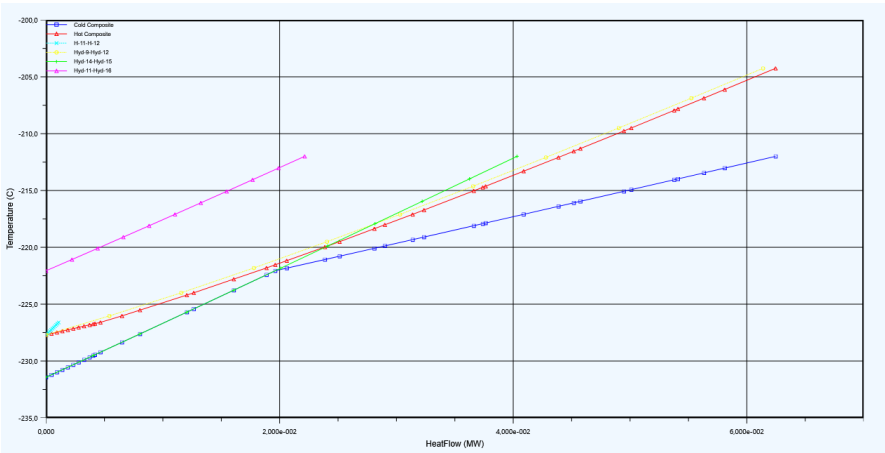

(a) Heating curves for the third heat exchanger HX-3

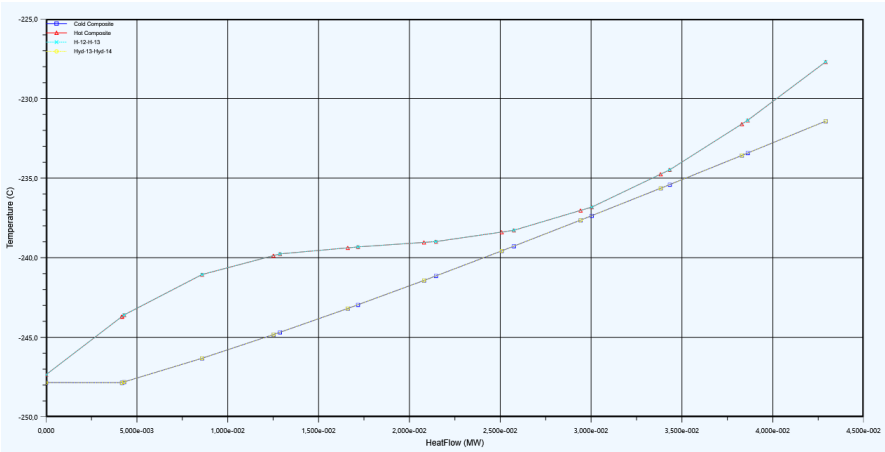

(b) Heating curves for the last heat exchanger HX-4

Figure B.4: Heating curves for the third and fourth heat exchanger for the hydrogen Claude process with the Joule-Thomson valve

Appendix C

Nelium reverse Brayton cycle

Parameter	Value	Unit
Hydrogen boil-off gas		
Reservoir volume	40 000	m^3
Boil-off rate	0.2	$\% \, d^{-1}$
Storage pressure	1.16	bar
Starting temperature	-235	°C
Mass flow	234.2	$kg \, h^{-1}$
Para-hydrogen concentration	100	mol %
Expander isentropic efficiency	80	%
Hydrogen piston compressor adiabatic efficiency	70	%
Pressure drop in a heat exchanger	1.6	%
Pressure drop in an inter/aftercooler	1	%
Mixed refrigerant		
Expander isentropic efficiency	80	%
Mixed refrigerant turbo compressor adiabatic efficiency	75	%
Helium and neon mole concentrations	80-20	%
Pressure drop in a heat exchanger	0.12	bar

Table C.1: Mixed refrigerant reverse Brayton cycle assumptions

Stream No.	T [°C]	p [kPa]	$\dot{m}$ [kg h^{-1}]	h [kJ kg^{-1}]	s [kJ kg^{-1} K]	$\dot{E}x$ [kW]
BOG	-252.4	116.0	0.0	192.0	29.6	0.0
H-1	-252.4	116.0	234.2	192.0	29.6	399.4
H-2	-235.0	116.0	234.2	385.1	36.4	284.4
H-3	-237.4	116.0	277.7	359.4	35.7	350.7
H-4	13.5	114.1	277.7	4001.0	63.6	11.0
H-5	101.3	228.3	277.7	5293.5	64.7	86.8
H-6	15.0	226.0	277.7	4023.9	60.9	73.6
H-7	103.3	452.0	277.7	5324.5	61.9	150.1
H-8	15.0	447.5	277.7	4025.0	58.1	136.4
H-9	103.3	895.0	277.7	5327.9	59.1	213.0
H-10	15.0	886.0	277.7	4027.0	55.2	199.3
H-11	-230.2	871.9	277.7	385.3	28.5	511.4
H-12	-235.8	857.9	277.7	311.9	26.8	545.2
H-13	-245.7	844.2	277.7	-162.6	11.4	849.8
H-14	-247.0	830.7	277.7	-181.9	10.7	864.1
H-15	-252.4	116.0	277.7	-181.9	11.6	845.4
H-16	-252.4	116.0	234.2	-251.3	8.2	771.3
H-17	-252.4	116.0	43.4	192.0	29.6	74.1
H-18	-250.0	116.0	43.4	220.9	30.9	69.9
H-RCY	-250.0	116.0	43.5	220.9	30.9	69.9
HeNe-1	13.0	664.0	6833.6	-35.0	10.4	1181.1
HeNe-2	55.2	863.2	6833.6	86.2	10.5	1359.9
HeNe-3	15.0	851.2	6833.6	-29.4	10.1	1337.1
HeNe-4	57.5	1106.6	6833.6	92.6	10.2	1517.5
HeNe-5	15.0	1094.6	6833.6	-29.6	9.8	1495.1
HeNe-6	57.5	1422.9	6833.6	92.4	9.9	1675.4
HeNe-7	15.0	1410.9	6833.6	-29.9	9.5	1654.5
HeNe-8	57.5	1834.2	6833.6	92.2	9.6	1834.9
HeNe-9	15.0	1822.2	6833.6	-30.2	9.2	1815.2
HeNe-10	57.5	2368.9	6833.6	91.9	9.3	1995.6
HeNe-11	15.0	2356.9	6833.6	-30.5	8.9	1976.8
HeNe-12	-235.8	2344.9	6833.6	-764.3	2.9	3895.8
HeNe-13	-243.5	1172.4	6833.6	-781.9	3.0	3779.6
HeNe-14	-245.7	1160.4	6833.6	-799.8	2.4	4088.0
HeNe-15	-247.5	700.0	6833.6	-809.8	2.5	4015.3
HeNe-16	-247.5	688.0	6833.6	-809.0	2.5	3991.1
HeNe-17	-241.7	676.0	6833.6	-771.8	3.9	3309.6

Table C.2: Material balance with exergy flows for nelium refrigeration process with the Joule-Thomson valve

Stream No.	T [°C]	p [kPa]	$\dot{m}$ [kg h^{-1}]	h [kJ kg^{-1}]	s [kJ kg^{-1} K]	$\dot{E}x$ [kW]
BOG	-252.4	116.0	0.0	192.0	29.6	0.0
H-1	-252.4	116.0	234.2	192.0	29.6	399.4
H-2	-235.0	116.0	234.2	385.1	36.4	284.4
H-3	-236.9	116.0	267.8	364.5	35.8	335.5
H-4	13.5	114.1	267.8	4001.0	63.6	10.6
H-5	101.3	228.3	267.8	5293.5	64.7	83.7
H-6	15.0	226.0	267.8	4023.9	60.9	71.0
H-7	103.3	452.0	267.8	5324.5	61.9	144.7
H-8	15.0	447.5	267.8	4025.0	58.1	131.5
H-9	103.3	895.0	267.8	5327.9	59.1	205.4
H-10	15.0	886.0	267.8	4027.0	55.2	192.2
H-11	-229.7	871.9	267.8	390.5	28.7	491.0
H-12	-235.6	857.9	267.8	313.4	26.8	525.0
H-13	-245.7	844.2	267.8	-162.6	11.4	819.5
H-14	-247.0	830.7	267.8	-181.9	10.7	833.3
H-15	-252.4	116.0	267.8	-195.9	10.9	828.6
H-16	-252.4	116.0	234.3	-251.2	8.2	771.6
H-17	-252.4	116.0	33.5	192.0	29.6	57.1
H-18	-250.0	116.0	33.5	220.9	30.9	53.8
H-RCY	-250.0	116.0	33.6	220.9	30.9	54.0
HeNe-1	13.0	664.0	6631.0	-35.0	10.4	1146.1
HeNe-2	55.2	863.2	6631.0	86.2	10.5	1319.6
HeNe-3	15.0	851.2	6631.0	-29.4	10.1	1297.5
HeNe-4	57.5	1106.6	6631.0	92.6	10.2	1472.5
HeNe-5	15.0	1094.6	6631.0	-29.6	9.8	1450.7
HeNe-6	57.5	1422.9	6631.0	92.4	9.9	1625.8
HeNe-7	15.0	1410.9	6631.0	-29.9	9.5	1605.5
HeNe-8	57.5	1834.2	6631.0	92.2	9.6	1780.5
HeNe-9	15.0	1822.2	6631.0	-30.2	9.2	1761.4
HeNe-10	57.5	2368.9	6631.0	91.9	9.3	1936.4
HeNe-11	15.0	2356.9	6631.0	-30.5	8.9	1918.2
HeNe-12	-235.6	2344.9	6631.0	-764.0	2.9	3776.0
HeNe-13	-243.5	1172.4	6631.0	-781.6	3.0	3663.0
HeNe-14	-245.7	1160.4	6631.0	-799.8	2.4	3966.7
HeNe-15	-247.5	700.0	6631.0	-809.8	2.5	3896.2
HeNe-16	-247.5	688.0	6631.0	-809.0	2.5	3872.8
HeNe-17	-241.6	676.0	6631.0	-771.6	3.9	3208.3

Table C.3: Material balance with exergy flows for nelium refrigeration process with the liquid expander

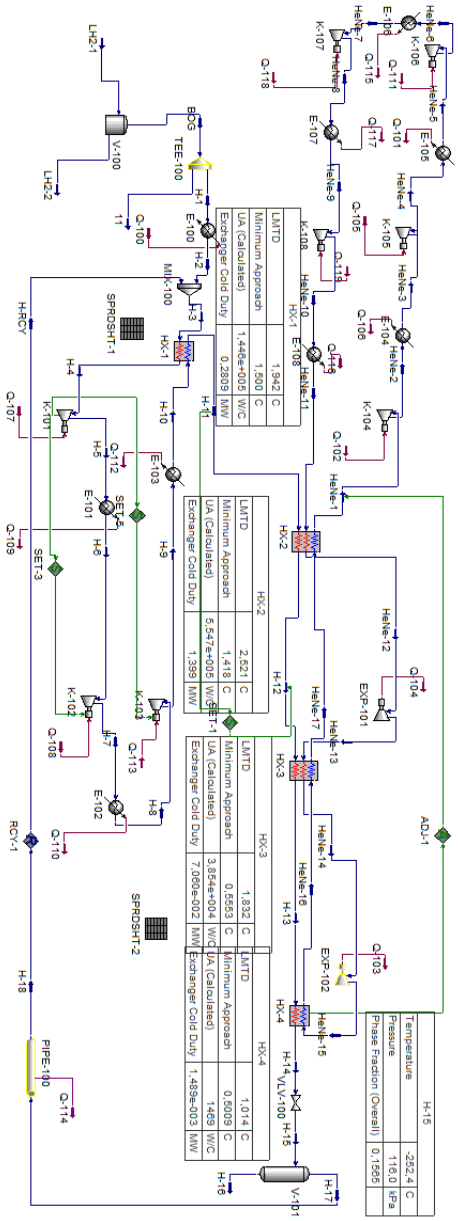

Figure C.1: Simplified process flow diagram for the simulation of nelium reverse Brayton process with the Joule-Thomson valve

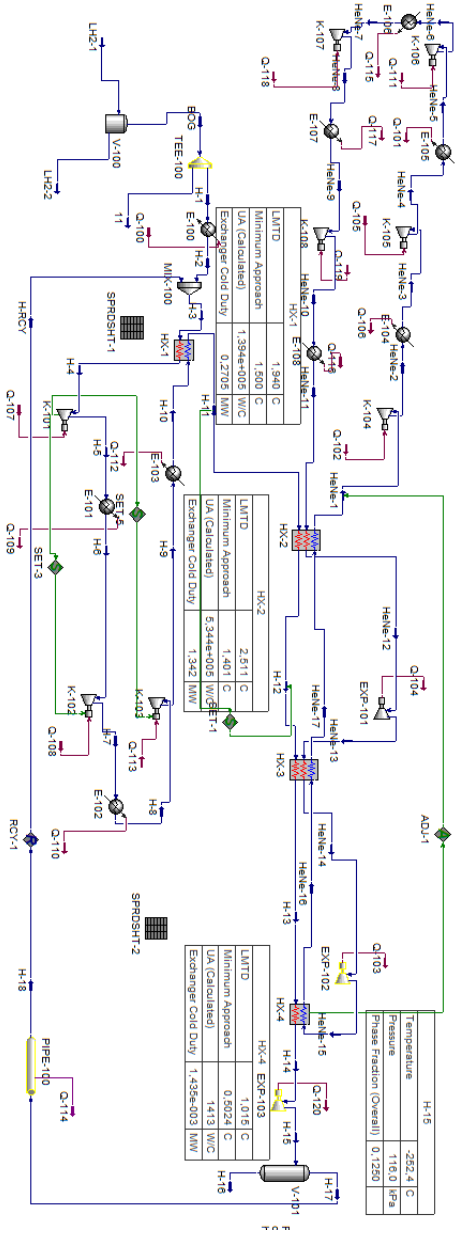

Figure C.2: Simplified process flow diagram for the simulation of nelium reverse Brayton process with the liquid expander

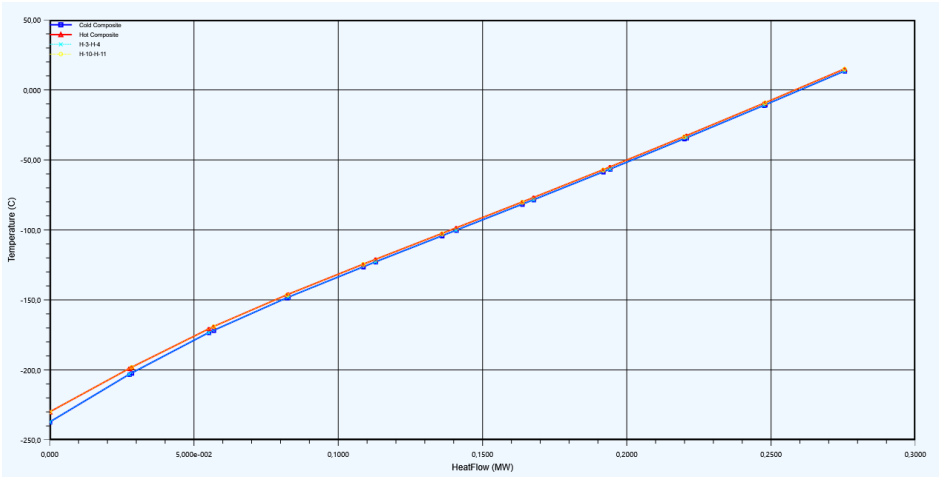

(a) Heating curves for the first heat exchanger HX-1

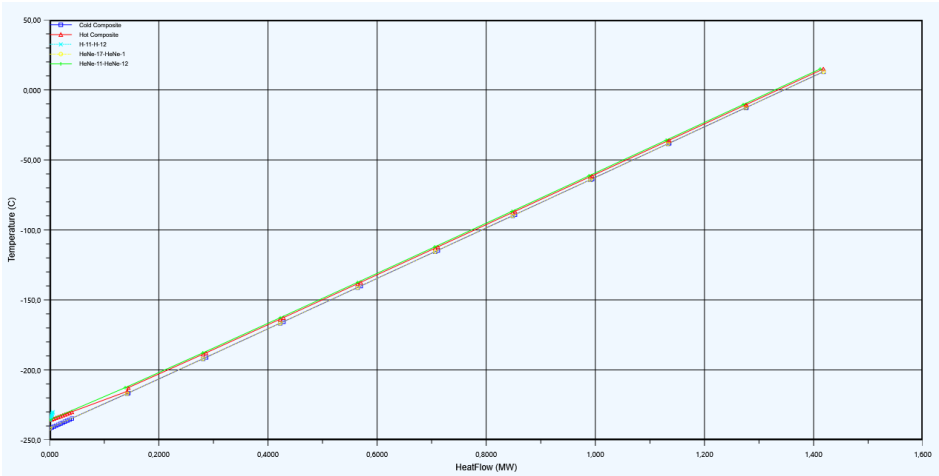

(b) Heating curves for the second heat exchanger HX-2

Figure C.3: Heating curves for the first and second heat exchanger for the best simulation case of mixed refrigerant with the Joule-Thomson valve

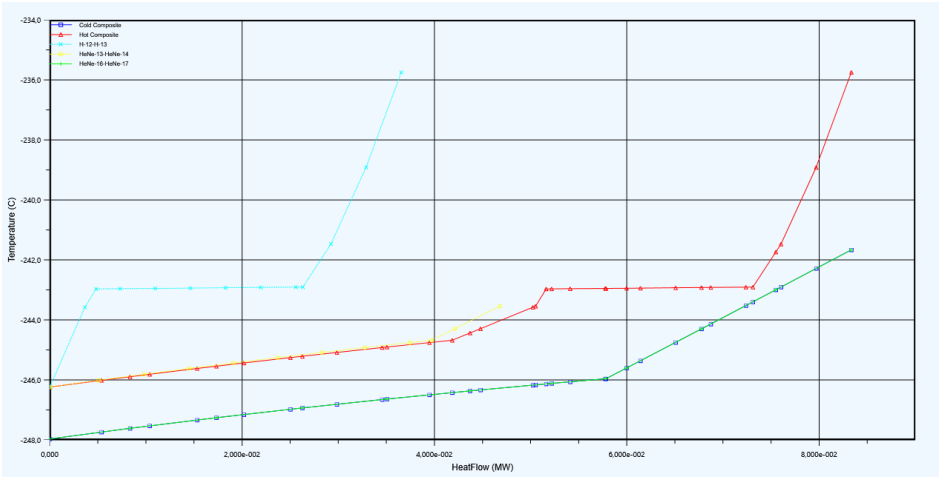

(a) Heating curves for the third heat exchanger HX-3

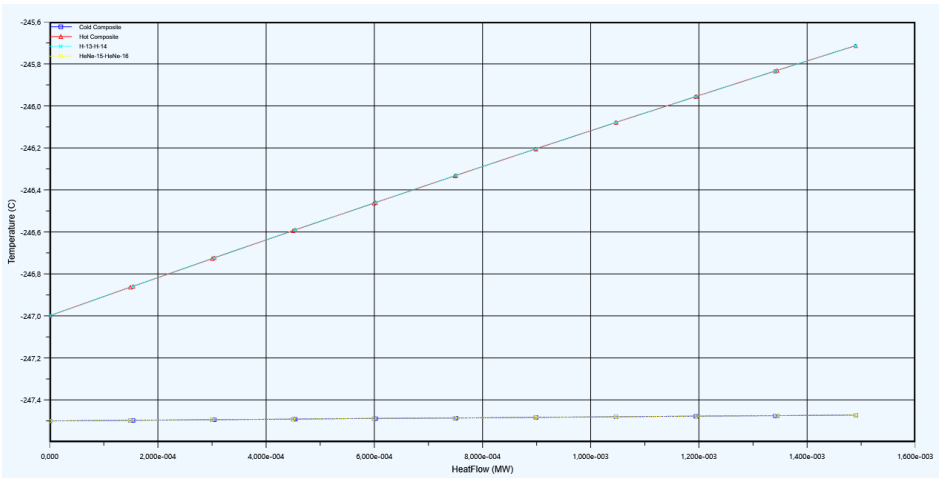

(b) Heating curves for the last heat exchanger HX-4

Figure C.4: Heating curves for the third and fourth heat exchanger for the best simulation case of mixed refrigerant with the Joule-Thomson valve